

MAGNETIC OSCILLATIONS IN TWO-DIMENSIONAL
DIRAC SYSTEMS

AND

SHEAR VISCOSITY AND SPIN DIFFUSION
IN A TWO-DIMENSIONAL FERMI GAS

Magnetische oscillaties in tweedimensionale Diracsystemen en
schuifviscositeit en spindiffusie in een tweedimensionale Fermigas

(met een samenvatting in het Nederlands)

Proefschrift

ter verkrijging van de graad van doctor aan de Universiteit Utrecht
op gezag van de rector magnificus, prof.dr. G.J. van der Zwaan,
ingevolge het besluit van het college voor promoties in het openbaar
te verdedigen op woensdag 28 oktober 2015 des middags te 12.45 uur

door

CAROLIN SARAH KÜPPERSBUSCH

geboren op 8 december 1984 te Essen, Duitsland

Promotoren: Prof.dr. C. de Morais Smith

Prof.dr. A. Rosch

Copromotor: Dr. L. Fritz

This degree is awarded as part of a Joint Doctorate with the University of Cologne.

This thesis was partly accomplished with financial support from the University of Cologne and the Bonn-Cologne Graduate School of Physics and Astronomy.

MAGNETIC OSCILLATIONS IN TWO-DIMENSIONAL
DIRAC SYSTEMS

AND

SHEAR VISCOSITY AND SPIN DIFFUSION
IN A TWO-DIMENSIONAL FERMI GAS

Inaugural-Dissertation

zur

Erlangung des Doktorgrades

der Mathematisch-Naturwissenschaftlichen Fakultät

der Universität zu Köln

vorgelegt von

CAROLIN SARAH KÜPPERSBUSCH

aus Essen

2015

Berichterstatter: Prof. Dr. Cristiane de Morais Smith

Prof. Dr. Achim Rosch

Tag der letzten mündlichen Prüfung: 28.10.2015

PUBLICATIONS

This thesis is partly based on the following publication:

- Tilman Enss, Carolin Küppersbusch and Lars Fritz, "*Shear viscosity and spin diffusion in a two-dimensional Fermi gas*", *Phys. Rev. A* **86**, 013617 (2012)

ABSTRACT

In the first part of this thesis I derive a full quantitative formula which describes the amplitude and frequency of magnetic oscillations in two-dimensional Dirac systems. The investigations are on the basis of graphene, but they generally also hold for other two-dimensional Dirac systems. Starting from the Luttinger-Ward functional [1] I derive an expression for the oscillatory part of the grand potential of graphene in a magnetic field. The amplitude of this expression is usually called the Lifshitz-Kosevich (LK) formula. I perform the computation for the clean and the disordered system, and I study the effect of electron-electron interactions on the oscillations. I discuss my results by comparing them to the analogue expressions for the two-dimensional electron gas (2DEG) which have been derived in Ref. [2]. I find that, unlike in the 2DEG, a finite temperature and impurity scattering also affects the oscillation frequency. Further I find that in graphene, compared to the 2DEG, additional interaction induced damping effects occur: To two-loop order electron-electron interactions do lead to an additional damping factor in the amplitude of the LK-formula. Moreover the renormalization effects cannot fully be accounted for by renormalizations of the Fermi velocity but they also have to be described by field renormalizations.

The publication of the results of this part of the thesis is currently in progress.

In the second part of this thesis I investigate the temperature dependence of the shear viscosity and spin diffusion in a two-dimensional, two-component Fermi gas, as realized in ultracold atomic gases [3]. I implement a contact interaction that only acts between fermions in different hyperfine states. The transport coefficients are obtained within a kinetic approach. I solve the linearized Boltzmann equation by using a variational principle and present a full numerical solution for the degenerate gas. In contrast to previous works [4, 5] I take the medium effect due to finite density fully into account. This effect reduces the viscosity to particle density ratio, η/n , by a factor of four for strong interactions; and similarly for spin diffusion. The lowest value I obtain for the viscosity to entropy ratio is $\eta/s = 0.15 \frac{\hbar}{k_B}$, and it occurs close to the phase transition to the superfluid phase. This value is about twice the conjectured lower bound [6] of $\eta/s = \frac{1}{4\pi} \frac{\hbar}{k_B}$, computed using the AdS/CFT correspondence [7]. I compare my result for the shear viscosity to the measurements by Vogt *et al.* [3], who measured the damping rate of the quadrupole mode of a trapped Fermi gas confined to two dimensions. This damping rate is related to the shear viscosity of the gas and our numerical results agree well with the experiment.

The results of this part of the thesis are published in *Phys. Rev. A* **86**, 013617 (2012).

KURZZUSAMMENFASSUNG

Im ersten Teil der Arbeit leite ich einen Ausdruck her, der Amplitude und Frequenz magnetischer Oszillationen in zweidimensionalen Dirac Systemen quantitativ beschreibt. Die Herleitung ist auf Grundlage von Graphen, sie ist jedoch auch gültig für andere zweidimensionale Dirac Systeme. Mein Ausgangspunkt ist das Luttinger-Ward Funktional [1], von dem aus ich einen Ausdruck für den oszillierenden Teil des großkanonischen Potentials ableite. Die Amplitude dieses Ausdrucks wird allgemein als Lifshitz-Kosevich (LK) Formel bezeichnet. Zuerst führe ich meine Berechnungen für reines Graphen aus, anschließend implementiere ich Unordnung und untersuche den Effekt von Elektron-Elektron Wechselwirkungen auf die Oszillationen. Die Diskussion meiner Ergebnisse erfolgt anhand eines Vergleichs mit den analogen Ausdrücken für das zweidimensionale Elektronengas (2DEG), die in Ref. [2] hergeleitet wurden. Im Vergleich zum 2DEG beeinflussen eine endliche Temperatur und die Streuung an Störstellen in Graphen auch die Oszillationsfrequenz. Außerdem treten in Graphen zusätzliche, wechselwirkungsinduzierte Dämpfungseffekte auf: In zweiter Ordnung in der Wechselwirkung finde ich einen zusätzlichen Dämpfungsfaktor in der Amplitude der LK-Formel. Zudem können die auftretenden Renormierungseffekte nicht ausschließlich als Renormierung der Fermigeschwindigkeit beschrieben werden, sondern sie renormieren auch das Feld.

Im zweiten Teil der Arbeit untersuche ich die Temperaturabhängigkeit der Scherviskosität sowie der Spindiffusion eines zweidimensionalen, zweikomponentigen Fermigases, wie es in ultrakalten Gasen realisiert wurde [3]. Ich implementiere eine Kontaktwechselwirkung, die nur zwischen Fermionen in verschiedenen Hyperfeinzuständen wirkt. Ich berechne die Transportkoeffizienten innerhalb eines kinetischen Ansatzes: Ich löse die linearisierte Boltzmann Gleichung unter Anwendung des Variationsprinzips und präsentiere eine numerische Lösung. Im Gegensatz zu bisherigen Arbeiten [4, 5] berücksichtige ich die Effekte des Mediums, die bei einer endlichen Dichte auftreten. Dies reduziert das Verhältnis von Viskosität zu Teilchendichte um einen Faktor von etwa vier. Ein ähnlicher Effekt ist bei der Spindiffusion zu beobachten. Der kleinste Wert, den ich für das Verhältnis der Viskosität zur Entropiedichte erhalte, ist $\eta/s = 0.15 \frac{\hbar}{k_B}$ und tritt nahe des Phasenübergangs zum Suprafluid auf. Dieser Wert ist ungefähr doppelt so groß wie die mutmaßliche untere Grenze von $\eta/s = \frac{1}{4\pi} \frac{\hbar}{k_B}$ [6], die anhand der AdS/CFT-Korrespondenz berechnet wurde [7]. Ich vergleiche meine Ergebnisse für die Viskosität mit den Messungen von Vogt *et al.* [3]. In diesem Experiment wird die Dämpfungsrate der Quadrupolmode eines auf zwei Dimensionen beschränkten Fermigases gemessen. Diese Dämpfungsrate lässt sich mit der Viskosität des Gases in Beziehung setzen und meine numerischen Ergebnisse stimmen gut mit dem Experiment überein.

SAMENVATTING

In het eerste gedeelte van de dissertatie leidt ik een volledig kwantitatieve formule af die de amplitude en frequentie van magnetische oscillaties in tweedimensionale Diracsystemen beschrijft. Hoewel het onderzoek is gericht op grafeen, geldt de toegepaste aanpak voor tweedimensionale Diracsystemen in het algemeen. Beginnend met de Luttinger-Ward functionaal [1] leidt ik een uitdrukking af voor het oscillerende gedeelte van de groot-canoneke potentiaal in een magnetisch veld. De amplitude van deze uitdrukking wordt gewoonlijk de Lifshitz-Kosevich (LK) formule genoemd. Ik pas de berekening in het geval van schone- en wanordelijke-systemen toe, en bestudeer het effect van de elektron-elektron interacties op de oscillaties. Ik controleer de overeenkomst van mijn resultaten met vergelijkbare uitdrukkingen voor het tweedimensionale Fermigas (2DEG) zoals berekend in Ref. [2]. In tegenstelling tot het 2DEG concludeer ik dat een eindige temperatuurs- en onzuiverheidsverstrooiing de frequentie van oscillatie beïnvloedt. Tevens bereken ik dat er in grafeen, afgezet tegen het 2DEG, extra door interacties geïnduceerde dempingseffecten optreden: Tot op de tweede lus-orde elektron-elektron interacties leidt dit tot een extra dempingsfactor in de amplitude van de LK formule. Bovendien kunnen de renormalisatie-effecten niet volledig door de renormalisatie van de Fermisnelheid verklaard worden. Om dit wel te kunnen verklaren, zullen veldenrenormalisaties ook meegenomen moeten worden.

In het tweede gedeelte van de dissertatie beschouw ik de temperatuursafhankelijkheid van de schuifviscositeit en spindiffusie in een tweedimensionaal Fermigas met twee componenten, gerealiseerd in een ultrakoud atomisch gas [3]. Ik pas een contactsinteractie toe die alleen werkt tussen fermionen in verschillende hyperfijn toestanden. De transportcoëfficiënten worden berekend via een kinetische aanpak. De gelineariseerde Boltzmannvergelijking wordt opgelost door middel van variatierekening. Ik presenteer de volledige numerieke resultaten voor het ontaarde gas. In tegenstelling tot eerder werk [4, 5] neem ik tevens het effect van de eindige dichtheid van het medium volledig mee. Dit effect reduceert de verhouding van de viscositeit tot de deeltjesdichtheid, η/n , met een factor vier in het geval van sterke interacties; hetzelfde geldt voor de spindiffusie. De laagste waarde die ik verkrijg voor de verhouding van de viscositeit tot de entropiedichtheid is $\eta/s = 0.15 \frac{\hbar}{k_B}$. Dit resultaat wordt verkregen dichtbij de faseovergang naar een superfluïde fase. Deze waarde is tweemaal de voorspelde minimale waarde van $\eta/s = \frac{1}{4\pi} \frac{\hbar}{k_B}$ [6] berekend door middel van de AdS/CFT correspondentie [7]. Mijn resultaten voor de schuifviscositeit vergelijk ik met metingen van Vogt *et al.* [3], welke de demping van een quadrupool van een tot twee dimensies beperkt Fermigas bestuderen. De mate van demping is gerelateerd aan de schuifviscositeit van het gas. De numerieke resultaten komen goed overeen met de resultaten van dit experiment.

CONTENTS

I	DE HAAS - VAN ALPHEN OSCILLATIONS IN GRAPHENE	1
1	MOTIVATION	3
2	GRAPHENE	5
2.1	Electronic properties of graphene	6
2.1.1	The tight binding model	6
2.1.2	The Dirac equation	9
2.2	The two-dimensional electron gas in a magnetic field	10
2.3	Graphene in a magnetic field	11
3	INTRODUCTION TO THE DE HAAS - VAN ALPHEN OSCILLATIONS	15
3.1	Semiclassical approach to the origin of the magnetic oscillations	16
4	THE LIFSHITZ-KOSEVICH FORMULA IN THE NON-INTERACTING SYSTEM	19
4.1	The Lifshitz-Kosevich formula for the two-dimensional electron gas	21
4.1.1	Effects of amplitude damping	22
4.2	The Lifshitz-Kosevich formula in clean graphene	23
4.2.1	The LK-formula in the Fermi liquid regime	25
4.2.2	The LK-formula near the Dirac point	25
4.3	The effect of disorder on the dHvA-oscillations	25
4.3.1	The self-energy within the self-consistent Born approximation	26
4.3.2	The Lifshitz-Kosevich formula with disorder	28
5	THE EFFECT OF ELECTRON-ELECTRON INTERACTIONS ON THE DHVA-OSCILLATIONS	31
5.1	The effect of electron-electron interactions in the 2DEG	31
5.1.1	The Fermi liquid self-energy for generic interactions.	33
5.2	The effect of electron-electron interactions in graphene	34
5.2.1	The interaction induced self-energy for graphene	36
6	DISCUSSION AND SUMMARY	43
6.1	Comparison of the dHvA-oscillations: graphene vs. 2DEG	43
6.1.1	Energy scales	43
6.1.2	The Lifshitz-Kosevich formula in a clean system	44
6.1.3	The Lifshitz-Kosevich formula in a disordered system	44
6.1.4	The effect of electron-electron interactions on the Lifshitz-Kosevich formula	45
6.2	Application of the Lifshitz-Kosevich formula	46
6.3	Outlook	47
A	APPENDIX	49
A.1	Computation of the oscillatory part of the self-energy due to disorder	49
A.2	The grand potential for disordered graphene in a magnetic field	51

II	SHEAR VISCOSITY AND SPIN DIFFUSION IN A TWO-DIMENSIONAL FERMION GAS	55
7	MOTIVATION	57
8	INTRODUCTION TO ULTRACOLD ATOMS	59
8.1	Scattering	59
8.2	Feshbach resonances	60
9	THE TRANSPORT COEFFICIENTS	61
9.1	Shear viscosity	61
9.2	Spin diffusion	63
10	SCATTERING IN TWO DIMENSIONS	65
10.1	The model	65
10.2	The scattering matrix	65
10.2.1	The two-body scattering matrix in the vacuum	65
10.2.2	The two-body scattering matrix in the medium	68
11	THE BOLTZMANN FORMALISM	71
11.1	Introduction to the Boltzmann formalism	71
11.2	The Boltzmann equation in linear response	72
11.2.1	The driving term	72
11.2.2	The collision integral	73
11.3	The variational approach	74
12	COMPUTATION OF THE TRANSPORT COEFFICIENTS	77
12.1	The shear viscosity within linear response	77
12.2	The spin diffusion coefficient within linear response	78
13	RESULTS	81
13.1	Thermodynamic quantities	81
13.2	Transport coefficients of the classical gas.	82
13.3	Numerical results for the transport coefficients	82
13.4	Relation to other theoretical work	84
13.4.1	Shear viscosity	84
13.4.2	Spin diffusion	85
13.5	Comparison to experiment	85
13.6	Conclusion and Outlook	89
B	APPENDIX	91
B.1	The many-body scattering matrix	91
B.2	Proof: maximizing $Q[\chi^{ij}]$ leads to the Boltzmann equation	92
	BIBLIOGRAPHY	97
	STATEMENT OF AUTHORSHIP / SELBSTSTÄNDIGKEITSERKLÄRUNG	101

LIST OF FIGURES

Figure 1	The honeycomb lattice	5
Figure 2	Honeycomb lattice with labeling	7
Figure 3	Reciprocal lattice of the honeycomb lattice	7
Figure 4	Bandstructure of graphene	8
Figure 5	Dirac cone	9
Figure 6	Measured dHvA-oscillations in single crystal bismuth	15
Figure 7	Landau tubes	17
Figure 8	k -states on Landau tubes	18
Figure 9	Poisson summation formula	20
Figure 10	Broadening of Landau levels	22
Figure 11	Integration path	25
Figure 12	Dirac cone reshaped by electron-electron interactions .	46
Figure 13	Feshbach resonance	60
Figure 14	Diverging scattering length a at a Feshbach resonance .	60
Figure 15	The shear viscosity	61
Figure 16	Ladder approximation for the scattering matrix	69
Figure 17	The computed transport coefficients vs. temperature .	84
Figure 18	Viscosity to entropy ratio η/s vs. temperature	85
Figure 19	Experimental quadrupole damping rate	89

LIST OF TABLES

Table 1	Energy scales	44
Table 2	The LK-formula in a clean system	44
Table 3	The LK-formula in a disordered system	45
Table 4	The LK-formula with electron-electron interactions . .	45

Part I

DE HAAS - VAN ALPHEN OSCILLATIONS IN
GRAPHENE

MOTIVATION

Electron-electron interactions in condensed matter systems have been subject to ample astonishment throughout the history of research on solid state systems. An important breakthrough was the Fermi liquid theory developed by Landau in 1957-59 [8]. It explains why a system of strongly interacting particles can be described by a system of non-interacting quasiparticles, which allows for simple theoretical models to describe phenomena in condensed matter system.

However, in Dirac systems, the Fermi liquid theory is not straightforwardly applicable. [9] It has been shown that graphene can be described by a marginal Fermi liquid. [10] And as the screening length diverges at the Dirac point, electron-electron interactions are expected to play a significant role.

In general there exist two different predictions on the effect of Coulomb-interactions in graphene. Assuming a weak coupling, electron-electron interactions are assumed to renormalize the Fermi velocity according to $v_F \rightarrow v_F \ln \frac{\Lambda}{k}$, where k is the momentum and Λ is a high-energy cutoff. [11, 12, 13] At strong couplings one expects the system to undergo a phase transition at low temperatures towards an excitonic insulator. [14] It is not yet ascertained if graphene is in the weak or the strong coupled regime. A Quantum Monte-Carlo simulation as well as experiments suggest that couplings are not strong enough for the insulating phase to occur. [15, 12]

There are only very few experiments which allow to deduce information about the electron-electron interactions in a system. A standard experiment is the measurement of magnetic oscillations. Generally they are described by the Lifshitz-Kosevich (LK) formula. [16] As electron-electron interactions affect the oscillation amplitude, one can extract their strength by fitting the LK-formula to the measured amplitude. [12, 16] However, in the Fermi liquid regime, the amplitude of the LK-formula does not contain an additional damping factor due to electron-electron interactions, but instead electron-electron interactions only affect the oscillations by renormalizing the cyclotron frequency. [2, 17]

Since graphene near the charge neutrality point is not a Fermi liquid [9, 10], it is questionable if this Fermi liquid result also holds for graphene. Yet, there are experiments reported where the Fermi liquid LK-formula was used to extract interaction effects from the damping of the amplitude of magnetic oscillations. [12]

GRAPHENE

Graphene is a two-dimensional system of carbon atoms arranged on a hexagonal lattice, the so called honeycomb lattice, see Figure 1. It is thus a single-atom thick sheet of graphite. This strictly two-dimensional crystal was discovered to be stable by the groups of Konstantin Novoselov and Andre Geim at the University of Manchester in 2004. [18, 19] They used a method called mechanical exfoliation to prepare thin films of graphite, including the monolayer. For this discovery they won the Nobel Prize in Physics in 2010.

Before this discovery it was thought that strictly two-dimensional systems would not be stable, according to the argument by Peierls and Landau [20, 21] that large thermal fluctuations should destroy the long-range crystal structure. Later, a theorem due to Mermin and Wagner stated that in one- and two-dimensional systems, a continuous symmetry cannot be broken. [22, 23] Consequently atoms in these systems cannot be arranged on a lattice which would break translational symmetry. Accordingly, the experimental finding of a stable graphene sheet were startling and groundbreaking.

A lot of debate has taken place about the reason why a stable graphene sheet can be produced. On the one hand there are doubts that the Mermin-Wagner theorem applies for finite graphene samples. [24] On the other hand, it has been found that a suspended graphene sample ripples in the third dimension [25], which suppresses the thermal fluctuations.

In this chapter we will review the electronic properties of graphene and the

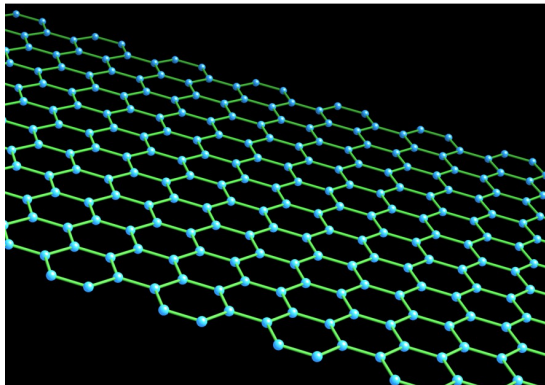


FIGURE 1: The honeycomb lattice of graphene. Image by Alan Stonebraker/APS [26].

behaviour of graphene in a magnetic field, assuming that it is perfectly flat. We will introduce the tight binding model for graphene from which the band structure can be obtained. Based on this we will discuss the low energy excitations, leading us to the Dirac theory. This effective low-energy theory will be used throughout this part of the thesis. Thereafter, we will address graphene

in a magnetic field. In this chapter we largely follow the review article by Castro neto *et al.* [27].

2.1 ELECTRONIC PROPERTIES OF GRAPHENE

Carbon is the element of atomic number six with electron configuration $1s^2 2s^2 2p^2$. In order to form a lattice structure the $2s$ -orbitals and the p_x - and p_y -orbitals of the carbon atoms hybridize and build three sp^2 hybrid orbitals. These three hybrid orbitals are located in one plane and form the maximal possible angle of 120° between each other. The p_z -orbital is perpendicular to the plane in which the hybrid orbitals are situated.

Three of the four valence electrons occupy the three sp^2 hybrid orbitals and form σ -bonds in all three directions with the electrons in hybrid orbital of adjacent carbon atoms. An image of the resulting hexagon structure is shown in Figure 1. The fourth electron is located in the p_z -orbital and forms a π -bond with the electrons of the p_z -orbitals of the adjacent carbon atoms. Hence the π -band, which is constituted in this way, is half filled and responsible for the electronic properties of graphene.

2.1.1 The tight binding model

Within the tight binding approach the mobile p_z electrons are considered to be located at the lattice sites. However they can hop to another lattice site. As the hopping amplitude depends on the overlap of the wave functions of the atoms on the lattice sites in most cases it is sufficient to consider only nearest neighbour hopping. In graphene, the hopping energy t (the tunneling matrix element) for nearest neighbour hopping is $t \approx 3 \text{ eV}$ [27], while the energy t' for next nearest neighbour hopping is much smaller, $t' \approx 0.3 \text{ eV}$ [28].

The honeycomb lattice can be seen as a triangular lattice with a bi-atomic unit cell and lattice vectors \mathbf{a}_1 and \mathbf{a}_2 , see Figure 2. The inter atomic distance of the graphene lattice is $a \approx 1.42 \text{ \AA}$. All three nearest neighbours of an atom of sublattice A (B) are located on sublattice B (A) and connected via the vectors

$$\delta_1 = (0, a), \quad \delta_2 = -\frac{a}{2}(\sqrt{3}, 1), \quad \delta_3 = \frac{a}{2}(\sqrt{3}, -1). \quad (1)$$

The nearest-neighbour tight-binding Hamiltonian, neglecting interactions, reads

$$\hat{H} = -t \sum_{\mathbf{r}} \sum_{i=1}^3 (a_{\sigma}^{\dagger}(\mathbf{r}) b_{\sigma}(\mathbf{r} + \delta_i) + h.c.), \quad (2)$$

where $a_{\sigma}(\mathbf{r})$ ($a_{\sigma}^{\dagger}(\mathbf{r})$) and $b_{\sigma}(\mathbf{r} + \delta_i)$ ($b_{\sigma}^{\dagger}(\mathbf{r} + \delta_i)$) annihilates (creates) an electron of spin σ on site \mathbf{r}_i of sublattice A and site $\mathbf{r} + \delta_i$ of sublattice B, respectively. In order to find the energy-momentum relation of the charge

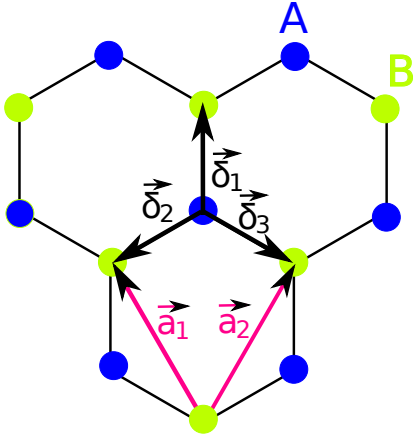


FIGURE 2: The honeycomb lattice of graphene. The vectors \mathbf{a}_1 and \mathbf{a}_2 are the lattice vectors of the triangular sublattices A and B.

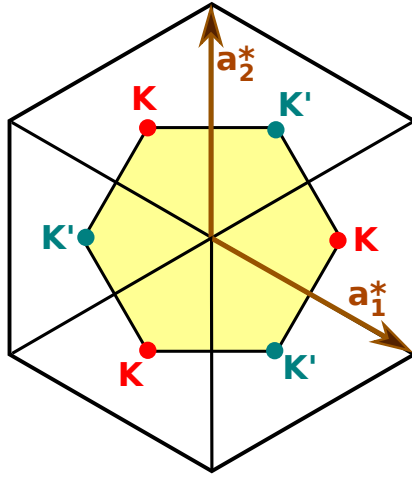


FIGURE 3: The reciprocal lattice of the honeycomb lattice with reciprocal lattice vectors \mathbf{a}_1^* and \mathbf{a}_2^* . The shaded area inside represents the first Brillouin zone.

carriers one needs to perform a Fourier transformation of the operators, $a_\sigma(\mathbf{r}) = \sum_{\mathbf{k}} a_{\sigma,\mathbf{k}} e^{i\mathbf{k}\mathbf{r}}$. The Hamiltonian in k -space reads

$$\begin{aligned} \hat{H} &= -t \sum_{i=1}^3 \sum_{\mathbf{k}} (e^{i\mathbf{k}\delta_i} a_{\sigma,\mathbf{k}}^\dagger b_{\sigma,\mathbf{k}} + h.c.) \\ &= \sum_{\mathbf{k}} \begin{pmatrix} a_{\sigma,\mathbf{k}}^\dagger & b_{\sigma,\mathbf{k}}^\dagger \end{pmatrix} \begin{pmatrix} 0 & -tf(\mathbf{k}) \\ -tf^*(\mathbf{k}) & 0 \end{pmatrix} \begin{pmatrix} a_{\sigma,\mathbf{k}} \\ b_{\sigma,\mathbf{k}} \end{pmatrix} \end{aligned} \quad (3)$$

with

$$f(\mathbf{k}) = e^{i\frac{a}{2}k_x} 2 \cos\left(k_y \frac{a\sqrt{3}}{2}\right) + e^{-iak_x}. \quad (4)$$

The energy eigenstates $E(\mathbf{k})$ of this Hamiltonian are

$$E_{\pm}(\mathbf{k}) = \pm t \sqrt{3 + 2 \cos(\sqrt{3}k_y a) + 4 \cos\left(\frac{\sqrt{3}}{2}k_y a\right) \cos\left(\frac{3}{2}k_x a\right)}. \quad (5)$$

This dispersion is plotted in Figure 4. It consists of two bands, the lower π -band and the upper π^* -band, each of which contains the same number of states. In six points at the corners of the Brillouin zone the two energy bands touch. Only two of these so called Dirac points are inequivalent as they cannot be connected by a reciprocal lattice vector. These inequivalent K and K' points are called 'valleys'.

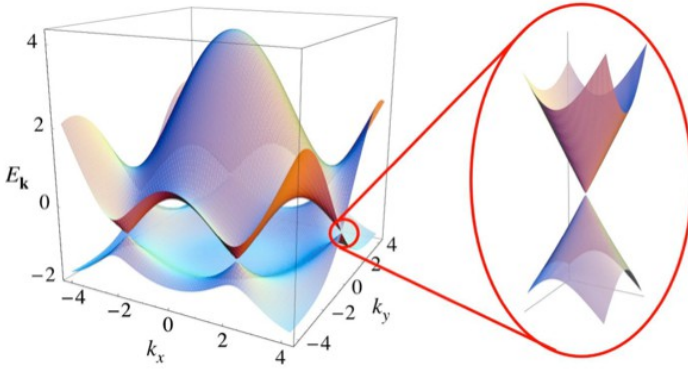


FIGURE 4: Bandstructure of graphene. In the six K-points of the Brillouin zone, shown in Figure 3, the two energy bands touch. The zoom in on the right shows the cone-shaped bandstructure in the vicinity of one of the Dirac points. Figure extracted from Ref. [27].

When expanding the dispersion around a Dirac point, the resulting energy-momentum relation is linear,

$$E_{\pm}(\mathbf{q}) \approx \pm \hbar v_F |\mathbf{q}| + \mathcal{O}\left\{\left(\frac{q}{K}\right)^2\right\}, \quad (6)$$

where \mathbf{q} is the momentum relative to the momentum \mathbf{K} of one Dirac point, $\mathbf{k} = \mathbf{K} + \mathbf{q}$, and v_F is the Fermi velocity defined by $v_F = \frac{3}{2\hbar} ta \approx 10^6 \frac{\text{m}}{\text{s}}$. Hence the energy-momentum relation near the Dirac points is rotationally-symmetric and cone-shaped, which is emphasized in Figure 4, with v_F being the slope of the cone. This bandstructure is also called the Dirac cone, which is plotted in Figure 5.

Since each carbon atom contributes one π -electron, which can occupy either a spin-up or a spin-down state, we have twice as many states as π -electrons. Hence in pristine graphene, the lower π -band, which is also called the valence band, is completely filled and the upper π^* -band, also called conduction band, is empty. Thus the chemical potential μ in pristine graphene crosses the Dirac points, meaning $\mu = 0$. In this sense, it is an ideal semi-metal. By doping the system, the chemical potential can be moved away from the Dirac point, $\mu > 0$ or $\mu < 0$. For chemical potential much larger than the temperature, $\mu \gg T$, the conoidal band structure is not striking and the system resembles a Fermi liquid. However, for chemical potentials near the Dirac point, meaning $\mu \ll T$, the cone-shaped dispersion plays an important role and the description as a pure Fermi liquid becomes questionable once interactions are taken into account. This relation of scales is sketched in Fig-

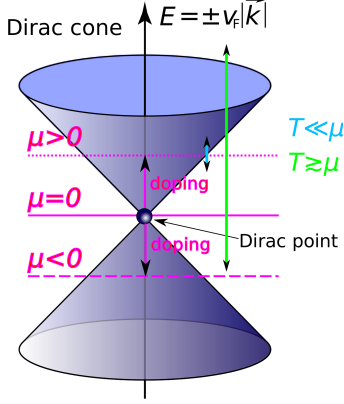


FIGURE 5: Excitations in the Dirac cone: If the temperature T is much smaller than the chemical potential μ , only states in the vicinity of the chemical potential are accessible. In this small energy range the system can be described as a Fermi liquid. This is illustrated by the blue arrow. Whereas for high temperatures also the other band becomes accessible, depicted by the green arrow, and the cone-shaped dispersion must be taken into account.

ure 5.

2.1.2 The Dirac equation

In the previous section we saw that near the Dirac points, the dispersion relation of graphene is linear. To describe the system in the vicinity of the Dirac points, we expand the Hamiltonian (3) around $\mathbf{K} = (\frac{4\pi}{3\sqrt{3}a}, 0)$ and $\mathbf{K}' = (-\frac{4\pi}{3\sqrt{3}a}, 0)$ and approximate the fermionic operators as a sum of two new operators

$$a_{\sigma}(\mathbf{r}) \approx e^{-i\mathbf{K}\mathbf{r}} a_{\mathbf{K}}(\mathbf{r}) + e^{-i\mathbf{K}'\mathbf{r}} a_{\mathbf{K}'}(\mathbf{r}) \quad (7)$$

$$b_{\sigma}(\mathbf{r}) \approx e^{-i\mathbf{K}\mathbf{r}} b_{\mathbf{K}}(\mathbf{r}) + e^{-i\mathbf{K}'\mathbf{r}} b_{\mathbf{K}'}(\mathbf{r}). \quad (8)$$

After Fourier transforming the new fields, the Hamilton operator reads

$$\begin{aligned} \hat{H} \approx \sum_{i=1}^3 \sum_{\mathbf{k}} e^{i\delta_i \mathbf{k}} & (a_{\mathbf{K}}^{\dagger}(\mathbf{k} - \mathbf{K}) b_{\mathbf{K}}(\mathbf{k} - \mathbf{K}) + a_{\mathbf{K}}^{\dagger}(\mathbf{k} - \mathbf{K}) b_{\mathbf{K}'}(\mathbf{k} - \mathbf{K}')) \\ & + a_{\mathbf{K}'}^{\dagger}(\mathbf{k} - \mathbf{K}') b_{\mathbf{K}}(\mathbf{k} - \mathbf{K}) + a_{\mathbf{K}'}^{\dagger}(\mathbf{k} - \mathbf{K}') b_{\mathbf{K}'}(\mathbf{k} - \mathbf{K}')). \end{aligned} \quad (9)$$

Since we want to develop a theory for low energy excitations, we neglect terms that couple electrons at the \mathbf{K} and the \mathbf{K}' -points. These terms only contribute at higher energies. Thereupon the Hamiltonian decouples into a Hamiltonian $H^{\mathbf{K}}$ and $H^{\mathbf{K}'}$, which describes the system at the \mathbf{K} -point and the \mathbf{K}' -point, respectively,

$$\hat{H}^{\mathbf{K}} = \sum_{i=1}^3 \sum_{\mathbf{k}} e^{i\delta_i \mathbf{k}} a_{\mathbf{K}}^{\dagger}(\mathbf{k} - \mathbf{K}) b_{\mathbf{K}}(\mathbf{k} - \mathbf{K}) + h.c. \quad (10)$$

$$\hat{H}^{\mathbf{K}'} = \sum_{i=1}^3 \sum_{\mathbf{k}} e^{i\delta_i \mathbf{k}} a_{\mathbf{K}'}^{\dagger}(\mathbf{k} - \mathbf{K}') b_{\mathbf{K}'}(\mathbf{k} - \mathbf{K}') + h.c. \quad (11)$$

We write $\mathbf{k} = \mathbf{K} + \mathbf{q}$ and expand to linear order in \mathbf{q} , i.e. we write $e^{i\mathbf{k}\delta_i} = e^{i(\mathbf{K}+\mathbf{q})\delta_i} \approx e^{i\mathbf{K}\delta_i} + i\mathbf{q}\delta_i e^{i\mathbf{K}\delta_i}$ and the Hamiltonian reads,

$$\begin{aligned} \hat{H}^K &= \frac{3}{2}at \sum_{\mathbf{q}} \left(a_K^\dagger(\mathbf{q}) b_K^\dagger(\mathbf{q}) \right) \begin{pmatrix} 0 & q_x - iq_y \\ q_x + iq_y & 0 \end{pmatrix} \begin{pmatrix} a_K(\mathbf{q}) \\ b_K(\mathbf{q}) \end{pmatrix} \\ &= \hbar v_F \sum_{\mathbf{q}} \left(a_K^\dagger(\mathbf{q}) b_K^\dagger(\mathbf{q}) \right) \hat{\sigma} \mathbf{q} \begin{pmatrix} a_K(\mathbf{q}) \\ b_K(\mathbf{q}) \end{pmatrix}, \end{aligned} \quad (12)$$

$$\begin{aligned} \hat{H}^{K'} &= \frac{3}{2}at \sum_{\mathbf{q}} \left(a_{K'}^\dagger(\mathbf{q}) b_{K'}^\dagger(\mathbf{q}) \right) \begin{pmatrix} 0 & q_x + iq_y \\ q_x - iq_y & 0 \end{pmatrix} \begin{pmatrix} a_{K'}(\mathbf{q}) \\ b_{K'}(\mathbf{q}) \end{pmatrix} \\ &= \hbar v_F \sum_{\mathbf{q}} \left(a_{K'}^\dagger(\mathbf{q}) b_{K'}^\dagger(\mathbf{q}) \right) \hat{\sigma}^* \mathbf{q} \begin{pmatrix} a_{K'}(\mathbf{q}) \\ b_{K'}(\mathbf{q}) \end{pmatrix}. \end{aligned} \quad (13)$$

Here, $\hat{\sigma} = (\hat{\sigma}_x, \hat{\sigma}_y)$ is the vector of Pauli matrices and $\hat{\sigma}^* = (\hat{\sigma}_x, -\hat{\sigma}_y)$ is its complex conjugate. We now see that the electron wave function $\psi(\mathbf{r})$ near the Dirac points obeys the two-dimensional Dirac equation

$$-i\hbar v_F \hat{\sigma} \nabla \psi_K(\mathbf{r}) = E \psi_K(\mathbf{r}) \quad \text{at the } K\text{-point, and} \quad (14)$$

$$-i\hbar v_F \hat{\sigma}^* \nabla \psi_{K'}(\mathbf{r}) = E \psi_{K'}(\mathbf{r}) \quad \text{at the } K'\text{-point.} \quad (15)$$

For this reason the quasiparticles in graphene are also called massless Dirac fermions.

2.2 THE TWO-DIMENSIONAL ELECTRON GAS IN A MAGNETIC FIELD

In order to be able to compare our results for graphene to the analogue expressions for the two-dimensional electron gas (2DEG) we will first discuss the energy spectrum of the 2DEG in a magnetic field before we turn to graphene. Thereby we follow the book by Landau and Lifshitz [29].

We consider a two-dimensional system of non-interacting electrons with a parabolic dispersion in the x - y -plane which is exposed to a perpendicular magnetic field, i.e. $\mathbf{B} = B\hat{e}_z$. The Hamilton operator of such a system is given by

$$\hat{H} = \frac{1}{2m} (\hat{p} - e\hat{A})^2, \quad (16)$$

where m is the electron mass, e the electron charge and \mathbf{A} is the magnetic vector potential defined by $\mathbf{B} = \nabla \times \mathbf{A}$. Within Landau gauge, i.e. $\mathbf{A} = \begin{pmatrix} -By \\ 0 \end{pmatrix}$, the Hamiltonian reads

$$\hat{H} = \frac{p_y^2}{2m} + \frac{1}{2} m \omega_c^2 \left(y + \frac{p_x}{eB} \right)^2, \quad (17)$$

where we have defined a cyclotron frequency

$$\omega_c = \frac{eB}{m}. \quad (18)$$

This Hamiltonian has the form of that of the harmonic oscillator with the minimum of the potential shifted by $\frac{p_x}{eB}$. Thus the energy levels of this system are those of the harmonic oscillator, namely

$$E_n = \hbar\omega_c \left(n + \frac{1}{2} \right) \quad (19)$$

with n being a non-negative integer. The magnetic field therefore leads to a quantization of energy. These degenerate quantized energy levels are called Landau levels.

2.3 GRAPHENE IN A MAGNETIC FIELD

In this section we restrict ourselves to low energies near the Dirac point such that the system is well described by the Dirac equation (14). All calculations in this section are performed for excitations near the K -point. The physics near the K' -point can be obtained in an analogue way.

In order to account for the magnetic field we assume a minimal coupling and the Dirac equation reads,

$$\hbar v_F [\hat{\sigma}(-i\nabla + e\mathbf{A})] \psi^K(\mathbf{r}) = E \psi^K(\mathbf{r}). \quad (20)$$

Using Landau gauge the solution of this equation has the generic form $\psi^K(\mathbf{r}) = \Phi^K(y) e^{ikx}$. With this ansatz the Dirac equation reads

$$\hbar v_F \begin{pmatrix} 0 & \partial_y - k + \frac{Bey}{c} \\ -\partial_y - k + \frac{Bey}{c} & 0 \end{pmatrix} \Phi^K(y) = E \Phi^K(y). \quad (21)$$

It is convenient to introduce the dimensionless variable $\xi = \frac{y}{l_B} - l_B k_x$ where $l_B = \sqrt{\frac{\hbar}{eB}}$ is the magnetic length. now the eigenvalue equation reads

$$\hbar\omega_c \begin{pmatrix} 0 & \frac{1}{\sqrt{2}}(\partial_\xi + \xi) \\ \frac{1}{\sqrt{2}}(-\partial_\xi + \xi) & 0 \end{pmatrix} \Phi^K(\xi) = E \Phi^K(\xi) \quad (22)$$

with the cyclotron frequency

$$\omega_c = \sqrt{2} \frac{v_F}{l_B} = v_F \sqrt{\frac{2eB}{\hbar}}. \quad (23)$$

The eigenstates of this matrix equation are spinors

$$\Phi_n^K(\xi) = \begin{pmatrix} \psi_{n-1}(\xi) \\ \pm \psi_n(\xi) \end{pmatrix} \quad (24)$$

where the first entry refers to sublattice A and the second entry to sublattice B. $\psi_n(\xi)$ are the solutions of the one-dimensional harmonic oscillator, with n being a positive integer. The eigenstates of the analogue matrix for the K' -point are given by

$$\Phi_n^{K'}(\xi) = \begin{pmatrix} \pm \psi_n(\xi) \\ \psi_{n-1}(\xi) \end{pmatrix}. \quad (25)$$

The many-body Hamiltonian of graphene in a perpendicular magnetic field is thus given by

$$\hat{H}^K = \int dy(\xi) \sum_{k_x} \Psi_{k_x}^\dagger(\xi) \hbar\omega_c \begin{pmatrix} 0 & \frac{1}{\sqrt{2}}(\partial_\xi + \xi) \\ \frac{1}{\sqrt{2}}(-\partial_\xi + \xi) & 0 \end{pmatrix} \Psi_{k_x}(\xi). \quad (26)$$

Since the translation symmetry in y -direction is broken by the Landau gauge and thus k_y is not a good quantum number we keep the integration over the y -coordinate while summing over the k_x coordinate in Fourier space. We write the wave functions as an expansion with respect to the Eigenfunctions (25) of the system.

$$\Psi_{k_x}(\xi) = \sum_n e^{ik_x x} \begin{pmatrix} a_{n,k_x} \psi_{n-1,k_x}(\xi) \\ b_{n,k_x} \psi_{n,k_x}(\xi) \end{pmatrix} \quad (27)$$

With this expansion the Hamiltonian reads

$$\begin{aligned} \hat{H}^K &= \hbar\omega_c l_B \int d\xi \sum_{k_x, n, n'} (a_{n,k_x}^\dagger \psi_{n-1,k_x}^*(\xi), b_{n,k_x}^\dagger \psi_{n,k_x}^*(\xi)) \\ &\times \begin{pmatrix} 0 & \frac{1}{\sqrt{2}}(\partial_\xi + \xi) \\ \frac{1}{\sqrt{2}}(-\partial_\xi + \xi) & 0 \end{pmatrix} \begin{pmatrix} a_{n',k_x} \psi_{n'-1,k_x}(\xi) \\ b_{n',k_x} \psi_{n',k_x}(\xi) \end{pmatrix}. \end{aligned} \quad (28)$$

Using $\frac{1}{\sqrt{2}}(\partial_\xi + \xi)\psi_{n',k_x}(\xi) = \sqrt{n'}\psi_{n'-1,k_x}$ and $\frac{1}{\sqrt{2}}(-\partial_\xi + \xi)\psi_{n'-1,k_x}(\xi) = \sqrt{n'}\psi_{n',k_x}$ yields

$$\begin{aligned} \hat{H}^K &= \hbar\omega_c l_B \int d\xi \sum_{k_x, n, n'} (a_{n,k_x}^\dagger b_{n',k_x} \sqrt{n'} \psi_{n-1,k_x}^*(\xi) \psi_{n'-1,k_x}(\xi) \\ &\quad + b_{n,k_x}^\dagger a_{n',k_x} \sqrt{n'} \psi_{n,k_x}^*(\xi) \psi_{n',k_x}(\xi)). \end{aligned} \quad (29)$$

now we can perform the integral by using the normalized property of the wave functions $\int d\xi \psi_n^*(\xi) \psi_{n'}(\xi) = \frac{1}{l_B} \delta_{nn'}$ and the Hamiltonian becomes

$$\begin{aligned} \hat{H}^K &= \hbar\omega_c \sum_{k_x, n} (a_{n,k_x}^\dagger b_{n,k_x} \sqrt{n} + b_{n,k_x}^\dagger a_{n,k_x} \sqrt{n}) \\ &= \hbar\omega_c \sum_{k_x, n} (a_{n,k_x}^\dagger b_{n,k_x}^\dagger) \begin{pmatrix} 0 & \sqrt{n} \\ \sqrt{n} & 0 \end{pmatrix} \begin{pmatrix} a_{n,k_x} \\ b_{n,k_x} \end{pmatrix}. \end{aligned} \quad (30)$$

The eigenvalues of this Hamiltonian are

$$E_\pm = \pm \hbar\omega_c \sqrt{n}. \quad (31)$$

Thus the Landau levels in graphene in a uniform magnetic field are not equally spaced as they are in a two-dimensional electron gas but they get closer with higher energy. As a consequence, phenomena which are negligible when the electrons in the system only occupy low Landau levels might

become important when also high Landau levels are occupied. Another peculiar feature is the existence of a Landau level with zero energy. It is responsible for the anomalous integer quantum hall effect without any Hall plateau at $n = 0$. From Eq. (25) one can see that the wave functions of the electrons and holes in this Landau level are fully localized in one of the sublattices of the honeycomb lattice: since ψ_{-1} is zero, the wavefunction at the K -point is localized in sublattice B and the wavefunction at the K' -point it is localized in sublattice A. In this way the magnetic field does not break inversion symmetry.

The Landau levels are degenerate according to (see Equation (43) and (23))

$$D = \frac{eBL^2}{\hbar\pi} = \frac{\omega_c^2 L^2}{2\pi v_F^2}, \quad (32)$$

where L is the size of the system.

INTRODUCTION TO THE DE HAAS - VAN ALPHEN OSCILLATIONS

In 1930 de Haas and van Alphen observed an oscillatory magnetic field dependence of the magnetization in single crystal bismuth at low temperatures. Later on this oscillatory behaviour of the magnetization was detected also in other systems, but the observation seemed to be confined to polyvalent metals, where more than one electron participates in a bond. In 1952 Onsager established a theory for the de Haas - van Alphen (dHvA) effect based on Landau quantization of the electron energy in an applied magnetic field. [30] According to his theory, the dHvA-frequency F which is the reciprocal of the period in $\frac{1}{B}$, with B being the magnetic field, is proportional to the extremal cross-section A of the Fermi surface. Moreover, the proportionality factor is a universal constant. The relation reads [16]

$$F = \frac{\hbar}{2\pi e} A, \quad (33)$$

with e being the electron charge. Thus measuring the dHvA-oscillations can be used as a tool of detecting the Fermi surface of a system: by measuring the dHvA-frequency for different crystal orientation one gains the structure of the Fermi surface. Relation (33) also explains why it is easier to observe the oscillations in polyvalent metals. Systems with more than one bonding electron exhibit a Fermi surface which crosses Brillouin zone boundaries, producing 'pockets'. These pockets, with their small extremal cross-section, result in oscillations with a small frequency, which are easier to observe.

In this chapter we will use a semiclassical approach in order to explain the physics behind the magnetic oscillations. We will see that this oscillatory behaviour is due to the quantization of electron motion in a magnetic field. We thereby follow the books by Shoenberg [16] and Kittel [31].

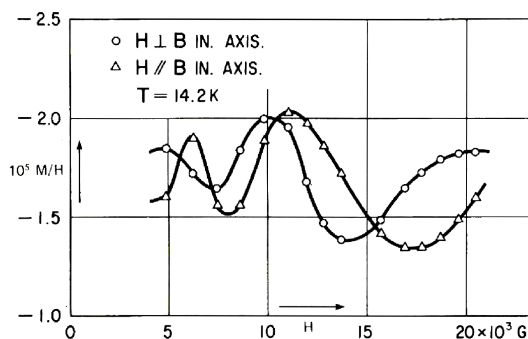


FIGURE 6: First observation of the oscillatory field dependence of the magnetization in single crystal bismuth (de Haas and van Alphen 1930) [16].

3.1 SEMICLASSICAL APPROACH TO THE ORIGIN OF THE MAGNETIC OSCILLATIONS

In a magnetic field \mathbf{B} an electron with charge e which moves with velocity \mathbf{v} is exposed to the Lorentz force \mathbf{F} according to

$$\mathbf{F} = -e(\mathbf{v} \times \mathbf{B}). \quad (34)$$

We now restrict ourselves to the situation of a magnetic field which is perpendicular to the velocity of the electron. In this case the electron motion due to the Lorentz force describes a circuit. Because of the closed orbit the wave function must fulfill a boundary condition. This results in the Bohr-Sommerfeld quantization rule for an electron in a magnetic field,

$$\oint \mathbf{p} d\mathbf{q} = (n + \gamma)2\pi\hbar, \quad (35)$$

where n is a non-negative integer and the integral over the electron momentum \mathbf{p} runs along the electron orbit described by the trajectory \mathbf{q} . The phase γ is exactly $\frac{1}{2}$ for a parabolic band and deviates slightly from $\frac{1}{2}$ for other Fermi liquids. This deviation depends on energy and magnetic field. In graphene, however, γ is zero. Within minimal coupling, the momentum \mathbf{p} of an electron in a magnetic field \mathbf{B} is

$$\mathbf{p} = \hbar\mathbf{k} - e\mathbf{A} \quad (36)$$

with \mathbf{A} being the magnetic vector potential. Using Stokes' theorem and the relation $\hbar\mathbf{k} = \mathbf{r} \times \mathbf{B}$ which follows from the definition of the Lorentz force we find

$$\begin{aligned} \oint \mathbf{p} d\mathbf{q} &= \oint \hbar\mathbf{k} d\mathbf{q} - e \oint \mathbf{A} d\mathbf{q} = -e \oint \mathbf{r} \times \mathbf{B} d\mathbf{q} - e \int_{S'} \nabla \times \mathbf{A} dS' \\ &= e\mathbf{B} \oint \mathbf{r} \times d\mathbf{q} - e \int_{S'} \mathbf{B} dS = eB2S - eBS \\ &= eBS = (n + \gamma)2\pi\hbar. \end{aligned} \quad (37)$$

The quantization rule for the closed electron orbit with area S follows as

$$S_n = (n + \gamma) \frac{2\pi\hbar}{eB}. \quad (38)$$

The quantization rule for the area a_n of the electron orbit in k -space reads

$$a_n = (n + \gamma) \frac{2\pi eB}{\hbar}. \quad (39)$$

This quantization rule is the so-called 'Onsager relation' [30]. Consequently the electrons move on so called Landau tubes in k -space whose cross-sectional area fulfill the quantization rule (39). For a spherical Fermi surface the Landau tubes are plotted in Figure 7. In terms of these quantized electron orbits one can understand the oscillatory behaviour of several physical quantities of a system in a varying magnetic field as follows: The electrons of a system

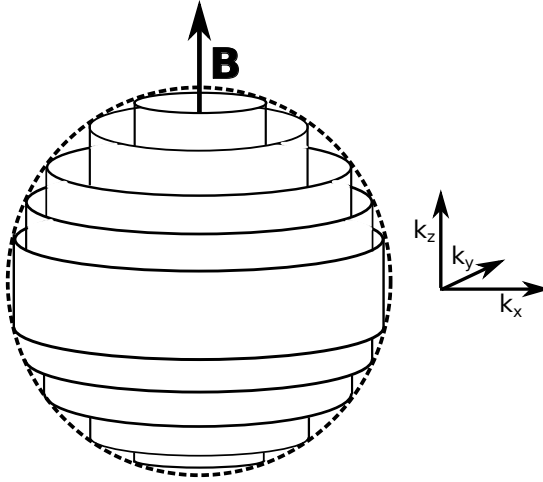


FIGURE 7: For a system with a spherical Fermi surface the Landau tubes are cylinders. The dashed line is the extremal cross-section of the Fermi surface. The cross-sectional area of the Landau tubes is given by the Onsager relation (39). Only the occupied part of the tubes is plotted which lies within the Fermi sphere.

occupy those Landau tubes which are located inside the Fermi surface. Let us assume that there is a large number of Landau tubes inside the Fermi surface, i.e. the magnetic field is sufficiently weak. When the magnetic field is increased, also the cross-section of the Landau tubes increases, see Eq. (39), and the occupied length of the Landau tubes decreases until the Landau tube separates from the Fermi surface. At this moment its occupation vanishes instantaneously. As these vanishings happen periodically the total energy of the system and all quantities which can be derived from it show a periodic behaviour. Equation (39) leads to the following relation for the magnetic field B_n at which the Landau tube n parts company with the Fermi surface,

$$\frac{1}{B_n} = (n + \gamma) \frac{2\pi e}{\hbar A}, \quad (40)$$

with A being the extremal cross-section of the Fermi surface. Thus the period of the oscillations is given by

$$\Delta \frac{1}{B} = \frac{1}{B_{n+1}} - \frac{1}{B_n} = \frac{2\pi e}{\hbar A} \quad (41)$$

and the frequency reads

$$F = \frac{\hbar A}{2\pi e}. \quad (42)$$

Due to the restriction of the electron location to orbits with quantized cross-section the Landau levels are degenerate. Per surface element there are $(\frac{2\pi}{L})^2$ allowed k -values. The area between two adjacent Landau tubes is according to Onsager's relation (39) $\Delta a = \frac{2\pi e B}{\hbar}$. Thus the degeneracy factor is

$$D = 2\Delta a \left(\frac{L}{2\pi} \right)^2 = \frac{eBL^2}{\hbar\pi}. \quad (43)$$

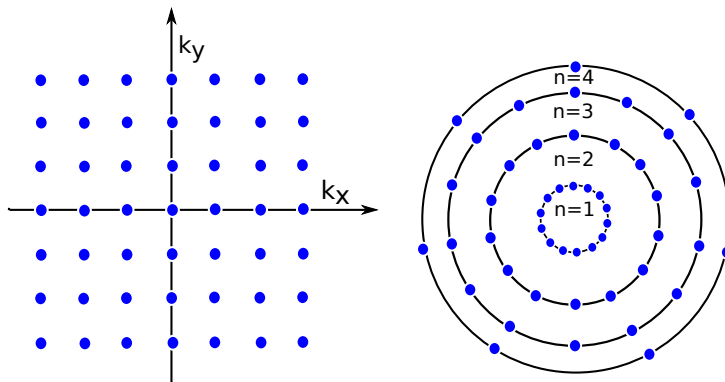


FIGURE 8: In an applied magnetic field, the k -states rearrange on the Landau tubes.

The factor of two stems from the spin. This degeneracy factor is independent of the dispersion and thus also graphene's Landau levels are degenerate according to Eq. (43), as referred to in Eq. (32).

THE LIFSHITZ-KOSEVICH FORMULA IN THE NON-INTERACTING SYSTEM

A full formula in order to describe quantitatively the magnetic oscillations was derived by Lifshitz and Kosevich already in 1954 [16]. This formula is an expression for the oscillatory part of the grand potential $\tilde{\Omega}_{osc}$ of a system in a magnetic field. Observables, such as the magnetization M or the specific heat c , can be derived from this expression via the corresponding derivatives,

$$\begin{aligned} M_{osc} &= \left(\frac{\partial \tilde{\Omega}_{osc}}{\partial B} \right)_{\mu} \\ c_{osc} &= -T \frac{\partial}{\partial T} \left(\frac{\partial \tilde{\Omega}_{osc}}{\partial T} \right)_B. \end{aligned} \quad (44)$$

In this chapter we will first outline the derivation of the Lifshitz-Kosevich (LK) formula for the two-dimensional electron gas (2DEG) as it has been performed by Adamov *et. al.* in [2]. (However, in this chapter we neglect electron-electron interactions.) On the basis of this result we will discuss the effects which lead to a damping of the oscillation amplitude. Thereafter we will compute the LK-formula for clean and disordered graphene. The effect of electron-electron interactions will be discussed in the following chapter. The results, in particular the differences between the LK-formula for the 2DEG and that for graphene, will be discussed in Chapter 6.

Our starting point is the Luttinger-Ward functional [1] which relates the thermodynamic potential Ω of the system to its Green function \hat{G} ,

$$\Omega = -T \operatorname{tr}\{\ln(-\hat{G}^{-1})\} - T \operatorname{tr}\{\hat{G}\hat{\Sigma}\} + \Omega'. \quad (45)$$

(From now on we will set the Boltzmann constant, $k_B \equiv 1$, as well as the Planck's constant, $\hbar \equiv 1$.) The trace implies summation over the Landau level index m , the fermionic Matsubara frequencies $\omega_n = \pi T(2n + 1)$, and the different degenerate states within one Landau level. The self-energy $\hat{\Sigma}$ accounts for disorder ($\hat{\Sigma}_{dis}$) or electron-electron interactions ($\hat{\Sigma}_{ee}$). T is the temperature. The terms $T \operatorname{tr}\{\hat{G}\hat{\Sigma}\}$ and Ω' are introduced to avoid overcounting of diagrams. Their oscillatory parts cancel each other [2] such that the magnetic oscillations are fully described by

$$\Omega_{mo} = -T \operatorname{tr}\{\ln(-\hat{G}^{-1})\} = -DT \sum_m \sum_{\omega_n} \ln(-g_m^{-1}(i\omega_n)). \quad (46)$$

In the last step we used the generic identity $\operatorname{tr}\{\ln\hat{G}\} = \sum_i \ln(g_{ii})$ which holds for any diagonalizable matrix \hat{G} with Eigenvalues g_{ii} . The factor D accounts for the sum over degenerate Landau levels, see Eq. (43). We use the Poisson

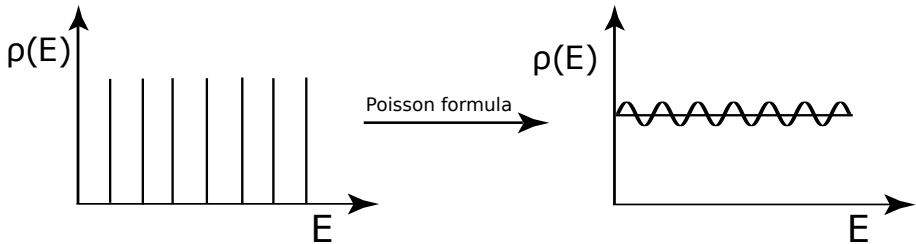


FIGURE 9: The transformation which is described by the Poisson summation formula: Instead of summing over discrete Landau levels one goes to a continuous picture with a constant density of states $\rho(E)$ which is modulated by a periodic function.

summation formula which relates the summation of a function to the function's continuous integral,

$$\begin{aligned} \sum_{m=0}^{\infty} f_m &= \lim_{\epsilon \rightarrow 0^+} \sum_{m=-\infty}^{\infty} \int_{-\epsilon}^{\infty} dx f(x) \delta(x-m) = \sum_{l=-\infty}^{\infty} \int_0^{\infty} dx f(x) e^{i2\pi l x} \\ &= \int_0^{\infty} dx f(x) + 2 \sum_{l=1}^{\infty} \int_0^{\infty} dx f(x) \cos(2\pi l x). \end{aligned} \quad (47)$$

Philosophically this transformation means that we go from discrete Landau levels to a continuous picture, where a constant density of states is modulated by oscillating modes, see Figure 9. This approach is appropriate when the Landau levels are sufficiently broadened due to e.g. disorder or temperature. In this case we obtain a small parameter, $\omega_c/\alpha_{\text{dis}}$ (α_{dis} is the disorder potential) and ω_c/T , respectively, such that the magnetic field can be treated perturbatively.

We neglect the first term as it only describes the $B = 0$ state, and insert the function defined in Eq. (46) into Eq. (47) and integrate by parts,

$$\begin{aligned} \Omega_{mo'} &= -2DT \sum_{\omega_n} \sum_{l=1}^{\infty} \int_{-\epsilon}^{\infty} dx \ln(-g^{-1}(x, i\omega_n)) \cos(2\pi l x) \\ &= -2DT \sum_{\omega_n} \sum_{l=1}^{\infty} \left[\ln[-g^{-1}(x, i\omega_n)] \frac{\sin(2\pi l x)}{2\pi l} \right]_0^{\infty} \\ &\quad + 2DT \sum_{\omega_n} \sum_{l=0}^{\infty} \int_0^{\infty} \frac{1}{-g^{-1}(x, i\omega_n)} \frac{d}{dx} \left(-g^{-1}(x, i\omega_n) \right) \frac{\sin(2\pi l x)}{2\pi l} dx. \end{aligned} \quad (48)$$

The first term is non-oscillatory and finite due to a cut-off in the Green function. The oscillatory part thus reads

$$\tilde{\Omega} = 2DT \sum_{\omega_n} \sum_{l=0}^{\infty} \int_0^{\infty} \frac{1}{-g^{-1}(x, i\omega_n)} \frac{d}{dx} \left(-g^{-1}(x, i\omega_n) \right) \frac{\sin(2\pi l x)}{2\pi l} dx. \quad (49)$$

4.1 THE LIFSHITZ-KOSEVICH FORMULA FOR THE TWO-DIMENSIONAL ELECTRON GAS

In this section we will compute the Lifshitz-Kosevich formula for the two-dimensional electron gas. Using the energy spectrum derived in Section 2.2 we can write down the Green function for the 2DEG in Landau level space,

$$\hat{G}_m(i\omega_n)^{-1} = (i\omega_n + \mu)\mathbb{1} - \hat{H} - \hat{\Sigma} = \left(i\omega_n + \mu - \omega_c \left(m + \frac{1}{2} \right) \right) \mathbb{1} - \hat{\Sigma}. \quad (50)$$

Here, we neglect interaction effects and consider white-noise disorder. That means that the impurities are randomly distributed in the system and that the disorder potentials $u(\mathbf{r})$ of the single impurities, located at \mathbf{r}_i , are not correlated, meaning [32]

$$\langle u(\mathbf{r}_i) \rangle = 0 \quad \text{and} \quad \langle u(\mathbf{r}_i)u(\mathbf{r}_j) \rangle = u_0^2 \delta_{ij}. \quad (51)$$

The strength of the scattering potential u_0 is related to the scattering time τ via

$$u_0^2 = \frac{1}{2\pi n_0 \tau}. \quad (52)$$

Here, n_0 is the free single-particle density of states. At weak magnetic fields, i.e. $\omega_c \tau \ll 1$, the self-energy can be computed in the k -basis and is given by [32]

$$\Sigma_{\text{dis}}(i\omega_n) = -\frac{i \text{sgn} \omega_n}{2\tau}. \quad (53)$$

The eigenvalues of the inverse Green function then follow as

$$g_m^{-1}(i\omega_n) = i\omega_n + \mu - \omega_c \left(m + \frac{1}{2} \right) + \frac{i \text{sgn} \omega_n}{2\tau} \quad (54)$$

and the oscillatory integral (49) reads

$$\tilde{\Omega} = \frac{\omega_c m L^2 T}{\pi^2} \sum_{\omega_n} \sum_{l=0}^{\infty} \frac{1}{l} \int_0^{\infty} \frac{\omega_c \sin(2\pi l x)}{-i\omega_n - \mu + \frac{1}{2}\omega_c + x\omega_c - \frac{i \text{sgn} \omega_n}{2\tau}} dx. \quad (55)$$

This integral can be solved using residue theorem and for $\mu > \frac{1}{2}\omega_c$ we get for the oscillatory part

$$\tilde{\Omega}_{\text{osc}} = 4\nu \omega_c T L^2 \sum_{l=1}^{\infty} \sum_{\omega_n > 0} \frac{(-1)^l}{l} e^{-\frac{2\pi l}{\omega_c} (\omega_n + \frac{1}{2})} \cos\left(\frac{2\pi l \mu}{\omega_c}\right), \quad (56)$$

with $\nu = \frac{m}{2\pi}$ being the density of states of the two-dimensional electron gas, where m is the electron mass. The sum over Matsubara frequencies $\omega_n = \pi T(2n+1)$ can be performed resulting in

$$\tilde{\Omega}_{\text{osc}} = 4\nu \omega_c T L^2 \sum_{l=1}^{\infty} \frac{(-1)^l}{l} \frac{1}{2 \sinh(\frac{2\pi^2 l T}{\omega_c})} e^{-\frac{\pi l}{\omega_c \tau}} \cos\left(\frac{2\pi l \mu}{\omega_c}\right). \quad (57)$$

4.1.1 Effects of amplitude damping

From Eq. (57) we see that there are two parameters that enter the amplitude and lead to a damping of the oscillations: a finite temperature T and a finite relaxation time τ . These damping effects are discussed qualitatively in the next two sections by following the book by Shoenberg [16].

4.1.1.1 Damping due to finite temperature

At finite temperature T the probability of occupation of a state with energy ϵ is given by the Fermi-Dirac distribution

$$f(\epsilon) = \frac{1}{1 + e^{\frac{\epsilon - \mu}{T}}} \quad (58)$$

where μ is the chemical potential. The following gedankenexperiment illustrates why this occupation distribution leads to a phase smearing, and thus to a damping of the oscillation amplitude. Let us assume that we have several copies i of our system at $T = 0$, but with different chemical potentials μ_i such that the μ_i are distributed according to the Fermi-Dirac distribution. Thus only the copies with $\mu > \epsilon$ are occupied. This situation is equivalent to a single system with occupation distribution (58). Since the frequency of the dHvA-oscillations depends on μ , the different copies are not phase-coherent, leading overall to a phase smearing. From Eq. (57) we can extract the reduction factor due to finite temperature,

$$R_T = \frac{T}{2 \sinh\left(\frac{2\pi^2 l T}{\omega_c}\right)}. \quad (59)$$

For high temperatures $2\pi^2 l T / \omega_c \geq 1$ this factor approaches

$$R_T \approx T e^{-2\pi^2 l T / \omega_c}. \quad (60)$$

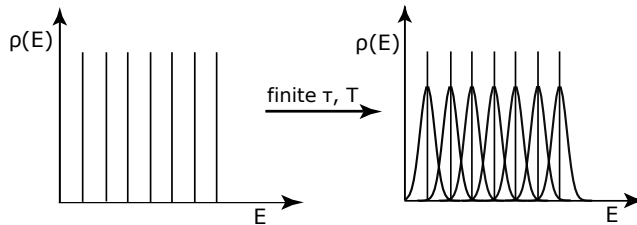


FIGURE 10: The density of states $\rho(E)$ versus the energy E for a system in a magnetic field. A finite relaxation time and/or a finite temperature broadens the otherwise sharp Landau levels.

4.1.1.2 Damping due to disorder

Impurity scattering leads to a finite relaxation time τ of the electrons. According to the uncertainty principle connecting time and energy this causes

a broadening of the otherwise sharp Landau levels. The levels broaden in a Lorentzian fashion. Thus the probability that a Landau level with energy ϵ_{LL} in the case of no level broadening effects lies between ϵ and $\epsilon + d\epsilon$ is given by

$$\frac{d\epsilon}{(\epsilon - \epsilon_{LL})^2 + (1/2\tau)^2}. \quad (61)$$

If it is reasonable to assume that the relaxation time τ is independent of the electron energy, the effect of this level broadening is similar to the case of finite temperature, but this time with a Lorentzian broadening,

$$\frac{d\mu}{(\mu - \xi)^2 + (1/2\tau)^2}. \quad (62)$$

This again leads to a phase smearing and thus to a damping of the amplitude. The reduction factor due to a finite relaxation time, first introduced by Herbert Dingle [16] and also called the 'Dingle factor', reads

$$R_D = e^{-\frac{\pi l}{\omega_c \tau}}. \quad (63)$$

If one introduces

$$x = \frac{1}{2\pi\tau} \quad (64)$$

the Dingle factor becomes

$$R_D = e^{-\frac{2\pi^2 l x}{\omega_c}}. \quad (65)$$

Comparing this Dingle factor to the temperature induced damping factor (60) suggests to identify x with a temperature. Hence x is the so called Dingle temperature.

4.2 THE LIFSHITZ-KOSEVICH FORMULA IN CLEAN GRAPHENE

Now we will derive the Lifshitz Kosevich formula for clean graphene. The inverse Green function of the clean, non-interacting system is given by

$$\hat{G}_0^{-1}(\omega_n) = (i\omega_n - \mu)\mathbb{1} - \hat{H} \quad (66)$$

where $\omega_n = (2n + 1)\pi T$ is the fermionic Matsubara frequency. We insert the Hamiltonian of graphene in a magnetic field, Eq. (30), to give

$$\hat{G}_0^{-1}(\omega_n, m) = \begin{pmatrix} i\omega_n + \mu & \omega_c \sqrt{m} \\ \omega_c \sqrt{m} & i\omega_n + \mu \end{pmatrix} \quad (67)$$

where m is the Landau level index. The Eigenvalues of this matrix are

$$g_{m,\pm}^{-1} = i\omega_n + \mu \pm \omega_c \sqrt{m}. \quad (68)$$

With these eigenvalues the Luttinger Ward functional (46) reads

$$\Omega_{mo} = -DT \sum_{m=0}^{\infty} \sum_{\omega_n} \sum_{\lambda=\pm 1} \ln(-i\omega_n - \lambda\omega_c\sqrt{m} - \mu) \quad (69)$$

and for the oscillatory potential (49) we get

$$\begin{aligned} \tilde{\Omega} &= 2DT \sum_{\omega_n} \sum_{l=1}^{\infty} \sum_{\lambda=\pm 1} \int_0^{\infty} \frac{1}{-i\omega_n - \mu - \lambda\omega_c\sqrt{x}} \frac{-\lambda\omega_c}{2\sqrt{x}} \frac{\sin(2\pi lx)}{2\pi l} dx \\ &= \frac{2T\omega_c^2 L^2}{\pi v_F^2} \sum_{\omega_n} \sum_{l=1}^{\infty} \frac{\omega_c^2}{2\pi l} \int_0^{\infty} dx \frac{\sin(2\pi lx)}{(i\omega_n + \mu)^2 - \omega_c^2 x}. \end{aligned} \quad (70)$$

Here, we have inserted the degeneracy factor $D = \frac{\omega_c^2 L^2}{2\pi v_F^2}$ (Eq. (43)) of the Landau levels. The integral of Eq. (70) can be evaluated using residue theorem, with the integration path shown in Figure 11.

$$\begin{aligned} &\int_0^{\infty} dx \frac{\sin(2\pi lx)}{(i\omega_n + \mu)^2 - \omega_c^2 x} = \frac{1}{2i} \int_0^{\infty} dx \frac{e^{i2\pi lx} - e^{-i2\pi lx}}{(i\omega_n + \mu)^2 - \omega_c^2 x} \\ &= \frac{1}{2} \int_0^{\infty} dx e^{-2\pi lx} \left(\frac{1}{(i\omega_n + \mu)^2 - i\omega_c^2 x} + \frac{1}{(i\omega_n + \mu)^2 + i\omega_c^2 x} \right) \\ &- \frac{\pi}{\omega_c^2} \Theta(\mu^2 - \omega_n^2) \left[e^{-\frac{4\pi l\omega_n\mu}{\omega_c^2}} e^{\frac{i2\pi l(\mu^2 - \omega_n^2)}{\omega_c^2}} \Theta(\omega_n\mu) + e^{\frac{4\pi l\omega_n\mu}{\omega_c^2}} e^{-\frac{i2\pi l(\mu^2 - \omega_n^2)}{\omega_c^2}} \Theta(-\omega_n\mu) \right] \end{aligned} \quad (71)$$

Using $\sum_{\omega_n} F(\omega_n) = \sum_{\omega_n > 0} (F(\omega_n) + F(-\omega_n))$, we get the following expression:

$$\begin{aligned} &\sum_{\omega_n} \int_0^{\infty} dx \frac{\sin(2\pi lx)}{(i\omega_n + \mu)^2 - \omega_c^2 x} = \\ &\sum_{\omega_n > 0} (\mu^2 - \omega_n^2) \int_0^{\infty} dx \left(\frac{e^{-2\pi lx}}{(\mu^2 - \omega_n^2)^2 + (2\omega_n\mu - \omega_c^2 x)} + \frac{e^{-2\pi lx}}{(\mu^2 - \omega_n^2)^2 + (2\omega_n\mu + \omega_c^2 x)} \right) \\ &- \frac{\pi}{\omega_c^2} \sum_{\omega_n > 0} e^{-\frac{4\pi l\omega_n|\mu|}{\omega_c^2}} 2 \cos\left(\frac{2\pi l(\mu^2 - \omega_c^2)}{\omega_c^2}\right) \Theta(\mu^2 - \omega_n^2). \end{aligned} \quad (72)$$

Importantly, the first term on the right-hand-side in Eq. (72) does not contribute an oscillatory term to the thermodynamic potential. Thus the oscillatory potential reads

$$\tilde{\Omega}_{\text{osc}} = \frac{2T\omega_c^2 L^2}{\pi v_F^2} \sum_{l=1}^{\infty} \sum_{\omega_n > 0} \frac{|\mu|}{l} e^{-\frac{4\pi l\omega_n|\mu|}{\omega_c^2}} \cos\left(\frac{2\pi l(\mu^2 - \omega_n^2)}{\omega_c^2}\right). \quad (73)$$

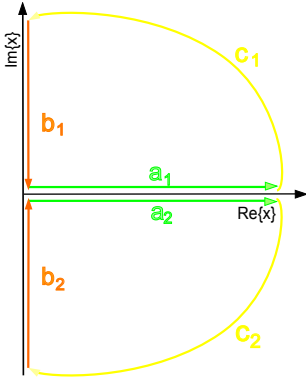


FIGURE 11: Integration path: we use the integration path 1 in the upper complex half-plane to evaluate the integral $\frac{e^{i2\pi lx}}{(i\omega_n + \mu)^2 - \omega_c^2 x}$ and the path 2 in the lower complex half-plane for the integral $\frac{e^{-i2\pi lx}}{(i\omega_n + \mu)^2 - \omega_c^2 x}$ such that the paths $c_{1,2}$ vanish for $x \rightarrow \infty$. Thus the original integral along the real axis, paths $a_{1,2}$, can be written as an integral along the imaginary axis, paths $b_{1,2}$, plus summation over residues.

4.2.1 The LK-formula in the Fermi liquid regime

In the limit $\mu \gg T$ the T -dependence of the frequency can be neglected. Furthermore, the sum over Matsubara frequencies can be extended to infinity. The LK-formula for graphene in the Fermi liquid regime thus reads

$$\tilde{\Omega}_{\text{osc}} = \frac{4T\omega_c^2 L^2}{\pi v_F^2} \sum_{l=1}^{\infty} \frac{1}{l \sinh\left(\frac{4\pi^2 l T |\mu|}{\omega_c^2}\right)} \cos\left(\frac{2\pi l \mu^2}{\omega_c^2}\right). \quad (74)$$

We therefore observe that the Fermi liquid regime of graphene almost reproduces the formula for a standard 2DEG, cf. Eq. (57), the difference arises simply from the different spacing of the Landau levels and the linear density of states.

4.2.2 The LK-formula near the Dirac point

Upon approaching the Dirac point we observe a number of peculiarities: (a) due to the restricted sum in Eq. (73) the oscillations completely die as soon as $\mu < \pi T$. (b) The effective oscillation frequency is not only a geometric quantity, but instead also depends on temperature via the dependence upon ω_n .

4.3 THE EFFECT OF DISORDER ON THE DHVA-OSCILLATIONS

As discussed in Section 4.1.1.2 disorder in the system leads to a damping of the amplitude of the de Haas - van Alphen oscillations. In this Section we will compute this damping factor in graphene. For this reason we will first compute the disorder related self-energy $\hat{\Sigma}_{\text{dis}}$ and subsequently we will solve the oscillatory integral Eq. (49) with the self-energy included in the Green function according to the Dyson equation [33],

$$\hat{G}^{-1} = \hat{G}_0^{-1} - \hat{\Sigma}_{\text{dis}}. \quad (75)$$

We do not attempt to make a realistic modelling of the properties of graphene with disorder; instead we treat disorder in the simplest way to gain a physical understanding of its effects.

4.3.1 The self-energy within the self-consistent Born approximation (SCBA)

We consider the self-energy within the SCBA to lowest order in the disorder potential, such that we have a non-vanishing imaginary part. That means the self-energy consists of the following two diagrams, where \Rightarrow is the dressed Green function.

$$\hat{\Sigma}_{\text{dis}}^{\text{SCBA}} = \begin{array}{c} \star \\ \vdots \\ \bullet \end{array} + \begin{array}{c} \star \\ \diagup \quad \diagdown \\ \bullet \quad \bullet \\ \Rightarrow \end{array} = U(\mathbf{r}) + \int U(\mathbf{r}) \hat{G}(\mathbf{r} - \mathbf{r}') U(\mathbf{r}') d\mathbf{r}' \quad (76)$$

The disorder potential $U(\mathbf{r})$ is given by the sum over the potentials that arise from scattering at the single impurities which are located at \mathbf{R}_j .

$$U(\mathbf{r}) = \sum_{j=1}^{N_{\text{imp}}} u(\mathbf{r} - \mathbf{R}_j) = u_0 \sum_{j=1}^{N_{\text{imp}}} \delta(\mathbf{r} - \mathbf{R}_j) \quad (77)$$

Here we have assumed short-ranged impurities with uniform strength u_0 . Since the single impurities are generally randomly distributed, it is reasonable to take the average over all possible configurations, meaning

$$\begin{aligned} \langle \hat{\Sigma}_{\text{dis}}^{\text{SCBA}} \rangle &= \underbrace{\langle u_0 \sum_{j=1}^{N_{\text{imp}}} \delta(\mathbf{r} - \mathbf{R}_j) \rangle}_0 + u_0^2 \sum_{j=1}^{N_{\text{imp}}} \sum_{l=1}^{N_{\text{imp}}} \int d\mathbf{r}' \underbrace{\langle \delta(\mathbf{r} - \mathbf{R}_j) \delta(\mathbf{r}' - \mathbf{R}_l) \rangle}_{\delta(\mathbf{r} - \mathbf{r}') \delta_{jl}} \langle \hat{G}(\mathbf{r} - \mathbf{r}') \rangle \\ &= u_0^2 \sum_{j=1}^{N_{\text{imp}}} \langle \hat{G}(0) \rangle = u_0^2 N_{\text{imp}} \langle \hat{G}(0) \rangle, \end{aligned} \quad (78)$$

where we assumed a translational invariant average. In momentum space the averaged self-energy then reads

$$\langle \hat{\Sigma}_{\text{dis}}^{\text{SCBA}} \rangle = u_0^2 N_{\text{imp}} \sum_k \langle \hat{G}(k) \rangle. \quad (79)$$

Since we want to perform the calculation within the Landau level (LL) basis, we need to transform the Green function into the LL-basis. The inverse Green

function of graphene in a magnetic field in the presence of disorder is then given by (cf. Eq. (67) and Eq. (75)),

$$\begin{aligned}\hat{G}^{-1} &= \begin{pmatrix} i\omega_n + \mu - \Sigma_{\text{dis}}^a & \omega_c \sqrt{m} \\ \omega_c \sqrt{m} & i\omega_n + \mu - \Sigma_{\text{dis}}^b \end{pmatrix} \\ \Rightarrow \hat{G} &= \frac{1}{(i\omega_n + \mu - \Sigma_{\text{dis}}^a)(i\omega_n + \mu - \Sigma_{\text{dis}}^b) - \omega_c^2 m} \\ &\times \begin{pmatrix} i\omega_n + \mu - \Sigma_{\text{dis}}^b & \omega_c \sqrt{m} \\ \omega_c \sqrt{m} & i\omega_n + \mu - \Sigma_{\text{dis}}^a \end{pmatrix}.\end{aligned}\quad (80)$$

Here we assumed that the self-energy is diagonal in the Landau level basis. Inserting this Green function into Eq. (79), we find a self-consistent expression for the self-energy,

$$\Sigma_{\text{dis}}^{a(b)} = N_{\text{imp}} u_0^2 \sum_{k,m} \frac{i\omega_n + \mu - \Sigma_{\text{dis}}^{b(a)}}{(i\omega_n + \mu - \Sigma_{\text{dis}}^a)(i\omega_n + \mu - \Sigma_{\text{dis}}^b) - \omega_c^2 m}.\quad (82)$$

We can perform the sum over k by simply multiplying by the degeneracy factor (32) of the Landau levels,

$$\Sigma_{\text{dis}}^{a(b)} = \alpha_{\text{dis}} \omega_c^2 \sum_m \frac{i\omega_n + \mu - \Sigma_{\text{dis}}^{b(a)}}{(i\omega_n + \mu - \Sigma_{\text{dis}}^a)(i\omega_n + \mu - \Sigma_{\text{dis}}^b) - \omega_c^2 m},\quad (83)$$

where $\alpha_{\text{dis}} = \frac{N_{\text{imp}} u_0^2 L^2}{2\pi v_F^2}$ is a dimensionless parameter characterizing the strength of the disorder potential.

In the following we assume that sufficiently high-lying Landau levels are populated such that the asymmetry between the sublattices is irrelevant. We then have

$$\Sigma_{\text{dis}} = \alpha_{\text{dis}} \omega_c^2 \sum_{m=0}^{\infty} \frac{i\omega_n + \mu - \Sigma_{\text{dis}}}{(i\omega_n + \mu - \Sigma_{\text{dis}})^2 - \omega_c^2 m}.\quad (84)$$

We use the Poisson summation formula, Equation (47), to dualize the sum over Landau levels making the expression more amenable to approximations for weak fields.

$$\begin{aligned}\Sigma_{\text{dis}} &= \alpha_{\text{dis}} \omega_c^2 \sum_{l=-\infty}^{\infty} \int_0^{\frac{v_F \Lambda}{\omega_c}} dx \frac{i\omega_n + \mu - \Sigma_{\text{dis}}}{(i\omega_n + \mu - \Sigma_{\text{dis}})^2 - \omega_c^2 x} e^{i2\pi l x} \\ &= \alpha_{\text{dis}} \int_0^{v_F^2 \Lambda^2} dx \frac{i\omega_n + \mu - \Sigma_{\text{dis}}}{(i\omega_n + \mu - \Sigma_{\text{dis}})^2 - x} \\ &+ \alpha_{\text{dis}} \sum_{l=1}^{\infty} \int_0^{v_F^2 \Lambda^2} dx \frac{(i\omega_n + \mu - \Sigma_{\text{dis}})}{(i\omega_n + \mu - \Sigma_{\text{dis}})^2 - x} \cos\left(\frac{2\pi l x}{\omega_c^2}\right) \\ &= \Sigma_{\text{dis}}^0 + \Sigma_{\text{dis}}^{\text{osc}}\end{aligned}\quad (85)$$

Here we introduced a cutoff Λ , restricting the analysis to the regime where the dispersion is linear. The first term Σ_{dis}^0 is the $l = 0$ term and corresponds

to the standard expression of the SCBA in a system without magnetic field. The second part $\Sigma_{\text{dis}}^{\text{osc}}$ describes the oscillations of the self-energy due to the magnetic field. Performing the integration yields

$$\Sigma_{\text{dis}}^0 = -\alpha_{\text{dis}}(i\omega_n + \mu - \Sigma_{\text{dis}}) \ln \frac{v_F^2 \Lambda^2 - (i\omega_n + \mu - \Sigma_{\text{dis}})^2}{-(i\omega_n + \mu - \Sigma_{\text{dis}})^2}. \quad (86)$$

This expression can be solved self consistently to leading order in α_{dis} and we obtain,

$$\Sigma_{\text{dis}}^0 = -\alpha_{\text{dis}}(i\omega_n + \mu) \ln \frac{v_F^2 \Lambda^2 - (i\omega_n + \mu)^2}{-(i\omega_n + \mu)^2}. \quad (87)$$

$\Sigma_{\text{dis}}^{\text{osc}}$ can be computed by using integration by parts, yielding an analytic expression. This calculation is performed in Appendix A.1. However, more insight is gained by treating the integral using residue theorem:

$$\begin{aligned} \Sigma_{\text{dis}}^{\text{osc}} &= \alpha_{\text{dis}}(i\omega_n + \mu - \Sigma_{\text{dis}}) \sum_{l=1}^{\infty} \int_0^{\infty} dx \frac{e^{\frac{i2\pi lx}{\omega_c^2}} + e^{-\frac{i2\pi lx}{\omega_c^2}}}{(i\omega_n + \mu - \Sigma_{\text{dis}})^2 - x} \\ &= \alpha_{\text{dis}}(i\omega_n + \mu - \Sigma_{\text{dis}}) 2\pi i \Theta(a) \sum_{l=1}^{\infty} e^{-\frac{2\pi}{\omega_c^2} |b|l} \left(e^{\frac{i2\pi}{\omega_c^2} al} \Theta(b) - e^{-\frac{i2\pi}{\omega_c^2} al} \Theta(-b) \right) \\ &\quad + \alpha_{\text{dis}}(i\omega_n + \mu - \Sigma_{\text{dis}}) \sum_{l=1}^{\infty} \int_0^{\infty} dx \left(\frac{e^{-\frac{2\pi}{\omega_c^2} xl}}{a + i(b-x)} - \frac{e^{-\frac{2\pi}{\omega_c^2} xl}}{a + i(b+x)} \right) \end{aligned} \quad (88)$$

with $a = (\mu - \Sigma'_{\text{dis}})^2 - (\omega_n - \Sigma''_{\text{dis}})^2$ and $b = 2(\omega_n - \Sigma''_{\text{dis}})(\mu - \Sigma'_{\text{dis}})$ where Σ'_{dis} is the real part of Σ_{dis} and Σ''_{dis} is its imaginary part. The first term stems from the residue. Whether the pole is located inside or outside the integration contour depends on the sign of a and b . The second term stems from integration along the imaginary axis and is a non-oscillatory correction term. The integration contours used here are plotted in Figure 11. In the regime $T \gtrsim \omega_c$ both terms in $\Sigma_{\text{dis}}^{\text{osc}}$ are suppressed exponentially due to the factors $\exp(-\frac{2\pi}{\omega_c^2} |b|l)$ and $\exp(-\frac{2\pi}{\omega_c^2} xl)$, respectively. Thus, in this regime, $\Sigma_{\text{dis}}^{\text{osc}}$ can be neglected, and the self-energy can be well-approximated as

$$\begin{aligned} \Sigma_{\text{dis}} &= -\alpha_{\text{dis}}(i\omega_n + \mu) \ln \left(\frac{v_F^2 \Lambda^2 - (i\omega_n + \mu)^2}{-(i\omega_n + \mu)^2} \right) \\ &\approx -\alpha_{\text{dis}}(i\omega_n + \mu) \ln \left(\frac{v_F^2 \Lambda^2}{-(i\omega_n + \mu)^2} \right). \end{aligned} \quad (89)$$

4.3.2 The Lifshitz-Kosevich formula with disorder

Now we can include the derived expression for the self-energy Eq. (89) into the Green function Eq. (80) and compute the oscillatory grand potential Eq. (49). As the self-energy is energy independent, the steps (67) to (70) can be

performed analogously to the calculation of the clean system but now with an additional summand, Σ_{dis} . We have,

$$g_m^{-1} = i\omega_n + \mu - \Sigma_{\text{dis}}(i\omega_n, \mu) \pm \omega_c \sqrt{m} \quad (90)$$

and therefore

$$\Omega = \frac{T\omega_c^4 L^2}{\pi^2 v_F^2} \sum_{\omega_n} \sum_{l=1}^{\infty} \frac{1}{l} \int_0^{\infty} dx \frac{\sin(2\pi lx)}{[i\omega_n + \mu - \Sigma_{\text{dis}}(i\omega_n, \mu)]^2 - \omega_c^2 x}. \quad (91)$$

This integral can again be computed using residue theorem (the computation is performed in appendix A.2). We find,

$$\begin{aligned} \tilde{\Omega}_{\text{osc}} &= \frac{2T\omega_c^2 L^2}{\pi v_F^2} \sum_{l=1}^{\infty} \frac{1}{l} \sum_{\omega_n > 0}^{\frac{|\mu|}{1+\alpha_{\text{dis}} \frac{\pi}{2}}} e^{-\frac{4\pi l}{\omega_c^2} ((\mu^2 - \omega_n^2)(\pi\alpha_{\text{dis}} - 2\phi\alpha_{\text{dis}}) + |\mu|\omega_n(1+2\alpha_{\text{dis}}\Gamma))} \\ &\quad \times \cos\left(\frac{2\pi l}{\omega_c^2} \left((\mu^2 - \omega_n^2)(1 + 2\alpha_{\text{dis}}\Gamma) - 4\alpha_{\text{dis}}|\mu|\omega_n(\pi - 2\phi)\right)\right). \end{aligned} \quad (92)$$

Now we can define a Dingle temperature according to Eq. (65). The damping factor that stems from disorder is

$$e^{-\frac{4\pi l}{\omega_c^2} ((\mu^2 - \omega_n^2)(\pi\alpha_{\text{dis}} - 2\phi\alpha_{\text{dis}}) + |\mu|\omega_n 2\alpha_{\text{dis}}\Gamma)} = e^{-\frac{4\pi l |\mu| \omega_n}{\omega_c^2} \left(\frac{(\mu^2 - \omega_n^2)}{|\mu|\omega_n} (\pi\alpha_{\text{dis}} - 2\phi\alpha_{\text{dis}}) + 2\alpha_{\text{dis}}\Gamma\right)}.$$

Thus the Dingle temperature T_D reads

$$T_D = \omega_n \left(\frac{(\mu^2 - \omega_n^2)}{|\mu|\omega_n} (\pi\alpha_{\text{dis}} - 2\phi\alpha_{\text{dis}}) + 2\alpha_{\text{dis}}\Gamma \right) \quad (93)$$

and at zero temperature it becomes

$$T_D = |\mu|\pi\alpha_{\text{dis}}. \quad (94)$$

From the expression for the grand potential, Eq. (92), we derive the oscillatory part of the magnetization (44),

$$\begin{aligned} M_{\text{osc}} &= \left(\frac{\partial \tilde{\Omega}_{\text{osc}}}{\partial B} \right)_{\mu} \\ &= \frac{4TL^2}{\pi} \sum_{l=1}^{\infty} \sum_{\omega_n > 0}^{\frac{|\mu|}{1+\alpha_{\text{dis}} \frac{\pi}{2}}} e^{-\frac{4\pi l}{\omega_c^2} ((\mu^2 - \omega_n^2)(\pi\alpha_{\text{dis}} - 2\phi\alpha_{\text{dis}}) + |\mu|\omega_n(1+2\alpha_{\text{dis}}\Gamma))} \\ &\quad \times \left[\left(\frac{1}{l} + \frac{4\pi}{\omega_c^2} \left((\mu^2 - \omega_n^2)(\pi\alpha_{\text{dis}} - 2\phi\alpha_{\text{dis}}) + |\mu|\omega_n(1 + 2\alpha_{\text{dis}}\Gamma) \right) \right) \right. \\ &\quad \times \cos\left(\frac{2\pi l}{\omega_c^2} \left((\mu^2 - \omega_n^2)(1 + 2\alpha_{\text{dis}}\Gamma) - 4\alpha_{\text{dis}}|\mu|\omega_n(\pi - 2\phi)\right)\right) \\ &\quad + \frac{2\pi}{\omega_c^2} \left((\mu^2 - \omega_n^2)(1 + 2\alpha_{\text{dis}}\Gamma) - 4\alpha_{\text{dis}}|\mu|\omega_n(\pi - 2\phi) \right) \\ &\quad \left. \times \sin\left(\frac{2\pi l}{\omega_c^2} \left((\mu^2 - \omega_n^2)(1 + 2\alpha_{\text{dis}}\Gamma) - 4\alpha_{\text{dis}}|\mu|\omega_n(\pi - 2\phi)\right)\right) \right]. \end{aligned} \quad (95)$$

THE EFFECT OF ELECTRON-ELECTRON INTERACTIONS ON THE DHVA-OSCILLATIONS

As the relaxation time due to electron-electron interactions is temperature dependent, it is natural to assume that electron-electron interactions also contribute to the Dingle temperature. Fowler and Prange showed that electron-phonon interactions do not lead to an additional damping but only renormalizes the effective mass. [34] This statement has been generalized to electron-electron interactions for $T \gtrsim \omega_c$ and it is independent of the specific form of the interaction potential. For the two-dimensional electron gas it can be found in Refs. [17, 2]. It states that the imaginary part of the self-energy due to electron-electron interactions, $\Sigma''_{ee}(i\omega_n)$, which formally leads to an additional damping factor, only yields a renormalization of the field for the first Matsubara frequency, i.e. $\Sigma''_{ee}(i\omega_0) \propto \omega_0$. Higher Matsubara frequencies can be neglected for temperatures $T \gtrsim \omega_c$. The real part of the self-energy, Σ'_{ee} , does not lead to an additional damping factor but only renormalizes the electron mass.

In this chapter we will first retrace the statement for the two-dimensional electron gas and then investigate the effect of electron-electron interactions in graphene. We find that while to one-loop order all interaction effects can be fully accounted for by the renormalized Fermi velocity, this ceases to be true to two-loop accuracy and additional renormalization effects play a role. Furthermore, at finite temperature, electron-electron interactions do lead to an additional damping factor due to inelastic scattering which is absent for standard metals.

5.1 THE EFFECT OF ELECTRON-ELECTRON INTERACTIONS IN THE TWO-DIMENSIONAL ELECTRON GAS

In contrast to the disorder self-energy Σ_{dis} , the self-energy for electron-electron interactions Σ_{ee} depends on energy, i.e. on the Landau level m . Thus we will first investigate the influence of an energy dependent self-energy on the oscillations. We will see that the real part of the self-energy only renormalizes the cyclotron frequency. Then we will compute the imaginary part and show that it is only a renormalization of the field for temperatures $T \gtrsim \omega_c$. The Green function of the two-dimensional electron gas, Eq. (50), was given by

$$\hat{G}(m, i\omega_n)^{-1} = \left(i\omega_n + \mu - \omega_c \left(m + \frac{1}{2} \right) \right) \mathbb{1} - \hat{\Sigma}. \quad (96)$$

We assume a self-energy that is diagonal in the Landau level basis. By following Adamov *et. al.* [2] we use the following ansatz for the self-energy,

$$\Sigma_{ee}(m, i\omega_n) = -i\alpha_0\omega_n + \delta\mu + \beta\omega_c m + \delta\Sigma(m, i\omega_n), \quad (97)$$

where $\delta\Sigma(m, i\omega_n)$ incorporates inelastic scattering processes. As these are in general small by a factor of T/E_F (E_F is the Fermi energy) we neglect the real part. The imaginary part does not depend on energy, meaning on the Landau level index m , and so we can write

$$\delta\Sigma(m, i\omega_n) \approx i\delta\Sigma''(i\omega_n). \quad (98)$$

In Chapter 4 we derived a generic expression for the oscillatory grand potential, Eq. (49), which was

$$\tilde{\Omega} = 2DT \sum_{\omega_n} \sum_{l=0}^{\infty} \int_0^{\infty} \frac{1}{-g^{-1}(x, i\omega_n)} \frac{d}{dx} \left(-g^{-1}(x, i\omega_n) \right) \frac{\sin(2\pi lx)}{2\pi l} dx. \quad (99)$$

Inserting the Green function of the two dimensional electron gas, Eq. (96), with eigenvalues

$$g^{-1}(x) = i\omega_n(1 + \alpha_0) + \mu - \delta\mu - \omega_c x(1 + \beta) - \frac{\omega_c}{2} - i\delta\Sigma''(i\omega_n), \quad (100)$$

the oscillatory integral reads

$$\tilde{\Omega} = \frac{DT}{\pi} \sum_{\omega_n} \sum_{l=0}^{\infty} \int_0^{\infty} \frac{\omega_c(1 + \beta) \sin(2\pi lx) dx}{(-i\omega_n(1 + \alpha_0) - \mu + \delta\mu + \omega_c x(1 + \beta) + \frac{\omega_c}{2} + i\delta\Sigma''(i\omega_n))}. \quad (101)$$

Solving this integral using residue theorem and neglecting the non-oscillatory summands we obtain

$$\tilde{\Omega}_{osc} = -2DT \sum_{\omega_n > 0} \sum_{l=1}^{\infty} \frac{1}{l} e^{-\frac{2\pi l(\omega_n(1 + \alpha_0) - \delta\Sigma'')}{\omega_c(1 + \beta)}} \cos\left(\frac{2\pi l \tilde{\mu}}{\omega_c(1 + \beta)}\right), \quad (102)$$

where we introduced an effective chemical potential $\tilde{\mu} \approx \mu - \delta\mu - \frac{\omega_c}{2}$. We see, that the self-energy Σ_{ee} influences the oscillation amplitude as follows: The real part of Σ_{ee} renormalizes the cyclotron frequency according to

$$\omega_c^* = \omega_c(1 + \beta). \quad (103)$$

A non-vanishing imaginary part would first lead to a renormalization of the Matsubara frequency according to

$$\omega_n^* = \omega_n(1 + \alpha_0), \quad (104)$$

and second it would lead, as in the case of disorder, to an additional damping factor

$$\exp\left\{\frac{2\pi l \delta\Sigma''}{\omega_c^*}\right\}. \quad (105)$$

5.1.1 The Fermi liquid self-energy for generic interactions.

Now we will derive a generic expression for the imaginary part of the self-energy of the Fermi liquid, in order to see if it meets the conditions for no additional damping factor in the amplitude due to electron-electron interactions.

We compute the electron self-energy within the 'random phase approximation' (RPA) [35],

$$\begin{aligned} \Sigma_{ee}(\mathbf{k}, i\omega_n) &= \begin{array}{c} \text{Diagram 1: A dashed semi-circular arc above a solid line with arrows pointing right. The top of the arc is labeled } k-k', i\omega-i\omega'. \text{ The bottom of the arc is labeled } k, i\omega \text{ on the left and } k', i\omega' \text{ on the right.} \\ \text{Diagram 2: A dashed semi-circular arc above a solid line with arrows pointing right.} \\ \text{Diagram 3: A dashed semi-circular arc above a solid line with arrows pointing right, with a loop on top.} \\ \text{Diagram 4: A dashed semi-circular arc above a solid line with arrows pointing right, with two loops on top.} \\ \dots \end{array} \\ &= -T \int \frac{d^2k'}{(2\pi)^2} \sum_{\omega'_n} V(\mathbf{k} - \mathbf{k}', i\omega_n - i\omega'_n) G_0(\mathbf{k}', i\omega'_n), \end{aligned} \quad (106)$$

where the interaction potential V is a resummed interaction line (double dashed line). We use the spectral representation for the potential $V(\mathbf{k} - \mathbf{k}', i\omega_n - i\omega'_n)$ and the Green function $G_0(\mathbf{k}', i\omega'_n)$ [35],

$$\begin{aligned} \Sigma_{ee}(\mathbf{k}, i\omega_n) &= -T \int \frac{d^2k'}{(2\pi)^2} \sum_{\omega'_n} \int_{-\infty}^{\infty} \frac{d\epsilon}{\pi} \frac{V''(\mathbf{k} - \mathbf{k}', \epsilon)}{i\omega_n - i\omega'_n - \epsilon} \int_{-\infty}^{\infty} \frac{d\tilde{\epsilon}}{\pi} \frac{G_0''(\mathbf{k}', \tilde{\epsilon})}{i\omega'_n - \tilde{\epsilon}} \\ &= -T \sum_{\omega'_n} \int \frac{d^2k'}{(2\pi)^2} \int_{-\infty}^{\infty} \frac{d\epsilon}{\pi} \int_{-\infty}^{\infty} \frac{d\tilde{\epsilon}}{\pi} V''(\mathbf{k} - \mathbf{k}', \epsilon) G_0''(\mathbf{k}', \tilde{\epsilon}) \\ &\quad \times \frac{-i\omega_n + i\omega'_n - \epsilon}{(\omega_n - \omega'_n)^2 + \epsilon^2} \frac{-i\omega'_n - \tilde{\epsilon}}{\omega_n'^2 + \tilde{\epsilon}^2}. \end{aligned} \quad (107)$$

Since for a collective mode or general interaction we have $V''(\epsilon) = -V''(-\epsilon)$, we can transform to

$$\begin{aligned} \Sigma_{ee}(\mathbf{k}, i\omega_n) &= -T \sum_{\omega'_n} \int \frac{d^2k'}{(2\pi)^2} \int_{-\infty}^{\infty} \frac{d\epsilon}{\pi} \int_{-\infty}^{\infty} \frac{d\tilde{\epsilon}}{\pi} V''(\mathbf{k} - \mathbf{k}', \epsilon) G_0''(\mathbf{k}', \tilde{\epsilon}) \\ &\quad \times \frac{-\epsilon}{(\omega_n - \omega'_n)^2 + \epsilon^2} \frac{-i\omega'_n - \tilde{\epsilon}}{\omega_n'^2 + \tilde{\epsilon}^2}. \end{aligned} \quad (108)$$

We thus have a real and an imaginary part of the self energy, where the imaginary part is given by

$$\begin{aligned} \Sigma_{ee}''(\mathbf{k}, i\omega_n) &= -T \sum_{\omega'_n} \int \frac{d^2k'}{(2\pi)^2} \int_{-\infty}^{\infty} \frac{d\epsilon}{\pi} \int_{-\infty}^{\infty} \frac{d\tilde{\epsilon}}{\pi} V''(\mathbf{k} - \mathbf{k}', \epsilon) G_0''(\mathbf{k}', \tilde{\epsilon}) \\ &\quad \times \frac{\epsilon}{(\omega_n - \omega'_n)^2 + \epsilon^2} \frac{\omega'_n}{\omega_n'^2 + \tilde{\epsilon}^2}. \end{aligned} \quad (109)$$

In the special case of a Fermi liquid we can linearize the dispersion around the Fermi surface. The resulting density of states is particle-hole symmetric and the integral over $\tilde{\epsilon}$ yields just π meaning

$$\begin{aligned}
\Sigma''_{ee}(\mathbf{k}, i\omega_n) &\propto -\pi T \sum_{\omega'_n} \int \frac{d^2k'}{(2\pi)^2} \int_{-\infty}^{\infty} \frac{d\epsilon}{\pi} V''(\mathbf{k} - \mathbf{k}', \epsilon) \frac{\epsilon \operatorname{sgn} \omega'_n}{(\omega_n - \omega'_n)^2 + \epsilon^2} \\
&= -\pi T \sum_{\omega'_n > 0} \int \frac{d^2k'}{(2\pi)^2} \int_{-\infty}^{\infty} \frac{d\epsilon}{\pi} V''(\mathbf{k} - \mathbf{k}', \epsilon) \epsilon \\
&\quad \times \left(\frac{1}{(\omega_n - \omega'_n)^2 + \epsilon^2} - \frac{1}{(\omega_n + \omega'_n)^2 + \epsilon^2} \right) \\
&= -\pi T \int \frac{d^2k'}{(2\pi)^2} \int_{-\infty}^{\infty} \frac{d\epsilon}{\pi} V''(\mathbf{k} - \mathbf{k}', \epsilon) \sum_{\nu_n \geq 0} \frac{\epsilon}{\nu_n^2 + \epsilon^2}.
\end{aligned} \tag{110}$$

This implies that on the first Matsubara mode, i.e. $\omega_n = \pi T$, there is a contribution

$$\Sigma''_{ee}(\mathbf{k}, i\pi T) \propto -\pi T \int \frac{d^2k'}{(2\pi)^2} \int_{-\infty}^{\infty} \frac{d\epsilon}{\pi} V''(\mathbf{k} - \mathbf{k}', \epsilon) \frac{1}{\epsilon}, \tag{111}$$

but no T^2 dependence. This leads to

$$\Sigma_{ee}(\mathbf{k}, i\pi T) = \Sigma'_{ee}(i\pi T, \mathbf{k}) - i\pi T f(\mathbf{k}) = \Sigma'_{ee}(i\pi T, \mathbf{k}) - i\omega_0 f(\mathbf{k}). \tag{112}$$

The imaginary part of the self-energy is simply a renormalization of the field and incorporated in the parameter α_0 in the general form of the self energy, Eq. (97).

We conclude that at sufficiently high temperatures, i.e. when it is reasonable to only consider the first Matsubara frequency ω_0 , electron-electron interactions do not lead to an additional damping factor in the amplitude of the Lifshitz-Kosevich formula for the two-dimensional electron gas.

5.2 THE EFFECT OF ELECTRON-ELECTRON INTERACTIONS IN GRAPHENE

In this section we will investigate the effect of electron-electron interaction on the oscillation amplitude in graphene. Thereby, we will follow the same logic as in the case of the 2DEG. We will first calculate the oscillatory part of the grand potential with a self-energy $\hat{\Sigma}_{ee}$ that depends on energy. Then we will compute the interaction induced self-energy for graphene and see that for finite temperatures the imaginary part contributes an additional damping factor to the LK-amplitude.

We make the following ansatz for the self-energy, which we will motivate below by means of an explicit calculation.

$$\begin{aligned}
\hat{\Sigma}_{ee}(m, i\omega_n) &= \begin{pmatrix} i\omega_n(1 - Z^{-1}) & (1 - Z_{v_F})\omega_c\sqrt{m} \\ (1 - Z_{v_F})\omega_c\sqrt{m} & i\omega_n(1 - Z^{-1}) \end{pmatrix} \\
&+ \begin{pmatrix} i\delta\Sigma''(\omega_c\sqrt{m}, \omega_n) & \delta\Sigma'(\omega_c\sqrt{m}, \omega_n) \\ \delta\Sigma'(\omega_c\sqrt{m}, \omega_n) & i\delta\Sigma''(\omega_c\sqrt{m}, \omega_n) \end{pmatrix}.
\end{aligned} \tag{113}$$

Here, we assumed that Z and Z_{v_F} account for logarithmic renormalizations and do not explicitly depend on energy. $\delta\Sigma''(\omega_c\sqrt{m}, \omega_n)$ and $\delta\Sigma'(\omega_c\sqrt{m}, \omega_n)$ are real and correspond to non-logarithmic contributions and potentially depend on temperature. The Green function thus reads

$$\hat{G}^{-1}(m, i\omega_n) = \begin{pmatrix} i\omega_n Z^{-1} + \mu & Z_{v_F} \omega_c \sqrt{m} \\ Z_{v_F} \omega_c \sqrt{m} & i\omega_n Z^{-1} + \mu \end{pmatrix} - \begin{pmatrix} i\delta\Sigma''(\omega_c\sqrt{m}, \omega_n) & \delta\Sigma'(\omega_c\sqrt{m}, \omega_n) \\ \delta\Sigma'(\omega_c\sqrt{m}, \omega_n) & i\delta\Sigma''(\omega_c\sqrt{m}, \omega_n) \end{pmatrix}. \quad (114)$$

The eigenvalues of this matrix are

$$g_m^{-1} = i\omega_n Z^{-1} + \mu - i\delta\Sigma'' \mp (\sqrt{m}\omega_c Z_{v_F} - \delta\Sigma') \quad (115)$$

$$= g_1 - \lambda g_2, \quad (116)$$

with $\lambda = \pm 1$. Inserting these eigenvalues into Eq. (99), the grand potential reads

$$\tilde{\Omega} = \frac{DT}{\pi} \sum_{\omega_n} \sum_{l=1}^{\infty} \frac{1}{l} \sum_{\lambda=\pm 1} \int_0^{\infty} \left[\frac{\sin(2\pi lx) \frac{d}{dx}(-g_1 + \lambda g_2)}{-g_1 + \lambda g_2} \right] dx. \quad (117)$$

Merging the two poles yields

$$\begin{aligned} \tilde{\Omega} &= \frac{DT}{\pi} \sum_{\omega_n} \sum_{l=1}^{\infty} \frac{1}{l} \int_0^{\infty} \left[\frac{\sin(2\pi lx) (2(\frac{d}{dx}g_1)g_1 - 2(\frac{d}{dx}g_2)g_2)}{g_1^2 - g_2^2} \right] dx \\ &= \frac{DT}{\pi} \sum_{\omega_n} \sum_{l=1}^{\infty} \frac{1}{l} \int_0^{\infty} \left[\frac{\sin(2\pi lx) \frac{d}{dx}(g_1^2 - g_2^2)}{g_1^2 - g_2^2} \right] dx. \end{aligned} \quad (118)$$

Now we will linearize the denominator around the pole x_0 with $g_1^2 - g_2^2|_{x=x_0} = 0$,

$$\tilde{\Omega} = \frac{DT}{\pi} \sum_{\omega_n} \sum_{l=1}^{\infty} \frac{1}{l} \int_0^{\infty} \left[\frac{\sin(2\pi lx) \frac{d}{dx}(g_1^2 - g_2^2)}{(x - x_0) \frac{d}{dx}(g_1^2 - g_2^2)|_{x=x_0}} \right] dx. \quad (119)$$

We expand the pole in powers of the interaction parameter α , which we will define below ($\delta\Sigma'$ and $\delta\Sigma''$ are quadratic in α),

$$x_0 = x_0^{(0)} + x_0^{(2)} + \dots$$

To lowest order we have

$$\begin{aligned} &(-i\omega_n Z^{-1} - \mu)^2 - \left(\sqrt{x_0^{(0)}} \omega_c Z_{v_F} \right)^2 = 0 \\ \Rightarrow \quad &\omega_c^2 Z_{v_F}^2 x_0^{(0)} = \left(i\omega_n Z^{-1} + \mu \right)^2 = -\omega_n^2 Z^{-2} + \mu^2 + 2i\omega_n Z^{-1} \mu. \end{aligned} \quad (120)$$

To quadratic order we find

$$\left(-i\omega_n Z^{-1} - \mu + i\delta\Sigma''(x_0^{(0)}) \right)^2 - \left(\sqrt{x_0^{(0)} + x_0^{(2)}} \omega_c Z_{v_F} - \delta\Sigma'(x_0^{(0)}) \right)^2 = 0$$

$$\begin{aligned}
\Rightarrow \omega_c^2 Z_{v_F}^2 x_0^{(2)} &= 2i\delta\Sigma''(-i\omega_n Z^{-1} - \mu) + 2\delta\Sigma'(x_0^{(0)})\sqrt{x_0^{(0)}}\omega_c Z_{v_F} \\
&= i\left(2\Im\{\delta\Sigma''\}\omega_n Z^{-1} - 2\Re\{\delta\Sigma''\}\mu + 2\Im\{\delta\Sigma'\}\sqrt{x_0^{(0)}}\omega_c Z_{v_F}\right) \\
&\quad + 2\Re\{\delta\Sigma''\}\omega_n Z^{-1} + 2\Im\{\delta\Sigma''\}\mu + 2\Re\{\delta\Sigma'\}\sqrt{x_0^{(0)}}\omega_c Z_{v_F}.
\end{aligned} \tag{121}$$

Computing the integral using residue theorem, we obtain

$$\begin{aligned}
\tilde{\Omega}_{osc} &= 2DT \sum_{l=1}^{\infty} \frac{1}{l} \sum_{\omega_n > 0}^{\approx |\mu|} e^{-\frac{4\pi l}{\omega_c^2 Z_{v_F}^2}(\omega_n Z^{-1}\mu + (\Im\{\delta\Sigma''\} + \Re\{\delta\Sigma'\})\omega_n Z^{-1} + (\Im\{\delta\Sigma'\} - \Re\{\delta\Sigma''\})\mu)} \\
&\quad \times \cos\left(\frac{2\pi l}{\omega_c^2 Z_{v_F}^2} \left(-\omega_n^2 Z^{-2} + \mu^2 + 2(\Re\{\delta\Sigma''\} - \Im\{\delta\Sigma'\})\omega_n Z^{-1} \right. \right. \\
&\quad \left. \left. + 2(\Im\{\delta\Sigma''\} + \Re\{\delta\Sigma'\})\mu\right)\right).
\end{aligned} \tag{122}$$

5.2.1 The interaction induced self-energy for graphene

In this section we will compute the electron-electron interaction induced self-energy $\hat{\Sigma}_{ee}$ for graphene in the 'random phase approximation' (RPA). We will perform our computation in k -space. We believe that this is a reasonable approximation at weak magnetic fields since in the case of disorder we showed that the part of the self-energy due to a finite magnetic field, Σ_{dis}^{osc} (Eq. (88)), can be neglected for $T \gtrsim \omega_c$.

$\hat{\Sigma}_{ee}$ in the RPA was given in Eq. (106),

$$\hat{\Sigma}_{ee}(\mathbf{k}, i\omega_n) = -T \sum_{\omega'_n} \int \frac{d^2 k'}{(2\pi)^2} V(\mathbf{k} - \mathbf{k}', i\omega_n - i\omega'_n) \hat{G}_0(\mathbf{k}', i\omega'_n). \tag{123}$$

Graphene's free electron Green function for zero chemical potential is given by

$$\hat{G}_0(\mathbf{k}, i\omega_n) = \frac{-i\omega_n \mathbb{1} - v_F \mathbf{k} \hat{\sigma}}{\omega_n^2 + v_F^2 k^2} \tag{124}$$

and the Coulomb interaction in the RPA at zero temperature is given by

$$V(\mathbf{k}, i\omega_n) = \frac{2\pi\alpha v_F}{|\mathbf{k}| + \frac{2\pi\alpha v_F}{4} \frac{k^2}{4\sqrt{v_F^2 k^2 + \omega_n^2}}}, \tag{125}$$

with $\alpha = e^2/(\epsilon v_F)$ (ϵ corresponds to the dielectric constant) being graphene's dimensionless fine structure constant. In the following we will only work to two-loop accuracy and consequently expand the dressed Coulomb interaction to quadratic order yielding

$$V(\mathbf{k}, i\omega_n) = \text{-----} + \text{-----} \circlearrowleft \text{-----} + O(\alpha^3)$$

$$= \frac{2\pi\alpha v_F}{k} - \frac{(2\pi)^2\alpha^2 v_F^2}{4\sqrt{v_F^2 k^2 + \omega_n^2}} + \mathcal{O}(\alpha^3). \quad (126)$$

We decompose the self-energy into a first and a second order part according to

$$\hat{\Sigma}_{ee}(\mathbf{k}, i\omega_n) \approx \hat{\Sigma}^{(1)}(\mathbf{k}, i\omega_n) + \hat{\Sigma}^{(2)}(\mathbf{k}, i\omega_n) \quad (127)$$

where $\hat{\Sigma}^{(1)}(\mathbf{k}, i\omega_n)$ is linear in α , while $\hat{\Sigma}^{(2)}(\mathbf{k}, i\omega_n)$ is quadratic in α . They read

$$\hat{\Sigma}^{(1)}(\mathbf{k}, i\omega_n) = 2\pi\alpha v_F T \sum_{\omega'_n} \int \frac{d^2 k'}{(2\pi)^2} \frac{1}{|\mathbf{k} - \mathbf{k}'|} \frac{i\omega'_n \mathbb{1} + v_F \mathbf{k}' \hat{\sigma}}{\omega_n'^2 + v_F^2 k'^2} \quad (128)$$

and

$$\begin{aligned} \hat{\Sigma}^{(2)}(\mathbf{k}, i\omega_n) = & -\frac{(2\pi)^2\alpha^2 v_F^2}{4} T \sum_{\omega'_n} \int \frac{d^2 k'}{(2\pi)^2} \frac{1}{\sqrt{v_F^2(\mathbf{k} - \mathbf{k}')^2 + (\omega_n - \omega'_n)^2}} \\ & \times \frac{i\omega'_n \mathbb{1} + v_F \mathbf{k}' \hat{\sigma}}{\omega_n'^2 + v_F^2 k'^2}. \end{aligned} \quad (129)$$

We see that the imaginary part is strictly diagonal, while the real part is off-diagonal. This motivates ansatz (113) for the self-energy.

We start with the calculation of $\hat{\Sigma}^{(1)}$. From symmetry we observe that the diagonal part vanishes and only the off-diagonal part survives,

$$\hat{\Sigma}^{(1)}(\mathbf{k}, i\omega_n) = 2\pi\alpha v_F T \sum_{\omega'_n} \int \frac{d^2 k'}{(2\pi)^2} \frac{1}{|\mathbf{k} - \mathbf{k}'|} \frac{v_F \mathbf{k}' \hat{\sigma}}{\omega_n'^2 + v_F^2 k'^2}. \quad (130)$$

We apply an integral identity,

$$\int_{-\infty}^{\infty} \frac{dx}{\pi} \frac{1}{a^2 + x^2} = \frac{1}{a}, \quad (131)$$

and rescale \mathbf{k}' and x with v_F , and obtain

$$\hat{\Sigma}^{(1)}(\mathbf{k}, i\omega_n) = 2\pi\alpha T \sum_{\omega'_n} \int \frac{d^2 k'}{(2\pi)^2} \int_{-\infty}^{\infty} \frac{dx}{\pi} \frac{1}{(\mathbf{k}' - v_F \mathbf{k})^2 + x^2} \frac{\mathbf{k}' \hat{\sigma}}{\omega_n'^2 + k'^2}.$$

We use the Feynman parameter and write

$$\begin{aligned}
\hat{\Sigma}^{(1)}(\mathbf{k}, i\omega_n) &= 2\pi\alpha T \sum_{\omega'_n} \int \frac{d^2k'}{(2\pi)^2} \int_{-\infty}^{\infty} \frac{dx}{\pi} \int_0^1 du \\
&\times \frac{\mathbf{k}' \hat{\sigma}}{(u(\mathbf{k}' - v_F \mathbf{k})^2 + ux^2 + (1-u)(\omega_n'^2 + k'^2))^2} \\
&= 2\pi\alpha T \sum_{\omega'_n} \int \frac{d^2k'}{(2\pi)^2} \int_{-\infty}^{\infty} \frac{dx}{\pi} \int_0^1 du \\
&\times \frac{\mathbf{k}' \hat{\sigma}}{((\mathbf{k}' - uv_F \mathbf{k})^2 + ux^2 + u(1-u)v_F^2 k^2 + (1-u)\omega_n'^2)^2} \\
&= 2\pi\alpha T \sum_{\omega'_n} \int \frac{d^2k'}{(2\pi)^2} \int_{-\infty}^{\infty} \frac{dx}{\pi} \int_0^1 du \\
&\times \frac{1}{\sqrt{u}} \frac{(\mathbf{k}' + uv_F \mathbf{k}) \hat{\sigma}}{(k'^2 + x^2 + u(1-u)v_F^2 k^2 + (1-u)\omega_n'^2)^2}.
\end{aligned}$$

In the last step we shifted $\mathbf{k} \rightarrow \mathbf{k}' + uv_F \mathbf{k}$ and rescaled x and ω'_n . The \mathbf{k}' integral over the first summand vanishes as the integrand is odd, the second summand contributes

$$\begin{aligned}
\hat{\Sigma}^{(1)}(\mathbf{k}, i\omega_n) &= -\frac{\alpha T v_F \mathbf{k} \hat{\sigma}}{2} \sum_{\omega'_n} \int_{-\infty}^{\infty} \frac{dx}{\pi} \int_0^1 du \sqrt{u} \\
&\times \left(\frac{1}{\Lambda^2 + x^2 + u(1-u)v_F^2 k^2 + (1-u)\omega_n'^2} \right. \\
&\quad \left. - \frac{1}{x^2 + u(1-u)v_F^2 k^2 + (1-u)\omega_n'^2} \right) \\
&= -\frac{\alpha T v_F \mathbf{k} \hat{\sigma}}{2} \sum_{\omega'_n} \int_0^1 du \sqrt{u} \\
&\times \left(\frac{1}{\sqrt{\Lambda^2 + u(1-u)v_F^2 k^2 + (1-u)\omega_n'^2}} \right. \\
&\quad \left. - \frac{1}{\sqrt{u(1-u)v_F^2 k^2 + (1-u)\omega_n'^2}} \right). \tag{132}
\end{aligned}$$

The sum over ω'_n can only be performed analytically in the limit $T \rightarrow 0$ when one can transform the sum into an integral,

$$\begin{aligned}
\hat{\Sigma}^{(1)}(\mathbf{k}, i\omega_n) &= -\frac{\alpha v_F \mathbf{k} \hat{\sigma}}{4\pi} \int d\omega' \int_0^1 du \sqrt{\frac{u}{1-u}} \\
&\times \left(\frac{1}{\sqrt{\Lambda^2 + u(1-u)v_F^2 k^2 + \omega'^2}} - \frac{1}{\sqrt{u(1-u)v_F^2 k^2 + \omega'^2}} \right). \\
&= -\frac{\alpha v_F \mathbf{k} \hat{\sigma}}{4\pi} \int_0^1 du \sqrt{\frac{u}{1-u}} \ln \left(\frac{u(1-u)v_F^2 k^2}{\Lambda^2 + u(1-u)v_F^2 k^2} \right) \\
&\approx -\frac{\alpha v_F \mathbf{k} \hat{\sigma}}{4\pi} \int_0^1 du \sqrt{\frac{u}{1-u}} \ln \left(\frac{u(1-u)v_F^2 k^2}{\Lambda^2} \right) \\
&= \frac{\alpha v_F \mathbf{k} \hat{\sigma}}{4} \ln \left(\frac{4\Lambda}{v_F k} \right). \tag{133}
\end{aligned}$$

Now we calculate $\hat{\Sigma}^{(2)}(\mathbf{k}, i\omega_n)$. We use an integral identity and write

$$\begin{aligned}
\hat{\Sigma}^{(2)}(\mathbf{k}, i\omega_n) &= -\frac{(2\pi)^2 \alpha^2 v_F^2 T}{4} \sum_{\omega'_n} \int \frac{d^2 k'}{(2\pi)^2} \int_{-\infty}^{\infty} \frac{dx}{\pi} \\
&\times \frac{1}{x^2 + v_F^2 (\mathbf{k} - \mathbf{k}')^2 + (\omega_n - \omega'_n)^2} \frac{i\omega'_n \mathbb{1} + v_F \mathbf{k}' \hat{\sigma}}{\omega_n'^2 + v_F^2 k'^2}.
\end{aligned}$$

Using the standard Feynman parameter we can rewrite it as

$$\begin{aligned}
\hat{\Sigma}^{(2)}(\mathbf{k}, i\omega_n) &= -\pi^2 \alpha^2 v_F^2 T \sum_{\omega'_n} \int \frac{d^2 k'}{(2\pi)^2} \int_{-\infty}^{\infty} \frac{dx}{\pi} \int_0^1 du \\
&\times \frac{i\omega'_n \mathbb{1} + v_F \mathbf{k}' \hat{\sigma}}{ux^2 + v_F^2 (\mathbf{k}' - u\mathbf{k})^2 + (\omega'_n - u\omega_n)^2 + u(1-u)\Omega^2}
\end{aligned}$$

where $\Omega^2 = v_F^2 k^2 + \omega_n^2$. In the following we analyze this expression in the zero temperature limit. We note, however, that we have also analyzed the finite temperature behaviour of this expression numerically, which is discussed later. In the limit $T \rightarrow 0$ we can rewrite the expression after an appropriate shift as

$$\begin{aligned}
\hat{\Sigma}^{(2)}(\mathbf{k}, i\omega_n) &= -\pi^2 \alpha^2 v_F^2 \int \frac{d\omega'}{2\pi} \int \frac{d^2 k'}{(2\pi)^2} \int_{-\infty}^{\infty} \frac{dx}{\pi} \int_0^1 du \\
&\times \frac{(i\omega' + ui\omega_n) \mathbb{1} + v_F (\mathbf{k}' + u\mathbf{k}) \hat{\sigma}}{ux^2 + v_F^2 k'^2 + \omega'^2 + u(1-u)\Omega^2}.
\end{aligned}$$

For symmetry reasons we can simplify the expression to yield

$$\begin{aligned}
\hat{\Sigma}^{(2)}(\mathbf{k}, i\omega_n) &= -\pi^2 \alpha^2 (i\omega_n \mathbb{1} + v_F \mathbf{k} \hat{\sigma}) \int \frac{d\omega'}{2\pi} \int \frac{d^2 k'}{(2\pi)^2} \int_{-\infty}^{\infty} \frac{dx}{\pi} \int_0^1 du \\
&\times \frac{\sqrt{u}}{x^2 + k'^2 + \omega'^2 + u(1-u)\Omega^2}.
\end{aligned}$$

The integrals over k' with a cutoff Λ and ω' are elementary and we obtain

$$\begin{aligned} \hat{\Sigma}^{(2)}(\mathbf{k}, i\omega_n) &= -\frac{\alpha^2}{8}(i\omega_n\mathbb{1} + v_F\mathbf{k}\hat{\sigma}) \int_0^1 du \sqrt{u} \int_{-\infty}^{\infty} dx \\ &\times \left(\frac{1}{\sqrt{x^2 + u(1-u)\Omega^2}} - \frac{1}{\sqrt{x^2 + u(1-u)\Omega^2 + \Lambda^2}} \right). \end{aligned}$$

Integrating over x leaves us with

$$\hat{\Sigma}^{(2)}(\mathbf{k}, i\omega_n) = -\frac{\alpha^2}{8}(i\omega_n\mathbb{1} + v_F\mathbf{k}\hat{\sigma}) \int_0^1 du \sqrt{u} \ln \frac{u(1-u)\Omega^2 + \Lambda^2}{u(1-u)\Omega^2},$$

which we can integrate to give

$$\begin{aligned} \hat{\Sigma}^{(2)}(\mathbf{k}, i\omega_n) &= -\frac{\alpha^2}{8}(i\omega_n\mathbb{1} + v_F\mathbf{k}\hat{\sigma}) \int_0^1 du \sqrt{u} \ln \left(\frac{u(1-u)\Omega^2 + \Lambda^2}{u(1-u)\Omega^2} \right) \\ &= \frac{\alpha^2}{24}(i\omega_n\mathbb{1} + v_F\mathbf{k}\hat{\sigma}) \\ &\times \left[\frac{\sqrt{2}}{\Omega^{\frac{3}{2}}} \left(\left(-\Omega + \sqrt{4\Lambda^2 + \Omega^2} \right)^{3/2} \arctan \left[\frac{\sqrt{2\Omega}}{\sqrt{-\Omega + \sqrt{4\Lambda^2 + \Omega^2}}} \right] \right. \right. \\ &\quad \left. \left. + \left(-\Omega - \sqrt{4\Lambda^2 + \Omega^2} \right)^{3/2} \arctan \left[\frac{\sqrt{2\Omega}}{\sqrt{-\Omega - \sqrt{4\Lambda^2 + \Omega^2}}} \right] \right) \right. \\ &\quad \left. + 2 \ln \left[\frac{4\Omega^2}{\Lambda^2} \right] \right]. \end{aligned} \quad (134)$$

In the limit $\Omega^2 \ll \Lambda^2$ this reduces to

$$\hat{\Sigma}^{(2)}(\mathbf{k}, i\omega_n) = -\frac{\alpha^2}{2}(i\omega_n\mathbb{1} + v_F\mathbf{k}\hat{\sigma}) \left(\frac{1}{6} \ln \left(\frac{\Lambda^2 v_F^2}{k^2 v_F^2 + \omega_n^2} \right) - \frac{1}{3} \ln(2) + \frac{5}{9} \right). \quad (135)$$

In defining the Z -factors we introduced in the ansatz for the self-energy, Eq. (113), we only include the logarithmically dependent parts since the other parts are irrelevant for the flow equations. They read

$$\begin{aligned} Z^{-1} &= \left(1 + \frac{\alpha^2}{12} \ln \frac{\Lambda^2}{v_F^2 k^2 + \omega_n^2} \right) \\ Z_{v_F} &= \left(1 + \frac{\alpha}{4} \ln \frac{4\Lambda}{v_F k} - \frac{\alpha^2}{12} \ln \frac{\Lambda^2}{v_F^2 k^2 + \omega_n^2} \right). \end{aligned} \quad (136)$$

While Z corresponds to the field renormalization, Z_{v_F} can be identified with the renormalization factor of the Fermi velocity. This implies that the Green function reads

$$\hat{G}^{-1}(\mathbf{k}, i\omega_n) = Z^{-1}(i\omega\mathbb{1} + Z\mu\mathbb{1} - v_F\mathbf{k}\hat{\sigma}ZZ_{v_F}) \quad (137)$$

and consequently we can define a renormalized Fermi velocity v_F^R as

$$v_F^R = v_F Z Z_{v_F}, \quad (138)$$

where v_F is the bare Fermi velocity. The calculation was performed within bare perturbation theory. In order to derive the flow equation we add a counter term in Z_{v_F} which is present in the renormalized perturbation theory. This counter term reads

$$\frac{\alpha^2}{16} \ln^2 \frac{4\Lambda}{v_F k}. \quad (139)$$

Exploiting $\frac{dv_F}{d \ln \Lambda} = 0$ we obtain the flow of the renormalized Fermi velocity as

$$\begin{aligned} \frac{dv_F^R}{d \ln \Lambda} &= v_F \left(\frac{\partial ZZ_{v_F}}{\partial \ln \Lambda} + \frac{\partial ZZ_{v_F}}{\partial \alpha} \frac{\partial \alpha}{\partial v_F^R} \frac{\partial v_F^R}{\partial \ln \Lambda} \right) \\ &= \frac{v_F^R}{ZZ_{v_F}} \left(\frac{\partial ZZ_{v_F}}{\partial \ln \Lambda} - \frac{\alpha}{ZZ_{v_F}} \frac{\partial ZZ_{v_F}}{\partial \alpha} \frac{\partial ZZ_{v_F}}{\partial \ln \Lambda} \right) \\ &= v_F^R \left(\frac{\alpha}{4} - \frac{\alpha^2}{3} \right) + \mathcal{O}(\alpha^3). \end{aligned} \quad (140)$$

The flow of α itself to lowest order in perturbation theory (one-loop) is given by $\frac{d\alpha}{d \ln \Lambda} = -\frac{\alpha^2}{4} + \mathcal{O}(\alpha^3)$. The flow equation implies a critical $\alpha_c = 3/4$, which potentially describes a repulsive critical point from weak coupling to strong coupling. However, in a strict large- N limit to all orders in α the absence of such a critical point was shown by Son in Ref. [36], meaning that the critical point most likely is an artefact of the order of approximation.

For additional effects of inelastic scattering we have also investigated $\hat{\Sigma}^{(2)}$ at finite temperatures. Here, we concentrate our discussion on the diagonal part of $\hat{\Sigma}^{(2)}$, called $\delta\Sigma'' = \Sigma_{\text{diag}}^{(2)}(T) - \Sigma_{\text{diag}}^{(2)}(T=0)$, which enters the amplitude and frequency of the oscillation, see Eq. (122), and was introduced in the ansatz for the self energy (113). We have found that

$$\delta\Sigma''(\mathbf{k}, \omega_n) = -\frac{\alpha^2 \pi \ln 2}{12} \omega_n \left(\frac{T^2}{\omega_n^2 + v_F^2 k^2} + \mathcal{O} \left\{ \left(\frac{T^2}{\omega_n^2 + v_F^2 k^2} \right)^2 \right\} \right). \quad (141)$$

A discussion of the results follows in the next chapter.

DISCUSSION AND SUMMARY

In this chapter we will give an overview of our main results and compare our findings for graphene to the two-dimensional electron gas. Further we will discuss an experiment where the LK-formula was applied and we will analyse our results. We will give an outlook at the end of the chapter.

6.1 COMPARISON OF THE DHVA-OSCILLATIONS: GRAPHENE VS. 2DEG

First we will discuss the different energy scales of the two systems and their consequences. Thereby we will set $\hbar \equiv 1$ and $k_B \equiv 1$, and the used unit for the energy is Kelvin (K). Thereafter we will compare the Lifshitz-Kosevich formula for graphene to that for the 2DEG, for clean, disordered, and interacting systems. However, we did not study the combined effect of disorder and interactions.

6.1.1 *Energy scales*

In Table 1 we contrast the energy characteristics of graphene which were derived in the introductory Chapter 2 with those of the two-dimensional electron gas. Graphene's linear dispersion leads to different energy scales in a magnetic field, compared to the 2DEG with its quadratic dispersion. The energy of the Landau levels does not depend linearly on the Landau level index but goes with its square root. Thus the Landau levels are not equally spaced but get closer with higher energy. As a consequence, phenomena which are negligible when the electrons in the system only occupy low Landau levels might become important when higher Landau levels are also occupied. For example, the Zeeman effect, which we neglected throughout the thesis, leads to an energy splitting for different spin species according to $E = \pm \vec{\mu} \vec{B}$, where $\vec{\mu}$ is the magnetic moment of spin-up electrons and $-\vec{\mu}$ that for spin-down electrons. For example at a magnetic field of $B = 0.1$ T it becomes important when Landau levels with index $n \approx 10000$ are occupied. Also the cyclotron frequency ω_c , which is linear in the magnetic field for the 2DEG, depends on the square root of the magnetic field in graphene. For the common magnetic fields and temperatures at which experiments are performed, $\omega_c \ll T$ holds in the 2DEG. But due to the different B -dependence of ω_c in graphene, $\omega_c \sim T$ applies for the same experimental parameters. An example is given in the last two lines of Table 1.

TABLE 1: Energy scales

	2DEG	Graphene
Dispersion	$E = \frac{k^2}{2m}$	$E = \pm v_F k$
Landau levels	$E_n = \omega_c (n + \frac{1}{2})$	$E_{n,\pm} = \pm \omega_c \sqrt{n}$
cyclotron frequency	$\omega_c = \frac{eB}{m}$	$\omega_c = v_F \sqrt{2eB}$
$B = 0.01$ T	$\omega_c \approx 0.01$ K	$\omega_c \approx 30$ K
$B = 0.1$ T	$\omega_c \approx 0.1$ K	$\omega_c \approx 100$ K

6.1.2 The Lifshitz-Kosevich formula in a clean system

In Table 2 we contrast the Lifshitz-Kosevich formula for the 2DEG and for graphene without disorder or interaction effects. The most striking difference is the limited sum. The oscillations in graphene die as soon as $\pi T > \mu$. The other noticeable difference in graphene's magnetic oscillations is the dependence of the frequency on the temperature through ω_n . This also has strong consequences if temperature becomes comparable to the chemical potential, which in contrast to metals is easily achievable in graphene.

TABLE 2: The LK-formula in a clean system

2DEG	$\tilde{\Omega}_{osc} = 4\nu\omega_c T \sum_{l=1}^{\infty} \sum_{\omega_n > 0}^{\infty} \frac{(-1)^l}{l} e^{-\frac{2\pi l \omega_n}{\omega_c}} \cos\left(\frac{2\pi l \mu}{eB}\right)$
Graphene	$\tilde{\Omega}_{osc} = \frac{2T\omega_c^2 L^2}{\pi v_F^2} \sum_{l=1}^{\infty} \sum_{\omega_n > 0}^{\infty} \frac{1}{l} e^{-\frac{4\pi l \omega_n \mu }{\omega_c^2}} \cos\left(\frac{2\pi l (\mu^2 - \omega_n^2)}{\omega_c^2}\right)$

6.1.3 The Lifshitz-Kosevich formula in a disordered system

In this section we will discuss the effect of disorder on the oscillations in graphene and compare this effect to that discussed in Section 4.1.1.2 for the 2DEG.

In Table 3 we contrast the LK-formula with disorder for graphene and the 2DEG. Again, we see, that in contrast to the oscillations in the 2DEG, the oscillations in graphene die above a characteristic temperature T_{osc} . This temperature depends on the strength α_{dis} of the scattering potential and is given by $\pi T_{osc} = \frac{|\mu|}{1 + \alpha_{dis} \frac{\pi}{2}}$. Disorder in graphene, unlike in the 2DEG, also affects the oscillation frequency.

In Section 4.1.1.2 we introduced the Dingle temperature T_D , which expresses the damping of the amplitude due to disorder. In Table 3 we specify the Dingle temperature for the 2DEG as well as for graphene. In graphene the Dingle temperature depends on the chemical potential and on the temperature, unlike in the 2DEG.

TABLE 3: The LK-formula in a disordered system

$$\begin{aligned}
\mathbf{2DEG} \quad \tilde{\Omega}_{osc} &= 4\nu\omega_c T \sum_{l=1}^{\infty} \sum_{\omega_n > 0} \frac{(-1)^l}{l} e^{-\frac{2\pi l}{\omega_c}(\omega_n + \frac{1}{2\tau})} \cos\left(\frac{2\pi l \mu}{eB}\right) \\
T_D &= \frac{1}{2\pi\tau} \\
\mathbf{Graphene} \quad \tilde{\Omega}_{osc} &= -\frac{2T\omega_c^2 L^2}{\pi v_F^2} \sum_{l=1}^{\infty} \frac{1}{l} \sum_{\omega_n > 0}^{\frac{|\mu|}{1+\alpha\frac{\tau}{2}}} e^{-\frac{4\pi l}{\omega_c}((\mu^2 - \omega_n^2)(\pi\alpha - 2\phi\alpha) + |\mu|\omega_n(1+2\alpha\Gamma))} \\
&\quad \times \cos\left(\frac{2\pi l}{\omega_c}((\mu^2 - \omega_n^2)(1+2\alpha\Gamma) - 4\alpha|\mu|\omega_n(\pi - 2\phi))\right) \\
T_D &= \omega_n \left(\frac{(\mu^2 - \omega_n^2)}{|\mu|\omega_n} (\pi\alpha - 2\phi\alpha) + 2\alpha\Gamma \right) \\
T_D(T=0) &= |\mu|\pi\alpha
\end{aligned}$$

6.1.4 The effect of electron-electron interactions on the Lifshitz-Kosevich formula

TABLE 4: The LK-formula with electron-electron interactions

$$\begin{aligned}
\mathbf{2DEG} \quad \tilde{\Omega}_{osc} &= -2DT \sum_{\omega_n > 0} \sum_{l=1}^{\infty} \frac{1}{l} e^{-\frac{2\pi l(\omega_n(1+\alpha_0) - \delta\Sigma'')}{\omega_c(1+\beta)}} \cos\left(\frac{2\pi l \tilde{\mu}}{\omega_c(1+\beta)}\right) \\
\mathbf{Graphene} \quad \tilde{\Omega}_{osc} &= 2DT \sum_{l=1}^{\infty} \frac{1}{l} \sum_{\omega_n > 0}^{\approx|\mu|} \\
&\quad \times e^{-\frac{4\pi l}{\omega_c^2 Z v_F^2}(\omega_n Z^{-1} \mu + (\Im\{\delta\Sigma''\} + \Re\{\delta\Sigma'\})\omega_n Z^{-1} + (\Im\{\delta\Sigma'\} - \Re\{\delta\Sigma''\})\mu)} \\
&\quad \times \cos\left(\frac{2\pi l}{\omega_c^2 Z v_F^2} \left(-\omega_n^2 Z^{-2} + \mu^2 + 2(\Re\{\delta\Sigma''\} - \Im\{\delta\Sigma'\})\omega_n Z^{-1} \right. \right. \\
&\quad \left. \left. + 2(\Im\{\delta\Sigma''\} + \Re\{\delta\Sigma'\})\mu \right)\right)
\end{aligned}$$

We have derived the LK-formula for weak interactions in both, the 2DEG and graphene, see Table 4. One of the main features of the 2DEG is that in-

elastic processes on the first Matsubara mode do not lead to an additional damping, since $\delta\Sigma''$ vanishes on the first Matsubara mode. (see Eq. (112)) This implies that interaction effects can fully be absorbed in renormalization factors.

The situation is different in graphene. Here, both inelastic effects as well as renormalization effects influence the amplitude. The inelastic effects are expressed by $\delta\Sigma'(x_0^{(0)}, i\omega_n)$ and $\delta\Sigma''(x_0^{(0)}, i\omega_n)$. The latter is given by (cf. Eq. (141))

$$\delta\Sigma''(x_0^{(0)}, i\omega_n) = -\frac{\alpha^2\pi\ln 2}{12}\omega_n\left(\frac{T^2}{\omega_n^2(1-Z^{-2})+\mu^2+2i\omega_nZ^{-1}\mu}\right) + \mathcal{O}\left\{\left(\frac{T^2}{\omega_n^2(1-Z^{-2})+\mu^2+2i\omega_nZ^{-1}\mu}\right)^2\right\}. \quad (142)$$

However, unlike in the case of disorder, the inelastic effects vanish for zero temperature.

Another interesting property is that the dominant damping term

$$e^{-\frac{4\pi l}{\omega_c^2 Z v_F^2}\omega_n Z^{-1}\mu} \quad (143)$$

cannot fully be accounted for by renormalizations of the Fermi velocity, since it goes like $\frac{1}{\omega_c^2 Z v_F^2}$ instead of $\frac{1}{\omega_c^2 Z v_F^{*2}}$, which would be required for that. So this result is in contrast to a recent analysis, where this has tacitly been assumed [12] and which we will discuss in the following section.

6.2 APPLICATION OF THE LIFSHITZ-KOSEVICH FORMULA

In the Nature article by Elias *et. al.* [12] the authors report their experimental finding on how electron-electron interactions in graphene renormalize the Fermi velocity $v_F \rightarrow v_F^*$. They find a momentum dependent renormalized Fermi velocity $v_F^*(k)$ which reshapes the Dirac cone.

In their experiment, Shubnikov-de Haas (SdH) oscillations in graphene are measured as a function of temperature T . These oscillations in the conductivity of graphene in a magnetic field are usually also described by the Lifshitz-Kosevich formula. By fitting the first harmonic $l = 1$ of the LK-formula (57) for the two-dimensional electron gas,

$$A_1 \sim \frac{T}{2\sinh\left(\frac{2\pi^2 T m_c^*}{\hbar e B}\right)}, \quad (144)$$

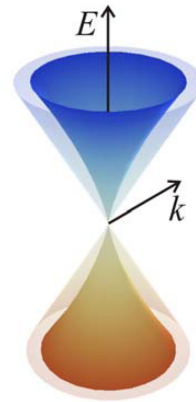


FIGURE 12: Dirac cone reshaped by electron-electron interactions as reported in Ref. [12].

to the measured amplitude, the effective mass m^* is extracted. It is related to the effective Fermi velocity v_F^* via

$$m_c^* = \frac{\hbar\sqrt{\pi n}}{v_F^*} = \frac{\mu}{v_F^{*2}}. \quad (145)$$

By repeating this procedure for different doping levels (meaning different momenta), a momentum-dependent effective mass is obtained. The analysis of the experimental data suggests a logarithmic renormalization of the Fermi velocity, caused by electron-electron interactions,

$$v_F^*(k) \sim \ln k. \quad (146)$$

The reshaped Dirac cone is plotted in Figure 12. As a consequence, electron-electron interactions effectively reduce the density of states at low energies. In the experiment the doping level, embodied by the electron and hole concentrations, n_e and n_h , respectively, is varied between $|n| \sim 10^9 \text{ cm}^{-2}$ and $|n| \sim 10^{12} \text{ cm}^{-2}$. The chemical potential μ is related to the particle concentration via $\mu = \hbar\sqrt{\pi n}v_F$. Thus we find $40 \text{ K} < |\mu| < 1400 \text{ K}$ (for $v_F = 10^6$). The magnetic field is varied from $B \approx 0.01 \text{ T}$ to $B \approx 0.1 \text{ T}$ and the temperature regime of the measurements is $0 \text{ K} < T < 60 \text{ K}$. With these parameters we find

$$\begin{aligned} \mu &\gtrsim T \\ \omega_c &\sim T, \end{aligned} \quad (147)$$

meaning in the experiment the non-Fermi liquid regime of graphene is reached. From our analysis we can say that the statement that a renormalization of v_F is the only damping effect due to electron-electron interactions is only true to one-loop order. Our two-loop calculation of the self-energy in Chapter 5 shows that electron-electron interactions in graphene also lead to inelastic processes, see Eq. (142) as well as field renormalization effects, see Eq. (143). Furthermore the frequency of the oscillations is also affected by temperature, impurity scattering and interactions, as seen in Table 3, 2, and 4. However, it should be mentioned that it is not clear to what extent our analysis for dHvA-oscillations also applies to Shubnikov - de Haas oscillations.

6.3 OUTLOOK

From the theoretical point of view it would be interesting to also study the interplay of electron-electron interactions and impurity scattering. In the two-dimensional electron gas this coupling was studied in Ref. [2]. The authors find that in the diffusive regime the electron mass is renormalized, meaning that impurity scattering does not change qualitatively the effect of electron-electron interactions on the amplitude of the dHvA-oscillations. As we found additional damping effects due to electron-electron interactions in graphene, it would be interesting to see how impurity scattering influences this result, meaning if our results still hold in the diffusive regime of graphene.

On the experimental side there are so far no reported experimental investigations of the dHvA-effect in graphene. In Section 6.2 we compare our results to the measurements of Shubnikov de - Haas oscillations, as they were performed in Ref. [12]. Usually these oscillations in the conductivity are also described using the LK-formula derived for dHvA-oscillations, since the derivation of the oscillating conductivity is more sophisticated and there are so far no theoretical descriptions which also include the effect of electron-electron interactions. (Theoretical work on SdH-oscillations neglecting any interaction effects can be found in Ref. [37] for graphene and in Refs. [38, 39] for the 2DEG.) However, it is not clear to what extent the LK-formula for dHvA-oscillations describes the oscillations in the conductivity well.

APPENDIX

A.1 COMPUTATION OF THE OSCILLATORY PART OF THE SELF-ENERGY DUE TO DISORDER

In this section we will derive an analytic expression for the oscillatory part of the disorder induced self-energy defined in Eq. (85).

$$\begin{aligned}
 \Sigma^{osc} &= \alpha_{\text{dis}}(i\omega_n + \mu - \Sigma) \sum_{l=1}^{\infty} \int_0^{\infty} dx \frac{\cos\left(\frac{2\pi lx}{\omega_c^2}\right)}{(i\omega_n + \mu - \Sigma)^2 - x} \\
 &= \alpha_{\text{dis}}(i\omega_n + \mu - \Sigma) \sum_{l=1}^{\infty} \left[\frac{\omega_c^2}{2\pi l} \sin\left(\frac{2\pi l x}{\omega_c^2}\right) \frac{1}{(i\omega_n + \mu - \Sigma)^2 - x} \right]_0^{\infty} \\
 &= \alpha_{\text{dis}} \frac{\omega_c^2}{2\pi} (i\omega_n + \mu - \Sigma) \sum_{l=1}^{\infty} \int_0^{\infty} dx \frac{1}{l} \frac{\sin\left(\frac{2\pi lx}{\omega_c^2}\right)}{([i\omega_n + \mu - \Sigma]^2 - x)^2},
 \end{aligned} \tag{148}$$

where we integrated by parts. Now we will first compute the sum over l , yielding

$$\begin{aligned}
 \sum_{l=1}^{\infty} \frac{\sin\left(\frac{2\pi lx}{\omega_c^2}\right)}{l} &= -\frac{1}{2} i (\ln e^{i\frac{2\pi x}{\omega_c^2}} + \ln(-1)) = \frac{1}{2} \left(\frac{2\pi x}{\omega_c^2} \text{mod}(2\pi) + \pi \right) \\
 &= \frac{1}{2} \left(\frac{2\pi}{\omega_c^2} (x \text{mod}(\omega_c^2)) + \pi \right).
 \end{aligned} \tag{149}$$

Now we use this expression to solve the integral,

$$\begin{aligned}
 &\int_0^{\infty} dx \frac{\frac{1}{2} \left(\frac{2\pi}{\omega_c^2} (x \text{mod}(\omega_c^2)) + \pi \right)}{([i\omega_n + \mu - \Sigma]^2 - x)^2} \\
 &= \frac{1}{2} \sum_{n=0}^{\infty} \int_0^{\omega_c^2} dx \frac{\frac{2\pi x}{\omega_c^2} + \pi}{([i\omega_n + \mu - \Sigma]^2 - x - n\omega_c^2)^2} \\
 &= \frac{1}{2\omega_c^2} \sum_{n=0}^{\infty} \int_0^1 dx \frac{2\pi x + \pi}{\left[\frac{(i\omega_n + \mu - \Sigma)^2}{\omega_c^2} - x - n \right]^2} \\
 &= \frac{\pi}{2\omega_c^2} \int_0^1 dx \text{Poly}\Gamma\left[1, x - \frac{(i\omega_n + \mu - \Sigma)^2}{\omega_c^2}\right] (1 - 2x) \\
 &= -\frac{\pi}{2(i\omega_n + \mu - \Sigma)^2} + \frac{\pi}{\omega_c^2} \left(\gamma - \sum_{k=0}^{\frac{(i\omega_n + \mu - \Sigma)^2}{\omega_c^2}} \frac{1}{k} + \ln\left[-\frac{(i\omega_n + \mu - \Sigma)^2}{\omega_c^2}\right] \right),
 \end{aligned} \tag{150}$$

where γ is Euler's constant. Thus we obtain the following expression for Σ^{osc} ,

$$\Sigma^{osc} = \frac{\alpha_{\text{dis}}}{2} \left(\frac{\omega_c^2}{2(i\omega_n + \mu - \Sigma)} - (i\omega_n + \mu - \Sigma) \left(\gamma - \sum_{k=0}^{\frac{(i\omega_n + \mu - \Sigma)^2}{\omega_c^2}} \frac{1}{k} + \ln \left[-\frac{(i\omega_n + \mu - \Sigma)^2}{\omega_c^2} \right] \right) \right). \quad (151)$$

A.2 THE GRAND POTENTIAL FOR DISORDERED GRAPHENE IN A MAGNETIC FIELD

In this section we will compute the oscillatory potential for disordered graphene. The corresponding self-energy Σ_{dis} is given by Eq. (89).

$$\tilde{\Omega} = \frac{T\omega_c^4 L^2}{\pi^2 v_F^2} \sum_{\omega_n} \sum_{l=1}^{\infty} \frac{1}{l} \int_0^{\infty} dx \frac{\sin(2\pi lx)}{[i\omega_n + \mu - \Sigma_{\text{dis}}(i\omega_n)]^2 - \omega_c^2 x}. \quad (152)$$

In order to evaluate the integral using residue theorem the location of the pole needs to be known. For this purpose we split the sum over ω_n , such that we have $\omega_n > 0$ from now on:

$$\tilde{\Omega} = \frac{T\omega_c^4 L^2}{\pi^2 v_F^2} \sum_{\omega_n > 0} \sum_{l=1}^{\infty} \frac{1}{l} \int_0^{\infty} dx \frac{\sin(2\pi lx)}{[i\omega_n + \mu - \Sigma_{\text{dis}}(i\omega_n)]^2 - \omega_c^2 x} + \frac{\sin(2\pi lx)}{[-i\omega_n + \mu - \Sigma_{\text{dis}}(-i\omega_n)]^2 - \omega_c^2 x}. \quad (153)$$

In the following we assume $\mu > 0$. For $\mu < 0$ it is expedient to sum over negative ω_n , i.e. to use the identity $\sum_{\omega_n} F(\omega_n) = \sum_{\omega_n < 0} (F(-\omega_n) + F(\omega_n))$. The two poles read

$$x_1 = \frac{1}{\omega_c^2} [i\omega_n + \mu - \Sigma_{\text{dis}}(i\omega_n)]^2 \quad (154)$$

$$x_2 = \frac{1}{\omega_c^2} [-i\omega_n + \mu - \Sigma_{\text{dis}}(-i\omega_n)]^2. \quad (155)$$

Here, we only perform the calculation for the first pole. The location of the second pole can be computed analogously.

First we will simplify the expression (89) for the self-energy

$$\begin{aligned} \Sigma_{\text{dis}}(i\omega_n) &\approx -\alpha_{\text{dis}}(i\omega_n + \mu) \ln \left(\frac{v_F^2 \Lambda^2}{-(i\omega_n + \mu)^2} \right) \\ &= -\alpha_{\text{dis}}(i\omega_n + \mu) \ln \left(\frac{e^{i\pi} v_F^2 \Lambda^2}{(\omega_n^2 + \mu^2) e^{2i\Phi}} \right) \\ &= -\alpha_{\text{dis}}(i\omega_n + \mu) (\Gamma + i\pi - 2i\phi) \end{aligned} \quad (156)$$

$$\text{with } \Gamma = \ln \left(\frac{(v_F \Lambda)^2}{\omega_n^2 + \mu^2} \right) \quad \text{and} \quad \phi = \arctan \left(\frac{\omega_n}{\mu} \right). \quad (157)$$

If we insert expression (156) for the self-energy into Eq. (154) we obtain

$$x_1 = \frac{1}{\omega_c^2} (i\omega_n + \mu)^2 (1 + \alpha_{\text{dis}} \Gamma + i\alpha_{\text{dis}} (\pi - 2\phi))^2. \quad (158)$$

We expand the pole to linear order in α_{dis} as we are interested in a weak disorder potential,

$$\begin{aligned} \omega_c^2 x_1 &\approx (\mu^2 - \omega_n^2) (1 + 2\alpha_{\text{dis}} \Gamma) - 4\alpha_{\text{dis}} \omega_n \mu (\pi - 2\phi) \\ &+ i2 \left(\omega_n \mu (1 + 2\alpha_{\text{dis}} \Gamma) + \alpha_{\text{dis}} (\mu^2 - \omega_n^2) (\pi - 2\phi) \right). \end{aligned} \quad (159)$$

In order to find the zero-crossing of the real part we use the ansatz $\mu = \omega_n + \delta\mu$ and expand again the real part up to first order in α_{dis} whereupon we assume that $\delta\mu$ is linear in α_{dis} .

$$(\mu^2 - \omega_n^2)(1 + 2\alpha_{\text{dis}}\Gamma) - 4\alpha_{\text{dis}}\omega_n\mu(\pi - 2\phi) \approx 2\omega_n\delta\mu - 4\alpha_{\text{dis}}\omega_n^2(\pi - 2\phi) \stackrel{!}{=} 0.$$

With $\phi = \arctan\left(\frac{\omega_n}{\omega_n + \delta\mu}\right) \approx \arctan(1) = \frac{\pi}{4}$ we get as a condition for the zero,

$$\delta\mu_0 = \alpha_{\text{dis}}\omega_n\pi \quad \Rightarrow \quad \mu_0 = \omega_n(1 + \alpha_{\text{dis}}\pi). \quad (160)$$

Hence the pole is located within our range of integration only for frequencies $\omega_n < \frac{\mu}{1 + \alpha_{\text{dis}}\pi}$. (We find the same condition for the second pole x_2 .) The imaginary part of the pole, see Eq. (159), is larger than zero. Thus the pole is located in the first quadrant. With this information we now can apply residue theorem to compute the integral,

$$\begin{aligned} & \int_0^\infty dx \frac{\sin(2\pi lx)}{[i\omega_n + \mu - \Sigma_{\text{dis}}(i\omega_n)]^2 - \omega_c^2 x} \\ &= \frac{1}{2i} \int_0^\infty dx \frac{e^{i2\pi lx}}{[i\omega_n + \mu - \Sigma_{\text{dis}}(i\omega_n)]^2 - \omega_c^2 x} \\ &- \frac{1}{2i} \int_0^\infty dx \frac{e^{-i2\pi lx}}{[i\omega_n + \mu - \Sigma_{\text{dis}}(i\omega_n)]^2 - \omega_c^2 x} = I_1 + I_2. \end{aligned} \quad (161)$$

The integration path is plotted in Figure 11. For the integral I_1 we use path c_1 since $e^{i2\pi lx}$ vanishes for $x \rightarrow i\infty$. This path contains the pole.

$$\begin{aligned} I_1 &= \frac{1}{2i} \int_0^\infty dx \frac{e^{i2\pi lx}}{[i\omega_n + \mu - \Sigma_{\text{dis}}(i\omega_n)]^2 - \omega_c^2 x} = \\ &- \frac{1}{2i} \int_{i\infty}^0 dx \frac{e^{i2\pi lx}}{[i\omega_n + \mu - \Sigma_{\text{dis}}(i\omega_n)]^2 - \omega_c^2 x} \\ &+ \frac{1}{2i} 2\pi i \sum_{\omega_n}^{\frac{\mu}{1 + \alpha_{\text{dis}}\pi}} \left(\frac{1}{-\omega_c^2} \right) e^{\frac{i2\pi l}{\omega_c^2} (i\omega_n + \mu - \Sigma_{\text{dis}}(i\omega_n))^2}. \end{aligned}$$

In the first term we substitute $y = -ix$ and in the second term we part the self-energy Σ_{dis} into a real part Σ'_{dis} and an imaginary part Σ''_{dis} ,

$$I_1 = \frac{1}{2} \int_0^\infty dy \frac{e^{-2\pi ly}}{[i\omega_n + \mu - \Sigma_{\text{dis}}(i\omega_n)]^2 - \omega_c^2 iy} \quad (162)$$

$$- \frac{\pi}{\omega_c^2} \sum_{\omega_n}^{\frac{\mu}{1 + \alpha_{\text{dis}}\pi}} e^{\frac{i2\pi l}{\omega_c^2} ((\mu - \Sigma'_{\text{dis}})^2 - (\omega_n - \Sigma''_{\text{dis}})^2)} e^{-\frac{4\pi l}{\omega_c^2} (\mu - \Sigma'_{\text{dis}})(\omega_n - \Sigma''_{\text{dis}})}. \quad (163)$$

The first term is a non-oscillatory correction term. Now we simplify the oscillatory part \tilde{I}_1 . We only keep terms linear in α_{dis} . We consider the self-energy (156) and split it into a real and an imaginary part:

$$\begin{aligned}\Sigma_{\text{dis}} &= -\alpha_{\text{dis}}(i\omega_n + \mu)(\ln \Gamma + i\pi - 2i\phi) \\ &= \alpha_{\text{dis}}(-\mu \ln \Gamma + \omega_n(\pi - 2\phi)) - i\alpha_{\text{dis}}(\omega_n \ln \Gamma + \mu(\pi - 2\phi)) \\ &= \Sigma'_{\text{dis}} + i\Sigma''_{\text{dis}}.\end{aligned}\quad (164)$$

We see that Σ'_{dis} and Σ''_{dis} are both linear in α_{dis} . Thus the oscillatory part in Eq. (163) simplifies to

$$\tilde{I}_1 = -\frac{\pi}{\omega_c^2} \sum_{\omega_n} \frac{\mu}{1+\alpha_{\text{dis}}\pi} e^{\frac{i2\pi l}{\omega_c^2}(\mu^2 - 2\mu\Sigma'_{\text{dis}} - \omega_n^2 + 2\omega_n\Sigma''_{\text{dis}})} e^{-\frac{4\pi l}{\omega_c^2}(\mu\omega_n - \mu\Sigma''_{\text{dis}} - \omega_n\Sigma'_{\text{dis}})}. \quad (165)$$

Now we examine integral I_2 defined in Eq. (161) using residue theorem. We use the integration contour c_2 as $e^{-i2\pi lx}$ vanishes for $x \rightarrow -i\infty$,

$$\begin{aligned}I_2 &= -\frac{1}{2i} \int_0^\infty dx \frac{e^{-i2\pi lx}}{[i\omega_n + \mu - \Sigma_{\text{dis}}(i\omega_n)]^2 - \omega_c^2 x} \\ &= \frac{1}{2i} \int_{-i\infty}^0 dx \frac{e^{-i2\pi lx}}{[i\omega_n + \mu - \Sigma_{\text{dis}}(i\omega_n)]^2 - \omega_c^2 x} \\ &= \frac{1}{2} \int_0^\infty dx \frac{e^{-2\pi ly}}{[i\omega_n + \mu - \Sigma_{\text{dis}}(i\omega_n)]^2 + \omega_c^2 iy},\end{aligned}\quad (166)$$

where we have used the substitution $y = ix$.

Now we add our results Eq. (162), Eq. (163) and Eq. (166) and obtain

$$\begin{aligned}& \int_0^\infty dx \frac{\sin(2\pi lx)}{[i\omega_n + \mu - \Sigma_{\text{dis}}(i\omega_n)]^2 - \omega_c^2 x} \\ &= \frac{1}{2} \int_0^\infty dy e^{-2\pi ly} \left(\frac{1}{[i\omega_n + \mu - \Sigma_{\text{dis}}(i\omega_n)]^2 + \omega_c^2 iy} \right. \\ & \quad \left. + \frac{1}{[i\omega_n + \mu - \Sigma_{\text{dis}}(i\omega_n)]^2 - \omega_c^2 iy} \right) \\ &= \frac{\pi}{\omega_c^2} \sum_{\omega_n} \frac{\mu}{1+\alpha_{\text{dis}}\pi} e^{\frac{i2\pi l}{\omega_c^2}(\mu^2 - 2\mu\Sigma'_{\text{dis}} - \omega_n^2 + 2\omega_n\Sigma''_{\text{dis}})} e^{-\frac{4\pi l}{\omega_c^2}(\mu\omega_n - \mu\Sigma''_{\text{dis}} - \omega_n\Sigma'_{\text{dis}})}.\end{aligned}\quad (167)$$

We also performed the analogue calculation, steps (156) to (167), for the second term in Eq. (153) which depends on $\Sigma_{\text{dis}}(-i\omega_n)$. Merging the two results we gain the following expression,

$$\begin{aligned}
\tilde{\Omega} &= \frac{T\omega_c^4 L^2}{\pi^2 v_F^2} \sum_{l=1}^{\infty} \frac{1}{l} \sum_{\omega_n > 0} \int_0^{\infty} dx e^{-2\pi l x} \left((\mu + \Sigma'_{\text{dis}})^2 - (\omega_n - \Sigma''_{\text{dis}})^2 \right) \\
&\times \left(\frac{1}{((\mu + \Sigma'_{\text{dis}})^2 - (\omega_n - \Sigma''_{\text{dis}})^2)^2 + (2(\mu + \Sigma'_{\text{dis}})(\omega_n - \Sigma''_{\text{dis}}) + \omega_c^2 x)} \right. \\
&+ \left. \frac{1}{((\mu + \Sigma'_{\text{dis}})^2 - (\omega_n - \Sigma''_{\text{dis}})^2)^2 + (2(\mu + \Sigma'_{\text{dis}})(\omega_n - \Sigma''_{\text{dis}}) - \omega_c^2 x)} \right) \\
&- \frac{T\omega_c^2 L^2}{\pi v_F^2} \sum_{l=1}^{\infty} \frac{1}{l} \sum_{\omega_n > 0} e^{-\frac{\mu}{1+\alpha_{\text{dis}}\pi}} e^{-\frac{4\pi l}{\omega_c^2}(\mu\omega_n - \mu\Sigma'_{\text{dis}} - \omega_n\Sigma'_{\text{dis}})} \\
&\times 2 \cos \left(\frac{2\pi l}{\omega_c^2} (\mu^2 - 2\mu\Sigma'_{\text{dis}} - \omega_n^2 + 2\omega_n\Sigma''_{\text{dis}}) \right). \tag{168}
\end{aligned}$$

We now see that the non-oscillatory correction terms are real and finite because of the factor $e^{-2\pi l x}$. We insert the expression for the self-energy defined in Eq. (164) and generalize our result to negative chemical potentials,

$$\begin{aligned}
\tilde{\Omega}_{\text{osc}} &= \frac{2T\omega_c^2 L^2}{\pi v_F^2} \sum_{l=1}^{\infty} \frac{1}{l} \sum_{\omega_n > 0} e^{-\frac{|\mu|}{1+\alpha_{\text{dis}}\frac{\pi}{2}}} e^{-\frac{4\pi l}{\omega_c^2}((\mu^2 - \omega_n^2)(\pi\alpha_{\text{dis}} - 2\phi\alpha_{\text{dis}}) + |\mu|\omega_n(1 + 2\alpha_{\text{dis}}\Gamma))} \\
&\times \cos \left(\frac{2\pi l}{\omega_c^2} \left((\mu^2 - \omega_n^2)(1 + 2\alpha_{\text{dis}}\Gamma) - 4\alpha_{\text{dis}}|\mu|\omega_n(\pi - 2\phi) \right) \right). \tag{169}
\end{aligned}$$

Part II

SHEAR VISCOSITY AND SPIN DIFFUSION IN A
TWO-DIMENSIONAL FERMI GAS

MOTIVATION

Transport properties provide particularly valuable probes which can reveal the nature and strength of the effective interaction between particles. The shear viscosity η , e.g., measures the internal friction in a quantum fluid, which is lowest for strongly interacting systems. For certain relativistic gauge theories the ratio of the shear viscosity to the entropy density s has been computed using the AdS/CFT correspondence and takes the value $(\eta/s)_{\min} = \hbar/(4\pi k_B)$ [7]. It has been conjectured that this value provides a lower bound also for a wider class of relativistic field theories [6], and quantum fluids which saturate this bound are therefore regarded as 'perfect fluids' [40]. Quantum fluids ranging from (non-relativistic) ultracold atoms to (relativistic) quark-gluon plasmas have been investigated in the search for such a perfect fluid [40]. In the solid state context, the viscosity of graphene layers has been shown to decrease logarithmically with increasing temperature [41] coming reasonably close to the lower limit. Another example is the viscosity of the unitary Fermi gas in three dimensions which has been measured [42, 43, 44] and again comes rather close to the hypothetical bound for temperatures below the Fermi temperature. This is in agreement with calculations based on kinetic theory for low [45, 46, 47] and high temperatures [48, 49, 50, 51]. These calculations have been confirmed and refined in approaches based on the Kubo formula with self-energy [52] and full vertex corrections [53] and recently also in the form of a Quantum Monte Carlo simulation [54]. Measurements for a trapped two-dimensional Fermi gas with strong interactions have found the viscosity to decrease with decreasing temperature and increasing interaction strength. [3]

The quantum limit for the spin diffusion coefficient, $D \sim \hbar/m$, has also been predicted to provide a similar lower bound for spin diffusion in any system [55]. Measurements of the spin diffusion coefficient for the three-dimensional Fermi gas [56, 57] come close to this lower bound and are in good agreement with calculations based on kinetic theory [56, 55].

Since in two dimensions the effect of interactions is stronger, one expects the transport coefficients to be even smaller than in three dimensions.

Ultracold atoms have emerged as a versatile system to study quantum effects in strongly interacting fermionic and bosonic many-body systems [58]. In particular, studies of ultracold fermionic systems are of special interest since they can reveal the physics behind complex phenomena in condensed matter systems. The advantage of systems of ultracold fermionic atoms over real condensed matter systems is the excellent control over the Hamiltonian parameters. Crystal structures can be simulated by optical lattices: Interfering laser beams form an intensity pattern in which neutral atoms can be trapped. Parameters such as lattice constant and on-site potential can be tuned in experiment. [58] Fermionic atoms in a trap obey a quadratic dispersion with a real mass which is not renormalized by a lattice potential. The interaction between the atoms can be tuned by Feshbach resonances, see Section 8.2. In this chapter we will introduce the most important features characterizing ultracold atomic systems and the tools used in ultracold atom experiments. Thereby we will follow the book by Stoof, Gubbels, and Dickerscheid [59] as well as the review article by Bloch, Dalibard and Zwerger [58].

8.1 SCATTERING

Collisions of two atoms in the quantum regime do a priori include scattering processes involving states at nonzero relative angular momentum. In order to scatter in these states, the incoming atoms need to have enough energy to overcome the centrifugal barrier due to the centrifugal potential which scales with $V \sim l(l+1)$ [60], where l is the quantized angular momentum of the final state. The energy of this threshold for small l corresponds to a temperature in the milli-Kelvin regime for the typical atomic masses that are used in experiments. [58] Below that temperature, only s -wave scattering processes can occur. This threshold temperature defines the regime of ultracold collisions. In many cases realistic interactions can be well approximated by a contact interaction. This has an important consequence on the scattering in ultracold fermionic systems: as fermions obey the Pauli exclusion principle and because ultracold temperatures only allow for s -wave scattering, only fermions in different intrinsic states are affected by a contact interaction. Therefore, in order to observe scattering events, fermionic gases are prepared in different intrinsic states - most often in two different hyperfine states.

A quantitative discussion on scattering in two dimensions will be given in Section 10.2, where we derive the two-body scattering matrix for collisions in a two-dimensional system.

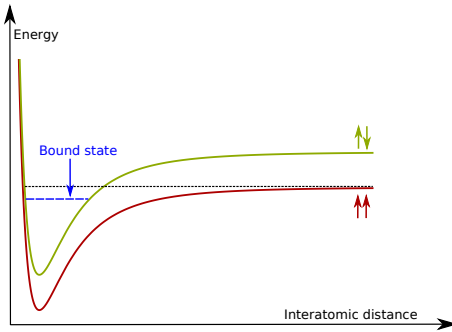


FIGURE 13: A system with two coupled scattering channels which have different magnetic moments. By varying the magnetic field it can be driven to a Feshbach resonance .

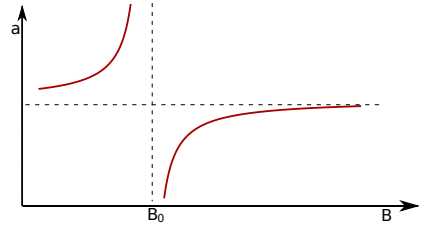


FIGURE 14: The dependence of the scattering length a on the magnetic field B according to $a \propto \frac{\Delta B}{B - B_0}$. The scattering length diverges when the magnetic field is tuned to its value B_0 of the Feshbach resonance.

8.2 FESHBACH RESONANCES

The Feshbach resonance is a very important feature of ultracold atomic gases which allows to study strongly correlated systems. By tuning the system towards a Feshbach resonance, the scattering length can be increased drastically.

A Feshbach resonance can occur in systems which exhibit two coupled scattering channels which differ in the internal configuration of the colliding atoms: the closed channel which contains a two-atom bound state close to the continuum of the other channel, called the open channel. This situation is depicted in Figure 13. For instance when the atoms in a gas can take two different spin states, the two colliding atoms can either form a singlet or a triplet. Let us assume that the singlet channel contains a bound state which is close in energy to the continuum of the triplet channel. The two channels are coupled via the hyperfine interaction which can provoke a spin flip. As the singlet and the triplet have a different magnetic moment, the two channels have a different Zeeman shift in a magnetic field. For that reason a magnetic field can be tuned such that the bound state of the singlet channel becomes resonant to the continuum of the triplet channel.

The resonating bound state is an eigenstate of the scattering process, as well as the plane waves of the continuum. For that reason the bound state is orthogonal to the plane waves and there is no overlap of the wave functions. In the resonant case, the plane waves of the continuum are repelled and the scattering length diverges.

THE TRANSPORT COEFFICIENTS

9.1 SHEAR VISCOSITY

The shear viscosity η of a fluid or a gas is a measure of the internal friction of the system. It characterizes the force required to create a velocity gradient in the system. The shear viscosity is the proportionality factor that relates the force F and the velocity gradient $\partial u / \partial y$,

$$F = A\eta \frac{\partial u}{\partial y}, \quad (170)$$

where A is the cross sectional area of the system. [40] Figure 15 illustrates this definition.

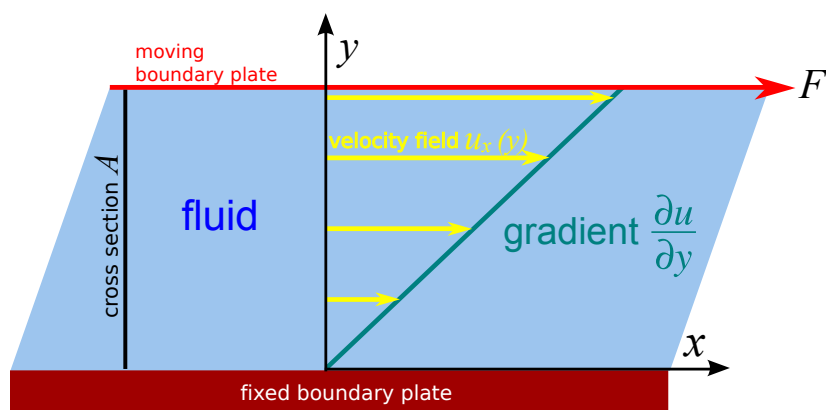


FIGURE 15: The shear viscosity η indicates how much force F is needed to create a velocity gradient $\frac{\partial u}{\partial y}$. The picture is based on Ref. [61].

By measuring the shear viscosity of a system one can gain information about the interaction between the particles of the system. The shear viscosity of strongly interacting systems is lower than that of weakly interacting systems. This at first sight contradictory correlation can be understood as follows: The viscosity measures the momentum transfer across a given distance: In a weakly interacting gas, as one boundary plate jolts a particle, the particle moves to the other plate and transfers its momentum. However, if the system is strongly interacting, the particle has already lost a part of its momentum through scattering with other particles by the time it arrives at the other side. In this case the momentum transfer is smaller, and hence the shear viscosity is also smaller. In terms of Eq. (170) and Figure 15 one can think in the following way: In strongly interacting systems, less force is needed to create a velocity gradient because the momentum transfer from one side of the capillary to the other is hindered by scattering.

In fact, the temperature dependence of the viscosity $\eta(T)$ is expected to have a minimum, as now discussed (we follow the article by Schäfer and Teaney [40]). In a classical picture, which goes back to Maxwell, the viscosity in a dilute gas is connected to the momentum transfer of the individual molecules. The relation reads as follows,

$$\eta = \frac{1}{3} n p l \quad (171)$$

where n is the particle density, p the momentum and l the mean free path. The mean free path is connected to the transport cross section σ via $l = \frac{1}{n\sigma}$. Since the molecules move according to their thermal energy, $\frac{p^2}{2m} = k_B T$, the viscosity of a dilute gas increases with increasing temperature in accordance with

$$\eta = \frac{\sqrt{2mk_B T}}{\sigma} \quad (172)$$

but it is approximately independent of the density. This counterintuitive behaviour was observed in experiments which were carried out by Maxwell himself. When the temperature is further lowered the gas condenses into a liquid and transport can no longer be described by the motion of the individual molecules. Here, transport processes are thermally activated transitions between local energy minima and the viscosity scales up with decreasing temperature according to

$$\eta \simeq h n e^{\frac{E}{k_B T}} \quad (173)$$

where E is the activation energy. Because of the opposite scalings of the viscosity for dilute gases, Eq. (172), and liquids, Eq. (173), there must be a minimum of the viscosity as a function of temperature. It is natural to expect that this minimum occurs in the vicinity of the gas-liquid phase transition.

Now we come to the question how to identify a "good" fluid. Experimental results show that the viscosity of liquids which are known to have a good flow characteristic differs by orders of magnitude. This observation suggests that the viscosity should be normalized with respect to some thermodynamic quantity. Eq. (171) and (173) indicate that the viscosity scales with particle density n . Indeed, the ratio $\frac{\eta}{n}$ of fluids with similar flow characteristics takes values of the same order of magnitude. However, as we are especially interested in a comparison to relativistic systems, normalization with respect to particle density is not applicable because in these systems the particle number is not conserved. A more suitable normalization quantity is the entropy density s . For many fluids the entropy density scales as $s \sim n k_B$. The uncertainty relation of quantum mechanics provides us with a rough estimate of a lower bound of the ratio $\frac{\eta}{s}$: The product of the momentum and the mean free path is restricted from below according to $p l \gtrsim \hbar$. From Eq. (171) it follows

$$\frac{\eta}{s} \gtrsim \frac{\hbar}{3k_B}. \quad (174)$$

But since kinetic theory is not reliable in the regime $\frac{\eta}{s} \sim \frac{\hbar}{k_B}$ other methods are needed in order to get a reliable lower bound. Based on the string theory framework, Kovtun *et. al.* [6] laid down a conjecture for the lower bound:

$$\frac{\eta}{s} \geq \frac{\hbar}{4\pi k_B}. \quad (175)$$

The existence of a lower bound of the viscosity raises the question if there is a "perfect fluid" whose ratio of viscosity to entropy density is equal to $\frac{\hbar}{4\pi k_B}$.

9.2 SPIN DIFFUSION

In a fermionic system which contains two different spin species, \uparrow and \downarrow , random collisions between the particles lead to spin currents which flow in such a way as to even out spatial gradients in the spin density. Here, spin refers to any intrinsic quantum number of the fermions. The spin diffusion coefficient D_s is a measure of this equilibration process and is defined by [56]

$$j_s = -D_s \nabla(n_\uparrow - n_\downarrow) \quad (176)$$

where j_s is the spin current density and $n_{\uparrow(\downarrow)}$ is the density of spin-up (spin-down) atoms. In our setup this translates to the two fermionic species with atomic masses m_\uparrow and m_\downarrow responding to gradients in the chemical potentials μ_\uparrow and μ_\downarrow , which are opposite for the two species.

An excellent set-up to measure the spin diffusivity is provided by ultracold atomic gases [56]: Two clouds of fermionic atoms which are prepared in two different spin states are separated from each other in a trap via a magnetic field gradient. Then strong interactions are induced by driving the system near a Feshbach resonance. The two atom clouds are released and collide in the middle of the trap. They "bounce" off each other, but subsequently collide again because the trapping potential pulls both clouds into the middle of the trap. This oscillating process is imaged selectively for the different spin components. The spin diffusivity D_s can be gained by comparing the relaxation rate to the gradient in the spin density.

In the strongly interacting regime, the spin diffusion coefficient exhibits a minimum as a function of temperature [55]. As spin diffusivity is smallest for strong interactions, this minimum is considered to be universal. This can be understood from the argument presented in Refs. [56] and [55]: At a high collision rate, a spin-up fermion is scattered back into the spin-up cloud when the two atom clouds collide, rather than diffusing into the opposite spin region. Hence the spin diffusion coefficient increases with increasing mean free path l_{mf} between scattering events, and with increasing velocity v of the atoms. In general we have for a d -dimensional system, [62]

$$D_s \sim \frac{1}{d} v l_{mf}. \quad (177)$$

l_{mf} is connected to the scattering cross section σ via $l_{mf} \sim \frac{1}{n\sigma}$, with $n = \frac{k_F^d}{d\pi^{d-1}}$ being the particle density. For temperatures T much higher than the Fermi

temperature T_F the scattering cross section is given by the thermal de Broglie wavelength, $\sigma \sim \lambda_T^{d-1}$ where $\lambda_T = \frac{2\pi\hbar}{\sqrt{2m\pi k_B T}}$, and the fermions move with the thermal velocity $v_T = \sqrt{2m\pi k_B T}$. This yields for the spin diffusion coefficient in two dimensions:

$$D_s \sim \frac{v_T}{2n\sigma} \sim \sqrt{2m\pi k_B T} \frac{2\pi}{2k_F^2} \frac{\sqrt{2m\pi k_B T}}{2\pi\hbar} = \frac{1}{\hbar k_F^2} (m\pi k_B T) \propto T \quad (178)$$

For temperatures far below the Fermi temperature only low energy states of the trap are occupied. Collisions into a low energy state are therefore suppressed due to the Pauli exclusion principle. Thus in the low-temperature regime the effective scattering cross section increases with increasing temperature and is found to scale according to $\sigma \propto T^2$. As the average velocity is of the order of the Fermi velocity $v_F = \frac{\hbar k_F}{m}$, the spin diffusion coefficient in two dimensions scales as

$$D_s \sim \frac{v_F}{2n\sigma} \sim \frac{\hbar}{m} \frac{\pi}{k_F} \frac{1}{T^2} \propto \frac{1}{T^2}, \quad (179)$$

and one expects a minimum to occur near the Fermi temperature before Pauli blocking becomes effective.

Now we will estimate the minimum value of the spin diffusion coefficient: The scattering cross section for strong interactions is related to the de Broglie wavelength via $\sigma \sim \lambda_B^{d-1} = \left(\frac{2\pi\hbar}{p}\right)^{d-1}$, where p is the momentum of the fermions. In the degenerate regime, p on average is the Fermi momentum $p_F = \hbar k_F$ and v the Fermi velocity $v_F = \frac{\hbar k_F}{m}$. This yields for the spin diffusion coefficient in two dimensions,

$$D_s \sim \frac{v_F}{2n\sigma} \sim \frac{\hbar k_F}{2m} \frac{2\pi}{k_F^2} \frac{k_F}{2\pi} = \frac{1}{2} \frac{\hbar}{m}. \quad (180)$$

This estimate of the universal quantum limit for spin diffusion in Fermi gases is independent of the temperature.

SCATTERING IN TWO DIMENSIONS

10.1 THE MODEL

We consider two species of interacting fermionic atoms, labeled by $\sigma = \uparrow, \downarrow$, in two dimensions. The corresponding Hamiltonian reads

$$H = \sum_{\mathbf{k}\sigma} (\varepsilon_{\mathbf{k}\sigma} - \mu_\sigma) c_{\mathbf{k}\sigma}^\dagger c_{\mathbf{k}\sigma} + \frac{g_0}{V} \sum_{\mathbf{k}\mathbf{k}'\mathbf{q}} c_{\mathbf{k}'-\mathbf{q}\downarrow}^\dagger c_{\mathbf{k}+\mathbf{q}\uparrow}^\dagger c_{\mathbf{k}\uparrow} c_{\mathbf{k}'\downarrow}. \quad (181)$$

The first term describes the energy of the free Fermi gas with the free single-particle dispersion $\varepsilon_{\mathbf{k}\sigma} = \mathbf{k}^2/2m_\sigma$ and species-dependent chemical potential μ_σ . (In this chapter as well as in Chapter 11 and 12 we will set $\hbar \equiv 1$ and $k_B \equiv 1$.) $c_{\mathbf{k}\sigma}^\dagger c_{\mathbf{k}\sigma}$ are fermionic creation and annihilation operators. The second term accounts for the interactions between the fermions where g_0 is an attractive contact interaction and V is the area of the system. We sum over all initial momenta \mathbf{k} and \mathbf{k}' and the momentum transfer \mathbf{q} . At ultracold temperatures the interaction only allows s -wave scattering (as higher scattering channels are suppressed due to the potential barrier, see Section 8.1). Due to the Pauli principle the s -wave contact interaction acts only between different species \uparrow and \downarrow .

10.2 THE SCATTERING MATRIX

In the dilute Fermi gas, the only important interaction processes are two-particle collisions. In this section we will derive an expression for the 2d two-body s -wave scattering matrix which describes such processes in two dimensions. First we will consider two-body scattering processes in the vacuum and derive the vacuum scattering matrix \mathcal{T}_0^{vac} for s -wave scattering. Thereby we follow the book by Stoof, Gubbels, and Dickerscheid [59] and the article by Adhikari [63]. Thereafter we also include the effect of a medium on the two-body scattering processes and we derive an integral expression for the the medium scattering matrix \mathcal{T} , which can only be computed numerically.

10.2.1 The two-body scattering matrix in the vacuum

We consider a spherically symmetric interaction potential $V(\mathbf{r}_1 - \mathbf{r}_2) = V(|\mathbf{r}_1 - \mathbf{r}_2|)$. In this case the two-body Schrödinger equation separates into a part describing the center-of-mass motion and one part describing the relative motion. The Schrödinger equation for the relative wave functions $\psi(\mathbf{r})$ reads

$$(\hat{H}_0 + \hat{V}(r))\psi(\mathbf{r}) = E\psi(\mathbf{r}) \quad (182)$$

with $\hat{H}_0 = \frac{-\nabla^2}{2m_r}$ being the free Hamiltonian with the reduced mass $m_r^{-1} = m_{\uparrow}^{-1} + m_{\downarrow}^{-1}$. E is the energy at which the elastic scattering process takes place. As $|k\rangle$ solves the problem for $\hat{V} = 0$ the solution of Eq. (182) is given by

$$|\psi_k\rangle = |k\rangle + \frac{1}{E - \hat{H}_0 + i\epsilon} \hat{V} |\psi_k\rangle. \quad (183)$$

The infinitesimal part $i\epsilon$ is introduced in order to deal with the singular nature of the operator $\frac{1}{E - \hat{H}_0}$. Eq. (183) is known as the Lippmann-Schwinger equation. For distances r much larger than the range R of the scattering potential, the wave function assumes the form

$$\psi_k(r, \theta) \approx e^{ikx} + \sqrt{\frac{i}{k}} f(\mathbf{k}, \mathbf{k}') \frac{e^{ik'r}}{\sqrt{r}}. \quad (184)$$

The first term describes the incoming state, which is assumed to be a plane wave in x -direction with wave vector \mathbf{k} . The outgoing state with wave vector \mathbf{k}' is rotationally invariant around the scattering potential \hat{V} at the origin and is determined by the momentum-dependent scattering amplitude $f(\mathbf{k}, \mathbf{k}')$, which is defined via the matrix element,

$$f(\mathbf{k}, \mathbf{k}') = -\sqrt{\frac{1}{2\pi}} m_r \langle \mathbf{k}' | \hat{V} | \psi_{\mathbf{k}} \rangle. \quad (185)$$

We now introduce the operator \hat{T}^{2B} , defined by

$$\hat{V} |\psi_k\rangle \equiv \hat{T}^{2B} |k\rangle \quad (186)$$

which is called the two-body scattering matrix. Multiplying Eq. (183) with \hat{V} and using Eq. (186) yields the Lippmann-Schwinger equation for the \hat{T} -matrix,

$$\hat{T}^{2B} = \hat{V} + \hat{V} \hat{G}_0 \hat{T}^{2B}, \quad (187)$$

where \hat{G}_0 is the free Green function

$$\hat{G}_0(z) = \frac{1}{z - \hat{H}_0} \quad (188)$$

with $z = E + i\epsilon$. When expanding this expression into a Born series,

$$\hat{T}^{2B} = \hat{V} + \hat{V} \hat{G}_0 \hat{V} + \hat{V} \hat{G}_0 \hat{V} \hat{G}_0 \hat{V} + \dots \quad (189)$$

one gains a formal solution for the scattering matrix

$$\hat{T}^{2B} = \hat{V} + \hat{V} \hat{G} \hat{V}, \quad (190)$$

where we introduced the full Green function

$$\hat{G} = (z - \hat{H})^{-1}. \quad (191)$$

When inserting the complete set of eigenstates $|\psi_\alpha\rangle \langle\psi_\alpha|$ of the perturbed Hamiltonian \hat{H} with eigenvalues ϵ_α one gets the following expression for the scattering matrix,

$$\hat{T}^{2B} = \hat{V} + \sum_{\epsilon_\alpha < 0} \hat{V} \frac{|\psi_\alpha\rangle \langle\psi_\alpha|}{z - \epsilon_\alpha} \hat{V} + \int_0^\infty \frac{d^2k}{4\pi^2} \hat{V} \frac{|\psi_k\rangle \langle\psi_k|}{z - \epsilon_k} \hat{V}. \quad (192)$$

From this expression we can see that the two-body scattering matrix exhibits poles in the complex plane that correspond to the bound states of the interaction potential and that it has a branch cut along the positive real axis due to the continuum of scattering states at positive energies.

From Eq. (185) we see that the two-body scattering matrix is related to the scattering amplitude $f(\mathbf{k}, \mathbf{k}')$ via

$$f(\mathbf{k}, \mathbf{k}') = -\sqrt{\frac{1}{2\pi}} m_r \langle\mathbf{k}'| \hat{T}^{2B} |\mathbf{k}\rangle. \quad (193)$$

As we consider elastic scattering processes, meaning $k = k'$, the scattering problem is fully described by k and θ , where θ is the angle between the wave vector \mathbf{k} of the incoming wave and the wave vector \mathbf{k}' of the outgoing wave. Since we are only interested in s -wave scattering it is convenient to expand the scattering amplitude in partial waves with amplitudes $f_l(k)$ and then only consider the first summand,

$$f(k, \theta) = \sqrt{\frac{2}{\pi}} \sum_{l=0}^{\infty} \epsilon_l \cos(l\theta) f_l(k). \quad (194)$$

We now write the incoming plane wave as a superposition of incoming and outgoing spherical waves by using

$$\begin{aligned} e^{ikx} = e^{ikr \cos \theta} &= \sum_{l=0}^{\infty} \epsilon_l i^l \cos(l\theta) j_l(kr) \\ &\xrightarrow{r \rightarrow \infty} \sum_{l=0}^{\infty} \epsilon_l i^l \cos(l\theta) \sqrt{\frac{1}{2\pi kr}} \left(e^{ikr} e^{-i\frac{\pi}{2}(l+\frac{1}{2})} + e^{-ikr} e^{i\frac{\pi}{2}(l+\frac{1}{2})} \right) \end{aligned} \quad (195)$$

with $\epsilon_l = 2$ for $l \neq 0$ and $\epsilon_0 = 1$. Here, we used the asymptotic form of the Bessel function $j_l(kr)$. From Eq. (184), Eq. (194), and Eq. (195) we can see that scattering at a potential leads to a change in the coefficient of the outgoing spherical wave according to

$$\frac{e^{ikr}}{\sqrt{r}} \rightarrow \frac{(1 + 2if_l(k))e^{ikr}}{\sqrt{r}}. \quad (196)$$

Since the probability flux is conserved during the scattering process, the coefficient $1 + 2if_l(k)$ is equal to unity. This can be taken into account by writing the coefficient as an exponential function,

$$1 + 2if_l(k) = e^{2i\delta_l(k)}. \quad (197)$$

And we find for the scattering amplitude f_l ,

$$f_l(k) = e^{i\delta_l(k)} \sin \delta_l(k) = \frac{1}{\cot \delta_l(k) - i}. \quad (198)$$

Consequently the partial wave expansion for the \hat{T} -matrix reads

$$\hat{T}^{2B}(k, \theta) = \sum_{l=0}^{\infty} \mathcal{T}_l(k, \theta) = -\frac{2}{m_r} \sum_{l=0}^{\infty} \epsilon_l \cos(l\theta) \frac{1}{\cot \delta(k)_l - i}. \quad (199)$$

When only considering s -wave scattering we can use the low energy expansion for $\cot \delta_0(k)$ with $E = \frac{k^2}{2m_r}$,

$$\pi \cot \delta_0(E) = \ln(E/\epsilon_B) + \mathcal{O}(E/\epsilon_R) \quad (200)$$

with constant $\epsilon_R = 1/2m_r R^2$ and R the range of the interaction potential. Inserting this expansion we find for s -wave scattering [63, 64],

$$\mathcal{T}_0(E) = \frac{2\pi/m_r}{\ln(\epsilon_B/E) + i\pi}. \quad (201)$$

The pole at $E = -\epsilon_B < 0$ corresponds to the two-body bound state. This bound state is always present in an attractive 2d Fermi gas [65, 64] and the binding energy

$$\epsilon_B = \frac{1}{2m_r a_{2D}^2} \quad (202)$$

defines the 2d scattering length a_{2D} .

In the following section we derive an expression for the two-body scattering matrix in the medium. Thereby we will use the notation $\mathcal{T}_0 = \mathcal{T}^{vac}$ for the vacuum two-body, s -wave scattering matrix (Eq. (201)) derived in this section.

10.2.2 The two-body scattering matrix in the medium

At finite density we need to consider the effect of the medium on the two-particle collisions. This scenario is described by the two-body scattering matrix $\mathcal{T}_{kk'}(\mathbf{q}, \omega)$ in the medium which is subject to the Bethe-Salpeter equation [33],

$$\mathcal{T}_{kk'}(\mathbf{q}, \omega) = \mathcal{T}_{kk'}^{vac}(\mathbf{q}, \omega) + \frac{1}{L^2} \sum_p \mathcal{T}_{kp}^{vac}(\mathbf{q}, \omega) G_{p\uparrow}(\omega) G_{p+q\downarrow}(\omega) \mathcal{T}_{pk'}(\mathbf{q}, \omega). \quad (203)$$

k is the momentum of one particle before the scattering event and k' is its momentum after the scattering event. q is the relative momentum of the particles which is not changed by the scattering process. The sum runs over all internal momenta p . The vacuum scattering matrix $\mathcal{T}_{kk'}^{vac}(\mathbf{q}, \omega)$ is given by Eq. (201) and [66]

$$\begin{aligned} G_{p\uparrow}(\omega) G_{p+q\downarrow}(\omega) &= -T \sum_{iv_m} \frac{1}{iv_m - \epsilon_{p\uparrow} + \mu_{\uparrow}} \frac{1}{i\omega_n - iv_m - \epsilon_{p+q\downarrow} + \mu_{\downarrow}} \\ &= \frac{f_{\uparrow\downarrow}(\epsilon_p) - f_{\uparrow\downarrow}(\epsilon_{p+q})}{i\omega_n - \epsilon_{p\uparrow} - \epsilon_{p+q\downarrow} + \mu_{\uparrow} + \mu_{\downarrow}} \end{aligned} \quad (204)$$

with $f_{\uparrow\downarrow}(\epsilon_p)$ being the Fermi-Dirac distribution [65]

$$f_{\uparrow\downarrow}(\epsilon_p) = \frac{1}{e^{\frac{1}{T}(\epsilon_{p\uparrow\downarrow} - \mu_{\uparrow\downarrow})} + 1}. \quad (205)$$

In a dilute gas with short-range interactions, where the average interparticle spacing k_F^{-1} is much larger than the range R of the potential (meaning we have a small parameter $k_F R$, where k_F is the Fermi momentum) only diagrams which have no crossing interaction lines survive. (This approximation is consistent with the lowest order approximation of the large- N expansion in Section 13.1.) The recursive formula reduces to the ladder structure sketched in Figure 16,

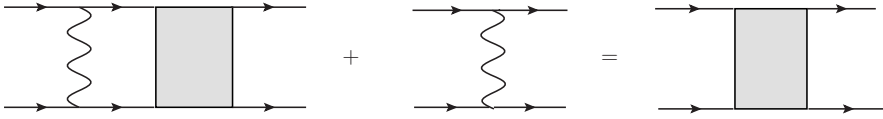


FIGURE 16: Ladder approximation for the scattering matrix $\mathcal{T}_{kk'}(\mathbf{q}, \omega)$

$$\mathcal{T}_{kk'}(\mathbf{q}, \omega) = V(\mathbf{q}, \omega) + V(\mathbf{q}, \omega) \frac{1}{L^2} \sum_p G_p^\uparrow(\omega) G_{p+q}^\downarrow(\omega) \mathcal{T}_{pk'}(\mathbf{q}, \omega), \quad (206)$$

where V is a single interaction line. Since the expression for $\mathcal{T}_{kk'}(\mathbf{q}, \omega)$ does not depend on k , we can solve this equation for $\mathcal{T}(\mathbf{q}, \omega)$ yielding

$$\mathcal{T}(\mathbf{q}, \omega) = \frac{V(\mathbf{q}, \omega)}{1 - V(\mathbf{q}, \omega) \frac{1}{L^2} \sum_p G_{p\uparrow}(\omega) G_{p+q\downarrow}(\omega)} \quad (207)$$

or

$$\begin{aligned} \mathcal{T}^{-1}(\mathbf{q}, \omega) &= \frac{1}{V(\mathbf{q}, \omega)} - \frac{1}{L^2} \sum_p G_{p\uparrow}(\omega) G_{p+q\downarrow}(\omega) \\ &= \mathcal{T}_0(E)^{-1} - \int \frac{d^2\mathbf{p}}{(2\pi)^2} \frac{f(\epsilon_{\mathbf{p}\uparrow} - \mu_\uparrow) + f(\epsilon_{\mathbf{p}+\mathbf{q}\downarrow} - \mu_\downarrow)}{i\omega + \mu_\uparrow + \mu_\downarrow - \epsilon_{\mathbf{p}\uparrow} - \epsilon_{\mathbf{p}+\mathbf{q}\downarrow}}. \end{aligned} \quad (208)$$

This integral is known analytically at $T = 0$ [67]. At finite temperature we can perform only the angular integral analytically which is done in appendix B.1. The radial part we have to compute numerically.

THE BOLTZMANN FORMALISM

The Boltzmann approach is a formalism to compute the distribution function of particles in a system. It was developed by Ludwig Boltzmann [68] in 1872 in order to describe the dynamics of classical gases. The approach is based on the semi-classical picture: particles move in phase space and scatter among each other or from external obstacles. It remains applicable in quantum systems provided quantum interference effects are negligible and the quasiparticles are well-defined.

In this introductory chapter we will derive a variational approach to solve the linearized Boltzmann equation. Thereby we will follow the book by Ziman [69] and the article by Arnold *et al.* [70].

11.1 INTRODUCTION TO THE BOLTZMANN FORMALISM

The distribution function $f_{\mathbf{k}}(\mathbf{r}, t)$ counts the average number of fermions in the momentum state \mathbf{k} in the neighbourhood of position \mathbf{r} at time t . In equilibrium the distribution function in a Fermi gas is given by the Fermi-Dirac distribution

$$f_{\mathbf{k}}^0(\mathbf{r}, t) = \frac{1}{e^{\frac{1}{T}(\epsilon_{\mathbf{k}} - \mu)} + 1}, \quad (209)$$

where μ is the chemical potential and $\epsilon_{\mathbf{k}}$ the energy of the state with momentum \mathbf{k} . The processes that lead to a disequilibrium and thus to a change of the distribution function in time, can be identified from $\frac{d}{dt}f_{\mathbf{k}}(\mathbf{r}, t) \neq 0$. It follows that,

$$\frac{d}{dt}f_{\mathbf{k}}(\mathbf{r}, t) = \partial_t f_{\mathbf{k}}(\mathbf{r}, t) + \dot{\mathbf{k}} \nabla_{\mathbf{k}} f_{\mathbf{k}}(\mathbf{r}, t) + \dot{\mathbf{r}} \nabla_{\mathbf{r}} f_{\mathbf{k}}(\mathbf{r}, t) = -I_{coll}[f_{\mathbf{k}}(\mathbf{r}, t)]. \quad (210)$$

We discuss each term now in turn. The term

$$\dot{\mathbf{r}} \nabla_{\mathbf{r}} f_{\mathbf{k}}(\mathbf{r}, t) = \mathbf{v} \nabla_{\mathbf{r}} f_{\mathbf{k}}(\mathbf{r}, t), \quad (211)$$

takes the group velocity \mathbf{v} into account, with which the different momentum states travel in k -space.

External fields \mathbf{F}_{ext} , which act as classical forces on the system are accounted for by

$$\dot{\mathbf{k}} \nabla_{\mathbf{k}} f_{\mathbf{k}}(\mathbf{r}, t) = \mathbf{F}_{ext} \nabla_{\mathbf{k}} f_{\mathbf{k}}(\mathbf{r}, t). \quad (212)$$

On the other hand we have

$$\frac{d}{dt}f_{\mathbf{k}}(\mathbf{r}, t) = \left(\frac{\partial f_{\mathbf{k}}(\mathbf{r}, t)}{\partial t} \right)_{coll} = -I_{coll}[f_{\mathbf{k}}(\mathbf{r}, t)], \quad (213)$$

describing the change of $f_{\mathbf{k}}(\mathbf{r}, t)$ due to collision processes. The collision integral $I_{coll}[f_{\mathbf{k}}(\mathbf{r}, t)]$ is a functional which induces a change in the distribution of momenta \mathbf{k} . It will be specified in Section 11.2.2. Collecting Eqs. (210) to (213) yields the Boltzmann equation,

$$[\partial_t + \mathbf{v}\partial_x + \mathbf{F}_{ext}\partial_{\mathbf{k}}]f_{\mathbf{k}}(\mathbf{r}, t) = -I_{coll}[f_{\mathbf{k}}(\mathbf{r}, t)], \quad (214)$$

which is an integro-differential equation for the quasiparticle distribution function $f_{\mathbf{k}}(\mathbf{r}, t)$. It can be written in the form,

$$D_{\alpha}f_{\mathbf{k}}(\mathbf{r}, t) = -I_{coll}[f_{\mathbf{k}}(\mathbf{r}, t)], \quad (215)$$

where we have introduced the tensor differential operator D_{α} , which is called the driving term as it accounts for perturbations driving the system away from the equilibrium situation. α specifies the type of the perturbation. In this thesis we will have $\alpha = \eta$ for the shear viscosity in Section 12.1 and $\alpha = sd$ for the spin diffusion in Section 12.2.

From now on we will simply write f_{σ} for the distribution function in order to discriminate between the different fermionic species but thereby skip the other dependences unless they are necessary for the comprehension.

11.2 THE BOLTZMANN EQUATION IN LINEAR RESPONSE

We will solve the Boltzmann equation for the non-equilibrium distribution function in the linear response regime, assuming that the deviation from the equilibrium distribution function can be obtained in an expansion in the perturbation. Schematically, it assumes the form

$$f_{\sigma} = f_{\sigma}^0 + \frac{1}{T}f_{\sigma}^0(1 - f_{\sigma}^0)f_{\sigma}^1, \quad (216)$$

where f_{σ}^0 is the Fermi-Dirac distribution of the equilibrium, see Eq. (209), and f_{σ}^1 is linear in the perturbation and otherwise a generic function (this is true for all types of perturbations considered here). The factor $\frac{1}{T}f_{\sigma}^0(1 - f_{\sigma}^0)$ is introduced for later convenience. In the next two sections we will linearize both sides of the Boltzmann equation, the driving term and the collision integral.

11.2.1 The driving term

Since the driving term D_{α} is linear in the perturbation one can replace $f_{\sigma} \rightarrow f_{\sigma}^0$ on the left-hand side of Eq. (215). We are interested in the stationary state of the system, i.e. $\partial_t f_{\sigma} = 0$, hence in general we have,

$$\begin{aligned} D_{\alpha}f_{\sigma}^0 &= \mathbf{v}(\partial_{\epsilon}f_{\sigma}^0\nabla_{\mathbf{r}}\epsilon_{\alpha} + \partial_{\mu}f_{\sigma}^0\nabla_{\mathbf{r}}\mu_{\alpha}) + \mathbf{F}_{ext}(\partial_{\epsilon}f_{\sigma}^0\nabla_{\mathbf{k}}\epsilon_{\alpha} + \partial_{\mu}f_{\sigma}^0\nabla_{\mathbf{k}}\mu_{\alpha}) \\ &= -\beta f_{\sigma}^0(1 - f_{\sigma}^0)(\mathbf{v}(\nabla_{\mathbf{r}}\epsilon_{\alpha} + \nabla_{\mathbf{r}}\mu_{\alpha}) + \mathbf{F}_{ext}(\nabla_{\mathbf{k}}\epsilon_{\alpha} + \nabla_{\mathbf{k}}\mu_{\alpha})) \\ &= -\frac{1}{T}f_{\sigma}^0(1 - f_{\sigma}^0)I_{\sigma,\alpha}^{ij}F_{\sigma,\alpha}^{ij} \equiv \mathcal{D}_{\alpha}^{\sigma}, \end{aligned} \quad (217)$$

where we use the Einstein summation convention. At this point we have introduced $F_{\sigma,\alpha}^{ij}$ as a generalized force field and $I_{\sigma,\alpha}^{ij}$ as a generalized projection. Both will be specified in Chapter 12, when we compute the transport coefficients. For reasons of a concise presentation we assume from now on that we can absorb the spin-dependence of $F_{\sigma,\alpha}^{ij}$ into the factor $I_{\sigma,\alpha}^{ij}$ and work with F_{α}^{ij} only, which acts in the same way on both spin species. For concreteness, in the case of an electrical conductivity it is $F_{\sigma,ec}^{ij} = E^i \delta_{ij}$ and $I_{\sigma,ec}^{ij} = e v_{\mathbf{k},\sigma}^i \delta_{ij}$ with E^i being the i th component of the external electric field, e the electron charge and $v_{\mathbf{k}}^i$ the i th component of the electron velocity. Since the driving term is linear in the perturbation f_{σ}^1 its general form also dictates the form of the ansatz for f_{σ}^1 , which we choose as

$$f_{\sigma}^1(\mathbf{k}) = F_{\alpha}^{ij} I_{\sigma,\alpha}^{ij}(\mathbf{k}) g_{\sigma,\alpha}(k) = F_{\alpha}^{ij} \chi_{\sigma,\alpha}^{ij}(\mathbf{k}). \quad (218)$$

$g_{\sigma,\alpha}(k)$ is the excited function and we will later write it as a linear combination of the excited modes of the system.

11.2.2 The collision integral

The collision integral describes the scattering between particles. It can be derived from Fermi's Golden Rule [71] and to lowest non-trivial order in the interaction, represented by the scattering matrix \mathcal{T} (Eq. (208)), it reads,

$$\begin{aligned} I_{\text{coll}}[f_{\sigma}, f_{-\sigma}] &= \frac{1}{T} \int_{\mathbf{k}', \mathbf{q}} \delta(\varepsilon_{\mathbf{k},\sigma} + \varepsilon_{\mathbf{k}',-\sigma} - \varepsilon_{\mathbf{k}+\mathbf{q},\sigma} - \varepsilon_{\mathbf{k}'-\mathbf{q},-\sigma}) \\ &\quad \times \left| \mathcal{T}(\mathbf{k} + \mathbf{k}', \varepsilon_{\mathbf{k},\sigma} + \varepsilon_{\mathbf{k}',-\sigma} - \mu_{\sigma} - \mu_{-\sigma}) \right|^2 \\ &\quad \times [f_{\sigma}(\mathbf{k}) f_{-\sigma}(\mathbf{k}') (1 - f_{\sigma}(\mathbf{k} + \mathbf{q})) (1 - f_{-\sigma}(\mathbf{k}' - \mathbf{q})) \\ &\quad - f_{\sigma}(\mathbf{k} + \mathbf{q}) f_{-\sigma}(\mathbf{k}' - \mathbf{q}) (1 - f_{\sigma}(\mathbf{k})) (1 - f_{-\sigma}(\mathbf{k}'))], \end{aligned} \quad (219)$$

where $\int_{\mathbf{k}} = \int \frac{d^2k}{(2\pi)^2}$. \mathbf{k} and \mathbf{k}' are the momenta of the particles before the scattering event, \mathbf{q} is the momentum transfer. The δ -function accounts for energy conservation and the product of distribution functions reduce the scattering amplitude according to how many states with momenta \mathbf{k} and \mathbf{k}' are occupied before the scattering event and how many states with momenta $\mathbf{k} + \mathbf{q}$ and $\mathbf{k}' - \mathbf{q}$ are available. In order to work consistently we also approximate the collision integral by using Eq. (216) and expand to linear order in f_{σ}^1 ,

$$\begin{aligned} I_{\text{coll}}[f_{\sigma}, f_{-\sigma}] &= C[f_{\sigma}^1, f_{-\sigma}^1] + \mathcal{O}((f_{\sigma}^1)^2, (f_{-\sigma}^1)^2) \\ &\approx C[f_{\sigma}^1, f_{-\sigma}^1], \end{aligned} \quad (220)$$

which yields

$$\begin{aligned}
C[f_{\sigma}^1, f_{-\sigma}^1] &= \frac{1}{T} \int_{\mathbf{k}', \mathbf{q}} \delta(\varepsilon_{\mathbf{k}\sigma} + \varepsilon_{\mathbf{k}'-\sigma} - \varepsilon_{\mathbf{k}+\mathbf{q}\sigma} - \varepsilon_{\mathbf{k}'-\mathbf{q}-\sigma}) \\
&\times \left| \mathcal{T}(\mathbf{k} + \mathbf{k}', \varepsilon_{\mathbf{k}\sigma} + \varepsilon_{\mathbf{k}'-\sigma} - \mu_{\sigma} - \mu_{-\sigma}) \right|^2 \\
&\times \left[f_{\sigma}^0(\mathbf{k}) f_{-\sigma}^0(\mathbf{k}') (1 - f_{\sigma}^0(\mathbf{k} + \mathbf{q})) (1 - f_{-\sigma}^0(\mathbf{k}' - \mathbf{q})) \right] \\
&\times \left[f_{\sigma}^1(\mathbf{k}) + f_{-\sigma}^1(\mathbf{k}') - f_{\sigma}^1(\mathbf{k} + \mathbf{q}) - f_{-\sigma}^1(\mathbf{k}' - \mathbf{q}) \right]. \tag{221}
\end{aligned}$$

With the ansatz for f_{σ}^1 introduced in Eq. (218) we can write the Boltzmann equation in linear response,

$$\mathcal{D}_{\sigma}^{\alpha} = -C[\chi_{\sigma}^{ij}, \chi_{-\sigma}^{ij}] F_{\alpha}^{ij}. \tag{222}$$

In the following we will skip the index α to preserve a clear view.

11.3 THE VARIATIONAL APPROACH

In this section we will find a solution for the linearized Boltzmann equation, Eq. (222). A seemingly straightforward approach to solve Eq. (222) would be to convert it to a matrix equation and solve it numerically. However, this method fails when the matrix is singular. A better strategy is to convert this integral equation into an equivalent variational problem. This variational approach will be introduced in a generic form in this section. In the following chapter we will specify it to compute the transport coefficients.

A conserved current j^{ij} in a system is given by the integration over the phase-space distribution function $f_{\sigma}(\mathbf{k})$. In general it is defined by

$$j^{ij} = \sum_{\sigma} \int_{\mathbf{k}} I_{\sigma}^{ij} f_{\sigma}(\mathbf{k}), \tag{223}$$

where I_{σ}^{ij} is the generalized projection defined in Section 11.2.1. If we use ansatz (216) for the distribution function the generalized current reads

$$\begin{aligned}
j^{ij} &= \sum_{\sigma} \frac{1}{T} \int_{\mathbf{k}} f_{\sigma}^0(1 - f_{\sigma}^0) I_{\sigma}^{ij} F^{kl} \chi_{\sigma}^{kl} \\
&= - \sum_{\sigma} \int_{\mathbf{k}} \chi_{\sigma}^{ij} \mathcal{D}^{\sigma} = - \langle \chi^{ij} | \mathcal{D} \rangle \\
&= - \langle \chi^{ij} | \mathcal{S} \rangle F^{ij} = - \mathcal{S}[\chi^{ij}] F^{ij}, \tag{224}
\end{aligned}$$

where $|\chi^{ij}\rangle = (\chi_{\uparrow}^{ij}, \chi_{\downarrow}^{ij})$ is a spinor and the components are themselves vectors in function space. In the last line we have introduced a scalar product and we have defined a functional,

$$\mathcal{S}[\chi^{ij}] = - \sum_{\sigma} \frac{1}{T} \int_{\mathbf{k}} f_{\sigma}^0(1 - f_{\sigma}^0) I_{\sigma}^{ij} \chi_{\sigma}^{ij}. \tag{225}$$

Using the definition of a scalar product we can also define the projection of $C[\chi^{ij}]$ on the spinor $|\chi^{ij}\rangle$,

$$C[\chi^{ij}] = \frac{1}{2} \langle \chi^{ij} | C[\chi^{ij}] \rangle, \quad (226)$$

where we write the collision integral as a vector whose entries refer to the different spin species, σ and $-\sigma$, thus

$$C[\chi^{ij}] = \begin{pmatrix} C_\sigma[\chi^{ij}] \\ C_{-\sigma}[\chi^{ij}] \end{pmatrix} = \begin{pmatrix} C[\chi_\sigma^{ij}, \chi_\sigma^{ij}] + C[\chi_\sigma^{ij}, \chi_{-\sigma}^{ij}] \\ C[\chi_{-\sigma}^{ij}, \chi_{-\sigma}^{ij}] + C[\chi_{-\sigma}^{ij}, \chi_\sigma^{ij}] \end{pmatrix} = \begin{pmatrix} C[\chi_\sigma^{ij}, \chi_{-\sigma}^{ij}] \\ C[\chi_{-\sigma}^{ij}, \chi_\sigma^{ij}] \end{pmatrix},$$

where in the last step we have used the fact that due to Pauli blocking there is no scattering between identical particles. The Boltzmann equation (222) dictates the relation between these functionals,

$$\mathcal{S}[\chi^{ij}] = -2C[\chi^{ij}]. \quad (227)$$

We can now introduce a functional

$$\mathcal{Q}[\chi^{ij}] = \mathcal{S}[\chi^{ij}] + C[\chi^{ij}] \quad (228)$$

whose extremum in function space

$$\left. \frac{\delta \mathcal{Q}[\chi^{ij}]}{\delta \chi_\sigma^{ij}} \right|_{\chi_\sigma^{ij, \max}} = 0 \quad (229)$$

can be shown to lead to the Boltzmann equation for the respective species σ :

$$\left. \frac{\delta \mathcal{S}[\chi^{ij}]}{\delta \chi_\sigma^{ij}} \right|_{\chi_\sigma^{ij, \max}} = - \left. \frac{\mathcal{C}[\chi^{ij}]}{\delta \chi_\sigma^{ij}} \right|_{\chi_\sigma^{ij, \max}} \Leftrightarrow D_\sigma^\alpha (F^{ij})^{-1} = -C[\chi_\sigma^{ij}, \chi_{-\sigma}^{ij}]. \quad (230)$$

Conversely, the Boltzmann equation implies that the current reads

$$\begin{aligned} j^{ij} &= -\mathcal{S}[\chi_\sigma^{ij, \max}] F^{ij} = 2C[\chi_\sigma^{ij, \max}] F^{ij} \\ &= -2\mathcal{Q}[\chi_\sigma^{ij, \max}] F^{ij}. \end{aligned} \quad (231)$$

The proper strategy to solve the Boltzmann equation is thus to maximize the functional $\mathcal{Q}[\chi_\sigma^{ij}]$ for $\chi_\sigma^{ij} = I_\sigma^{ij} g_\sigma(k)$ by varying $g_\sigma(k)$. This is done by identifying the physically most relevant modes $g_{n\sigma}(k)$ and writing $g_\sigma(k)$ as an expansion with respect to these modes,

$$g_\sigma(k) = \sum_n \lambda_n g_{n\sigma}(k), \quad (232)$$

$$\mathcal{Q}[I^{ij} \sum_n \lambda_n g_{n\sigma}(k)] = \sum_n \lambda_n \langle I^{ij} g_n | \mathcal{S} \rangle + \frac{1}{2} \sum_{n,m} \lambda_n \lambda_m \langle I^{ij} g_n | C[I^{ij} g_m] \rangle. \quad (233)$$

Taking the derivative of $\mathcal{Q}[I^{ij} \sum_n \lambda_n g_{n\sigma}(k)]$ with respect to a specific expansion coefficient λ_n yields

$$\begin{aligned} & \frac{\delta \mathcal{Q}[I^{ij} \sum_n \lambda_n g_{n\sigma}(k)]}{\delta \lambda_n} \\ &= \langle I^{ij} g_n | S \rangle + \frac{1}{2} \sum_m \lambda_m \langle I^{ij} g_n | C[I^{ij} g_m] \rangle + \frac{1}{2} \sum_m \lambda_m \langle I^{ij} g_m | C[I^{ij} g_n] \rangle \\ &= \mathcal{S}_n^{ij} + \frac{1}{2} \sum_m \lambda_m (C_{nm}^{ij} + C_{mn}^{ij}) = \mathcal{S}_n^{ij} + \sum_m \lambda_m C_{nm}^{ij}, \end{aligned} \quad (234)$$

where we used the fact that C_{nm}^{ij} is a symmetric matrix.

Maximizing $\mathcal{Q}[I^{ij} \sum_n \lambda_n g_{n\sigma}(k)]$ with respect to the expansion coefficients λ_n , i.e. $\left. \frac{\delta \mathcal{Q}[I^{ij} \sum_n \lambda_n g_{n\sigma}(k)]}{\delta \lambda_n} \right|_{\lambda_n^{\max}} = 0$ leads to a matrix equation for λ_n^{\max} which can be solved by matrix inversion,

$$-\hat{\mathcal{S}}^{ij} (\hat{\mathcal{C}}^{ij})^{-1} = \hat{\lambda}^{\max}. \quad (235)$$

The advantage of solving Eq. (235) over Eq. (222) is that the basis of $\hat{\mathcal{C}}^{ij}$ consists of the physical modes of the system. That means if there is a zero in the matrix, which leads to a singularity, it has a real physical meaning. For example in a system where the different fermionic species have different mass, the spin diffusion equilibration process will lead to an oscillation of the center of mass, which cannot be relaxed. This will lead to a singularity in $(\hat{\mathcal{C}}^{ij})^{-1}$. Usually the most relevant modes are the slow modes which are related to almost conserved quantities whose relaxation is described by the collision kernel.

COMPUTATION OF THE TRANSPORT COEFFICIENTS

12.1 THE SHEAR VISCOSITY WITHIN LINEAR RESPONSE

We consider a two-component Fermi gas in its most general form, allowing for different chemical potentials for the two species, i.e. μ_\uparrow and μ_\downarrow and a species dependent mass m_σ . We are concerned with a system without external forces, i.e. $\mathbf{F}_{\text{ext}} = \mathbf{0}$, in its stationary state, $\partial_t = 0$, such that the left hand side of the Boltzmann equation reduces to

$$D_\eta f_\sigma^0(\epsilon_\eta(\mathbf{k})) = \mathbf{v} \nabla_{\mathbf{r}} f_\sigma^0(\epsilon_\eta(\mathbf{k})). \quad (236)$$

Here, we specified the interaction according to a system with shear viscosity η and set $\alpha = \eta$. The energy of the system is given by

$$\epsilon_\eta(\mathbf{k}) = \frac{\mathbf{k}^2}{2m} - \mathbf{u}(r)k, \quad (237)$$

with $\mathbf{u}(r)$ being the velocity field. We assume a uniform flow in the x -direction and a velocity gradient in the y -direction as sketched in Figure 15 meaning $\mathbf{u}(r) = (u(y), 0)$. Now we can compute the spatial derivative of the equilibrium distribution function,

$$\nabla_{\mathbf{r}} f_\sigma^0 = \partial_\epsilon f_\sigma^0 \nabla_{\mathbf{r}} \epsilon = -\beta f_\sigma^0 (1 - f_\sigma^0) \nabla_{\mathbf{r}} (-u(y)k_x) = \beta f_\sigma^0 (1 - f_\sigma^0) \begin{pmatrix} 0 \\ \partial_y u(y) k_x \\ 0 \end{pmatrix}$$

and the left hand side of the Boltzmann equation reads

$$D_\eta f_\sigma^0 = \beta f_\sigma^0 (1 - f_\sigma^0) \mathbf{v} \begin{pmatrix} 0 \\ \partial_y u(y) k_x \\ 0 \end{pmatrix} = \beta f_\sigma^0 (1 - f_\sigma^0) \frac{k_x k_y}{m_\sigma} \partial_y u(y), \quad (238)$$

where we used $\mathbf{v} = \frac{\mathbf{k}}{m}$. Following the logic of Section 11.2.1 we find

$$I_{\sigma\eta}^{ij} = \frac{k_x k_y}{m_\sigma} \quad \text{and} \quad F_\eta^{ij} = \partial_y u(y). \quad (239)$$

In the more general case, we define for a generic velocity field $\mathbf{u}(r)$ of the fluid,

$$\begin{aligned} F_\eta^{ij} &= \partial_i u_j + \partial_j u_i - \frac{2}{d} \delta_{ij} \partial_l u_l \\ I_{\sigma\eta}^{ij} &= v_{\mathbf{k},\sigma}^i k^j, \end{aligned} \quad (240)$$

with u_i being the components of the flow velocity of the fluid. The generalized current is the viscous part of the stress tensor describing hydrodynamics in two spatial dimensions,

$$j_\eta^{ij} = T^{ij} = -\eta F_\eta^{ij} - \zeta \delta_{ij} \partial_l u_l, \quad (241)$$

where ζ the bulk viscosity. Combining Eq. (241) and Eq. (224) one obtains

$$\eta = \mathcal{S}_\eta[\chi^{ij}] \quad (242)$$

for the exact solution $|\chi^{ij}\rangle$. The variational principle provides us with a lower bound. If we make an ansatz $|\chi^{ij, \text{ansatz}}\rangle$ using a *finite* function set $\chi^{ij, \text{ansatz}} = I^{ij} \sum_n \lambda_n g_{n\sigma}(k)$ this implies [72]

$$\eta \geq \mathcal{S}_\eta[\chi_{\text{max}}^{ij, \text{ansatz}}], \quad (243)$$

where $|\chi_{\text{max}}^{ij, \text{ansatz}}\rangle$ corresponds to the optimal choice for a finite number of the parameters λ_n introduced in Eq. (232) which maximizes Eq. (229). In the case of the viscosity, the driving term does not couple to a conserved quantity such as the total energy or the momentum. Consequently, the variational approach can be employed straightforwardly, and very few modes suffice to solve the problem essentially exactly. We found that, just as in the three-dimensional case [52], the choice for the modes

$$g_\sigma(k) = 1 \quad (244)$$

yields results which are very close to the exact result. We have checked this statement for different sets of modes, for instance $g_{n\sigma}(k) = k^n$ for $n = 0, \dots, N$ up to $N = 10$ as well as Chebyshev polynomials up to the same order. The differences were in the low percent level, i.e. of order $\mathcal{O}\{10^{-2}\}$. With this choice of modes, Eq. (244), we find the following expression for the shear viscosity,

$$\eta = \mathcal{S}_\eta[I_\eta^{ij}] \lambda^{\text{max}} = \frac{\langle I_\eta^{ij} | \mathcal{S}_\eta \rangle^2}{\langle I_\eta^{ij} | C [I_\eta^{ij}] \rangle}, \quad (245)$$

where we used the expression (225) and (235) for $\mathcal{S}_\eta[I_\eta^{ij}]$ and λ^{max} , respectively.

12.2 THE SPIN DIFFUSION COEFFICIENT WITHIN LINEAR RESPONSE

Spin diffusion in a metal describes the response of a system of fermions to a gradient in a magnetic field. In our setup this translates to the two fermion species responding to gradients in the chemical potentials, which are opposite for the two species with atomic masses m_\uparrow and m_\downarrow . Again we assume a system with no external forces, i.e. $\mathbf{F}_{\text{ext}} = \mathbf{0}$, in its stationary state, $\partial_t f(\mathbf{k}) = 0$, such that the distribution function is accordingly driven out of equilibrium by

$$D_{\text{sd}} f^0(\mathbf{k}) = \mathbf{v} \nabla_{\mathbf{r}} f^0(\mathbf{k}). \quad (246)$$

The energy of our system $\epsilon(\mathbf{k})$ does not vary in space, meaning $\nabla_{\mathbf{r}}\epsilon(\mathbf{k}) = \mathbf{0}$, but we have $\nabla_{\mathbf{r}}\mu_{\sigma} \neq 0$, such that

$$\nabla_{\mathbf{r}}f_{\sigma}^0 = \partial_{\mu_{\sigma}}f_{\sigma}^0\nabla_{\mathbf{r}}\mu_{\sigma} = \beta f_{\sigma}^0(1 - f_{\sigma}^0)\nabla_{\mathbf{r}}\mu_{\sigma}. \quad (247)$$

We assume that the absolute value of the gradient is the same for both species but counteracts, meaning $\nabla_{\mathbf{r}}\mu_{\sigma} = \sigma\nabla_{\mathbf{r}}\mu$, and the driving term reads

$$\mathcal{D}_{\text{sd}}^{\sigma} = \sigma \frac{\mathbf{k}\nabla_{\mathbf{r}}\mu}{m_{\sigma}T} f_{\sigma}^0 (1 - f_{\sigma}^0). \quad (248)$$

Again, we identify the generalized force and projection from Eq. (217),

$$\begin{aligned} F_{\text{sd}}^{ij} &= \partial_i\mu\delta_{ij} \\ I_{\sigma,\text{sd}}^{ij} &= \sigma v_{\mathbf{k},\sigma}^i\delta_{ij}. \end{aligned} \quad (249)$$

The generalized current in this case is the spin current given by

$$j_s = -\sigma_s F_{\text{sd}}^{ij} \quad (250)$$

with σ_s being the spin conductivity. In accordance with Eq. (224) the spin conductivity is bounded from below by

$$\sigma_s \geq \mathcal{S}_{\text{sd}}[\chi_{\text{max}}^{ij, \text{ansatz}}]. \quad (251)$$

We can deduce the spin diffusion coefficient D via

$$D = \frac{\sigma_s}{\chi_s} \quad (252)$$

with the spin susceptibility of the free Fermi gas

$$\chi_s = \frac{m_{\uparrow}f_{\uparrow}^0(k=0) + m_{\downarrow}f_{\downarrow}^0(k=0)}{2\pi}. \quad (253)$$

In the case of the spin diffusion the driving term in general does not decouple from the momentum mode. Accordingly, finding the relevant modes of the system requires more care than in the case of the viscosity. The momentum mode corresponds to the choice

$$g_{\sigma} = \sigma m_{\sigma}. \quad (254)$$

The overlap of the momentum mode with the driving term within this variational ansatz is calculated as

$$\langle \chi | \mathcal{D}_{\text{sd}} \rangle = \frac{T}{\pi} \left(m_{\uparrow} \ln(1 + e^{\beta\mu_{\uparrow}}) - m_{\downarrow} \ln(1 + e^{\beta\mu_{\downarrow}}) \right). \quad (255)$$

This is zero if $\mu_{\uparrow} = \mu_{\downarrow} = \mu$ and $m_{\uparrow} = m_{\downarrow} = m$, meaning the momentum mode is not excited. If these conditions do not hold, the momentum mode is excited and it cannot be relaxed. This formally leads to an infinite spin conductivity σ_s . In metals the standard situation is spin balance with a finite spin conductivity [73]. In the experiments under discussion [56] two clouds

of different spin species are prepared to collide in the center of the trap. If the two clouds have the same number of particles and the masses are equal the unified cloud will reside in the center of the trap. On the other hand, the zero mode can be excited if one prepares different densities and/or different masses for the different spin species. The zero mode of the spin diffusion then has a very simple and intuitive physical interpretation as the center of mass motion.

In our concrete setup in a balanced system we work with the choice

$$g_\sigma = m \quad (256)$$

which is not a zero mode of the collision integral and has finite overlap with the driving term. We have again checked more generic mode choices and found this to provide an excellent variational ansatz.

With this choice of modes, Eq. (256), we find for the spin diffusion coefficient, as an analogue to Eq. (245) for the shear viscosity,

$$D = \frac{1}{\chi_s} \mathcal{S}_{\text{sd}}[I_{\text{sd}}^{ij}] m \lambda^{\text{max}} = \frac{m}{\chi_s} \frac{\langle I_{\text{sd}}^{ij} | \mathcal{S}_{\text{sd}} \rangle^2}{\langle I_{\text{sd}}^{ij} | C[I_{\text{sd}}^{ij}] \rangle}. \quad (257)$$

The numerical solution for the shear viscosity and the spin diffusion coefficient is presented in the next chapter.

RESULTS

In order to obtain results comparable to other systems we need to normalize the transport coefficients by the respective thermodynamic quantities, density, pressure, and entropy density, which we will compute in Section 13.1.

In order to be able to compare our results for the two-dimensional Fermi gas to the transport coefficients of the classical gas we will discuss those coefficients for the classical in Section 13.2 before we present our results in Section 13.3.

13.1 THERMODYNAMIC QUANTITIES

For consistency all thermodynamic quantities have to be computed at the same level of approximation. A definite prescription is provided by the large- N expansion described in [51]. Here, N identical copies of spin-up and spin-down fermions are introduced such that one can interpolate between free fermions ($N = \infty$) and the physical case of interacting fermions ($N = 1$). To order $\mathcal{O}(1/N)$ the grand potential reads [51]

$$\frac{\Omega}{N} = \sum_k \left\{ -2T \ln(1 + e^{-\beta(\epsilon_k - \mu)}) - \frac{1}{N} \int_{-\infty}^{\infty} \frac{d\omega}{\pi} b(\omega) \Im \ln \mathcal{T}(k, \omega) \right\}, \quad (258)$$

with the full medium scattering matrix $\mathcal{T}(k, \omega)$ and the Bose function $b(\omega) = (\exp(\beta\omega) - 1)^{-1}$, $\beta = 1/(k_B T)$. The total differential of the thermodynamic potential $d\Omega = -SdT - PdV - N_0 d\mu$ provides us with the required relations for thermodynamic quantities, pressure P , particle density n , and entropy density s . To leading order in $1/N$ the thermodynamic quantities within the large- N expansion are those of the free Fermi gas [51] with grand potential

$$\Omega = -k_B T \sum_k \ln(1 + e^{-\beta(\epsilon_k - \mu)}). \quad (259)$$

We find

$$n = \frac{N_0}{V} = -\frac{1}{V} \frac{\partial \Omega}{\partial \mu} = 2\lambda_T^{-2} \ln(1 + e^{\beta\mu}), \quad (260)$$

$$P = -\frac{\partial \Omega}{\partial V} = -nk_B T \theta \text{Li}_2(1 - e^{1/\theta}) \quad \text{and} \quad (261)$$

$$s = -\frac{\partial P}{\partial T} = nk_B \{ -2\theta \text{Li}_2(1 - e^{1/\theta}) - \ln(e^{1/\theta} - 1) \}, \quad (262)$$

with the thermal length $\lambda_T = \sqrt{2\pi/mk_B T}$ and reduced temperature $\theta = T/T_F$. $\text{Li}_s(z)$ is the polylogarithm function. In the high temperature classical limit $\theta \rightarrow \infty$ the entropy density becomes

$$s = nk_B \{ 2 + \ln \theta + \mathcal{O}(\theta^{-2}) \}. \quad (263)$$

13.2 TRANSPORT COEFFICIENTS OF THE CLASSICAL GAS.

In this section we present the shear viscosity and the spin diffusion coefficient for the classical gas. By comparing our results for the quantum gas to the coefficients of the classical gas we can reveal the quantum effect on the transport coefficients. In the classical limit $T \gg T_F = \frac{k_F^2}{2m}$ the Fermi-Dirac distribution, Eq. (205), becomes the Boltzmann distribution,

$$f^0(k) = e^{-E/k_B T}, \quad (264)$$

for which $f^0(k) \ll 1$ holds for high temperatures. In this case the integrals of Eq. (245) and Eq. (257) simplify and can be solved analytically. Including the vacuum scattering matrix, Eq. (201), in the collision integral in Eq. (245) and Eq. (257), respectively, yields for the shear viscosity [4]

$$\frac{\eta(\theta)}{n} = \frac{R\theta}{2\pi} \quad \text{with} \quad R = \pi^2 + \left[\ln\left(\frac{5}{2}\Theta\right) + 2\ln(k_F a_{2D}) \right]^2, \quad (265)$$

and for the spin diffusion coefficient [5]

$$D(\theta) = \frac{Q\theta}{4\pi} \quad \text{with} \quad Q = \pi^2 + \left[\ln\left(\frac{3}{2}\Theta\right) + 2\ln(k_F a_{2D}) \right]^2. \quad (266)$$

In the high-temperature limit the transport coefficients depend linearly on θ with logarithmic corrections.

13.3 NUMERICAL RESULTS FOR THE TRANSPORT COEFFICIENTS

In Figure 17 we plot our numerical results for the transport coefficients for the strongly interacting two-dimensional Fermi gas. In the left panel of Figure 17 we show the shear viscosity over particle density $\alpha = \eta/n$, and in the right panel we give the spin diffusion coefficient times the mass, Dm . The red lines represent the results with full medium effects, i.e. with the medium scattering matrix $\mathcal{T}(\mathbf{q}, \omega)$ (208) included in the collision integral \mathcal{C} (221) while the blue lines were calculated using the vacuum scattering matrix \mathcal{T}^{vac} (201). The black lines represent the transport coefficients for the classical gas, Eq. (265) and Eq. (266). Our main finding is that the medium increases scattering in an interacting system and thereby substantially lowers the transport coefficients. For strong interactions ($\epsilon_B/\epsilon_F = 2$, for further explanation regarding the interaction parameter $\epsilon_B/\epsilon_F = 2$ see below) we find a minimum value for the shear viscosity with medium scattering of

$$\frac{\eta}{n} \approx 0.83\hbar, \quad (267)$$

at a temperature $T/T_F \approx 1.3$. The shear viscosity with vacuum scattering at this temperature obtains the value

$$\frac{\eta}{n} \approx 3.6\hbar, \quad (268)$$

which is approximately four times larger.

For the spin diffusion coefficient with medium scattering at strong interactions we find a minimal value of

$$mD \approx 0.39\hbar, \quad (269)$$

at a temperature of $T/T_F \approx 1.4$. The spin diffusion coefficient with vacuum scattering at this temperature is

$$mD \approx 2.3\hbar, \quad (270)$$

which is approximately six times larger than with medium effects included. The reason for the very small value for the spin diffusion coefficient with medium effects could be due to the fact that our approach overestimates quantum fluctuations. As the calculation with only vacuum scattering included underestimates quantum fluctuations we expect the real minimum to be located between these two values. Consequently, we can conclude that the spin diffusion coefficient for the two-dimensional Fermi gas is close to the quantum limit of $\sim \frac{\hbar}{m}$.

For vacuum scattering the system always appears to be in the normal Fermi liquid phase and the upturn of the transport coefficients for low temperatures is due to Pauli blocking. With medium scattering the transport coefficients decrease down to a finite temperature T_c where the medium \mathcal{T} -matrix acquires a pole, $\mathcal{T}^{-1}(q=0, \omega=0)|_{T=T_c} = 0$. Below T_c this pole would formally lead to a diverging collision integral C , see Eq. (221), and according to Eq. (235), $\eta, D \rightarrow 0$ in this approximation. But in accordance with the Thouless criterion [74, 75, 76], at this temperature the system undergoes a phase transition to a superfluid phase where our approach is not valid. For the viscosity the following picture applies: In the superfluid phase, the viscosity of the superfluid component within the Landau two-fluid model [77] is indeed zero, but in the superfluid phase also the particle density is not defined, as there is no particle conservation. Therefore, the ratio η/n is not well defined. If one also considers the normal component of the fluid, the shear viscosity as well as the particle density are finite and the ratio η/n increases with decreasing temperature, such that the minimum value for η/n near the critical temperature is global. A calculation of the viscosity in the superfluid B phase of ^3He for $T < T_c$ in Ref. [46] found that Pauli blocking and enhanced scattering cancel precisely and the viscosity approaches a finite value for $T \rightarrow 0$.

In Figure 18 the ratio of the viscosity to entropy density η/s is compared for different values of the interaction strength. The interaction strength is expressed by the binding energy ϵ_B of the two-particle bound state scaled by the Fermi energy ϵ_F . For strong interactions the binding energy is larger and it is connected to the two-dimensional scattering cross section a_{2D} via $\epsilon_B = 1/(2m_r a_{2D}^2)$ with the reduced mass $m_r^{-1} = m_\uparrow^{-1} + m_\downarrow^{-1}$. As discussed in Section 9.1, the viscosity is lower when interactions are stronger. The phase transition, indicated by the endpoints of the solid lines at $T = 1.04 T_c$, to the superfluid phase occurs at higher temperatures when interactions are stronger. As an estimate, the smallest value we computed for the ratio η/s is

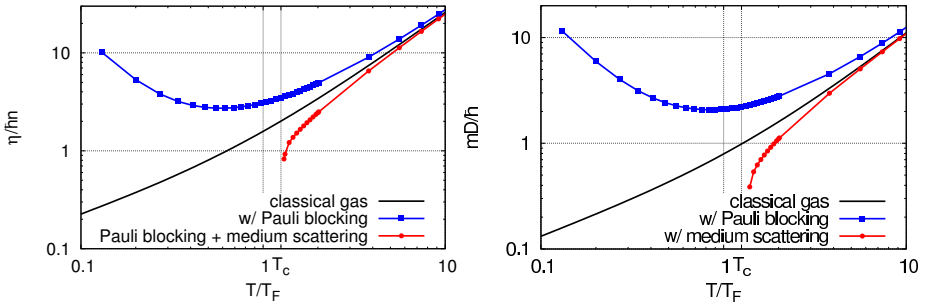


FIGURE 17: The temperature dependence of the transport coefficients, the shear viscosity left and the spin diffusion coefficient right, with and without medium effects, at strong interaction $\varepsilon_B/\varepsilon_F = 2$. While Pauli blocking (blue line) increases the transport coefficients with respect to the classical gas (black line), medium scattering (red line) substantially lowers the minimum as T_c is approached from above.

for an interaction parameter $\varepsilon_B/\varepsilon_F = 0.5$ (blue line). It is located at around $T/T_F \approx 0.6$ and has a value of

$$\eta/s \approx 0.15 \frac{\hbar}{k_B} \approx 1.9 \frac{1}{4\pi} \frac{\hbar}{k_B}. \quad (271)$$

This is only about twice the proposed string theory bound of $\eta/s = 1/(4\pi) \frac{\hbar}{k_B}$.

13.4 RELATION TO OTHER THEORETICAL WORK

13.4.1 Shear viscosity

The shear viscosity for the two-dimensional Fermi gas, calculated using only the vacuum scattering matrix, has also been discussed in [4, 5]. The authors find a minimum of $\eta/n \approx 2.7\hbar$ at a temperature of $T/T_F \approx 0.6$ and a minimum of $\eta/s \approx 1.5 \frac{\hbar}{k_B}$ at $T/T_F \approx 0.9$. These values agree exactly with the observed minima in our calculations with the vacuum scattering matrix, the blue line in the left panel of Figure 17.

The calculation for the shear viscosity with the full \mathcal{T} -matrix has been performed for the unitary three-dimensional Fermi gas by Enss *et. al.* [53]. In two dimensions, quantum and interaction effects are stronger than in three dimensions, and we expect the minimum of our computed shear viscosity for the two-dimensional Fermi gas to be smaller. Enss *et. al.* find the minimal value of $\eta/s \approx 0.6 \frac{\hbar}{k_B}$ at a temperature of $T/T_F \approx 0.3 - 0.4$ for the 3d Fermi gas. This is four times larger than our result of $\eta/s \approx 0.15 \frac{\hbar}{k_B}$ at $T/T_F \approx 0.6$ for the 2d Fermi gas.

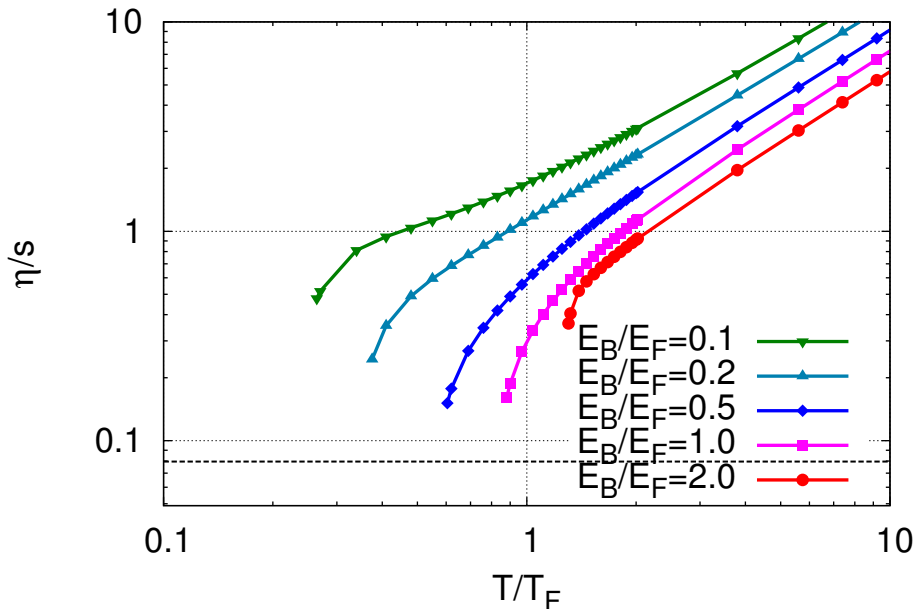


FIGURE 18: Viscosity to entropy ratio η/s in units of \hbar/k_B with medium scattering above T_c for different interaction strengths $\varepsilon_B/\varepsilon_F = 0.1, 0.2, 0.5, 1, 2$ (from top to bottom). The dashed line indicates the bound $\hbar/(4\pi k_B)$.

13.4.2 Spin diffusion

The spin diffusion coefficient for the two-dimensional Fermi gas with only the vacuum scattering matrix included in the calculations has also been discussed by Bruun in Ref. [5]. The author finds a minimum of $mD \approx 2.15\hbar$ at a temperature of $T/T_F \approx 0.85$. This value is in very good agreement with the lowest value we could find in our calculation with the vacuum scattering matrix, $mD \approx 2.07\hbar$.

The spin diffusion coefficient for the three-dimensional Fermi gas has been discussed by Bruun in Ref. [55]. For high temperatures the author used a kinetic approach while for low temperatures he includes strong correlation effects by using Fermi liquid theory. In the unitarity limit the minimum value of $mD \approx 1.1\hbar$ occurs somewhat below T_F but above the transition temperature of $T_c \sim 0.2T_F$. This value is very close to the universal quantum limit discussed in Section 9.2 and it is lower than our result for the spin diffusion in a two-dimensional Fermi gas with vacuum scattering, but larger than our result with medium effects included.

13.5 COMPARISON TO EXPERIMENT

We compare our computed result for the shear viscosity to the experimental finding of Vogt *et. al.* [3] in a strongly interacting ultracold Fermi gas constrained to two dimensions. Experimentally the shear viscosity can be measured via the damping rate of the quadrupole mode of an oscillating gas. In

this section we will sketch the experimental setup and derive an expression which relates the damping rate of the quadrupole mode to the shear viscosity, to allow comparison of our results with the experiment and the classical gas.

The experiment [3] is performed with a gas of ^{40}K -atoms prepared in a 50/50 ratio in two different hyperfine ground states and cooled down to temperatures of the order $\frac{T}{T_F}$. A standing wave potential creates an optical lattice which confines the gas to two dimensions. Within the plane the gas is trapped by a weaker isotropic, two-dimensional harmonic potential with trapping frequency ω_\perp . The quadrupole mode is excited by adiabatically introducing a small anisotropy and then abruptly returning to the original trapping configuration. This excites an oscillation of the atomic cloud with frequency ω_Q until the radial trapping potential is switched off and the cloud expands. From an absorption picture which is taken some milliseconds after switching off the potential one can determine the radii of the cloud in the x - and y -direction and fit their difference to determine ω_Q . The damping of the oscillations is caused by the viscosity of the gas. Hence one can calculate the viscosity from the damping rate Γ_Q which is connected to the time averaged energy dissipation rate $\langle \dot{E} \rangle_t$ via

$$\Gamma_Q = \frac{\langle \dot{E} \rangle_t}{2\langle E \rangle_t}. \quad (272)$$

The time-averaged mechanical energy is given by

$$\langle E \rangle_t = \frac{mb^2}{2} \int d^2r r^2 n(r), \quad (273)$$

with $n(r)$ being the two-dimensional particle density profile in the trap and the parameter b specifies the strength of the velocity field, cf. Eq. (277). In the temperature regime $\frac{T}{T_F} \geq 0.3$ in which the measurement of Vogt *et. al.* was performed we can apply the high temperature approximation for the cloud density which shows a gaussian decay with increasing distance r from the center of the gap [4]

$$n(r) = \frac{N}{\pi\sigma^2} e^{-\frac{r^2}{\sigma^2}} \quad (274)$$

with $\sigma^2 = \frac{2T}{m\omega_\perp^2}$ and particle number $N = \int d^2r n(r)$. With this density profile we obtain

$$\langle E \rangle_t = \frac{b^2 NT}{\omega_\perp^2}. \quad (275)$$

The time averaged energy dissipation rate follows from the stress tensor (241)

$$\langle \dot{E}^{ij} \rangle_t = -\frac{1}{2} \int d^2r \eta(r) (\partial_i u_j + \partial_j u_i - \delta_{ij} \nabla \cdot \mathbf{v})^2 - \int d^2r \zeta(r) (\nabla \cdot \mathbf{v})^2. \quad (276)$$

For the quadrupole mode the velocity field has the form

$$\mathbf{v}(r) = b[x\hat{e}_x - y\hat{e}_y] \cos(\omega t) \quad (277)$$

such that the time averaged energy dissipation rate of the quadruple mode is fully determined by the shear viscosity,

$$\langle \dot{E}^{ij} \rangle_t = -2b^2 \int d^2r \eta(r). \quad (278)$$

It is convenient to write

$$\eta(r) = n(r)\alpha(r) \quad (279)$$

with $\alpha(r)$ being a dimensionless function. The spatial integral over $\eta(r)$ can then be written as

$$\int d^2r \eta(r) = \int d^2r n(r)\alpha(r) = N\langle \alpha \rangle \quad (280)$$

With Eq. (275), Eq. (278) and Eq. (280) the quadrupole damping rate follows as

$$\Gamma_Q = -\frac{\omega_{\perp}^2}{T} \langle \alpha \rangle. \quad (281)$$

For a classical gas the viscosity is approximately independent of particle density, such that the spatial integral of $\eta(r)$ is infinite. This problem is solved by introducing a cutoff, which physically accounts for the nonapplicability of hydrodynamics in the dilute corona of the cloud. Within kinetic theory, this can be implemented by taking into account the frequency dependence of the shear viscosity [78, 4, 51],

$$\eta(\omega) = \frac{\eta(0)}{1 + \tau_R^2 \omega^2}, \quad (282)$$

where τ_R is the viscous relaxation time, which is the time it takes for the stress tensor to relax to the Navier-Stokes form $T^{ij} = -\eta(0)F^{ij}$. $\eta(0)$ is the shear viscosity at zero frequency (which still depends on the spatial coordinates). The relaxation time can be obtained from the sum rule which connects the shear viscosity to the pressure P within kinetic theory [79],

$$\frac{1}{\pi} \int d\omega \eta(\omega) = \frac{P}{2}. \quad (283)$$

Integrating Eq. (282) and comparing to Eq. (283) one finds an antiproportionality of the viscous relaxation time to the particle density: $\tau_R = \frac{\eta(r)}{P(r)} \sim \frac{\eta(r)}{n(r)T}$. Thus the spatial integral over $\eta(\omega)$ becomes finite. Now we can calculate the spatial average of α ,

$$\begin{aligned} \langle \alpha \rangle &= \frac{1}{N} \int d^2r \eta(\omega_Q, r) = \frac{1}{N} \int d^2r \frac{n(r)\alpha(r)}{1 + \omega_Q^2 \frac{n(r)^2 \alpha(r)^2}{P^2(r)}} \\ &= \frac{1}{N} \int d^2r \frac{n(r)\alpha(r)}{1 + \frac{\omega_Q^2}{\omega_{\perp}^2} \frac{\alpha^2(r)}{N \Theta^2 p^2(r)}}, \end{aligned} \quad (284)$$

where we introduced the global reduced temperature $\Theta = \frac{T}{T_F^{glob}} = \frac{T}{\sqrt{N}\omega_\perp}$ and the dimensionless pressure $p(r) = \frac{P(r)}{n(r)T}$. We now change variables to a local temperature, defined as

$$\theta(r) = \frac{T}{T_F^{loc}} = \frac{mT}{\pi n(r)}, \quad (285)$$

where we used the fact that the Fermi temperature is $T_F = \frac{k_F^2}{2m}$ and in two dimensions the Fermi momentum is related to the particle density via

$$k_F = \sqrt{2\pi n}. \quad (286)$$

After this change of variables the integral reads

$$\langle \alpha \rangle = 2\Theta^2 \int_{2\Theta^2}^{\infty} \frac{d\theta}{\theta^2} \frac{\alpha(\theta)}{1 + \frac{\omega_Q^2}{\omega_\perp^2} \frac{\alpha^2(\theta)}{N\Theta^2 p^2(\theta)}}. \quad (287)$$

Now we can compute $\langle \alpha \rangle$ numerically for the two-dimensional Fermi gas for different interaction strengths ϵ_B/ϵ_F , using our numerical result for $\eta/n = \alpha$ (see Section 12.1 and left panel of Figure 17). The damping rate of the quadrupole mode (Eq. (281)) over the trapping frequency ω_\perp can then be extracted. We use the parameters from the experiment, $\Theta = 0.3$, $\epsilon_F/h = 6.4$ kHz, $\omega_\perp = 2\pi \times 125$ Hz, $N = 2620$ particles and we use $p(\theta) = 1$. The frequency of the quadrupole mode ω_Q can be determined by measuring the radius of the cloud in x and y -direction from the absorption picture. In the hydrodynamic regime, i.e. for interaction parameters $\ln(k_F a_{2D}) \lesssim 2.5$, it is found to be $\omega_Q \simeq \sqrt{2}\omega_\perp$.

For the classical gas we find by using Eq. (265),

$$\langle \alpha(\Theta) \rangle = \frac{R\Theta^2}{2\pi} \ln \left[1 + \frac{\pi^2 N}{2R^2 \Theta^2} \right] \quad (288)$$

which yields for the damping rate

$$\frac{\Gamma_Q}{\omega_\perp} = \frac{R\Theta}{2\pi\sqrt{N}} \ln \left[1 + \frac{\pi^2 N}{2R^2 \Theta^2} \right]. \quad (289)$$

In Figure 19 we plot the computed damping rate over trapping frequency $\frac{\Gamma_Q}{\omega_\perp}$ for the classical gas, Eq. (289), and for the two-dimensional Fermi gas versus the interaction parameter $\ln(k_F a_{2D})$ together with the experimental data. (Here, a_{2D} is the two-dimensional scattering length.) The interaction parameter $\ln(k_F a_{2D})$ is smaller for stronger interactions, and $k_F a_{2D}$ is connected to the energy of the two-particle bound state ϵ_B via $\frac{\epsilon_B}{\epsilon_F} = \frac{1}{(k_F a_{2D})^2}$. We see that the function for the classical gas fails to describe the experimental data. In the 2d Fermi gas the damping is strongly enhanced compared with the classical gas and the peak height $\Gamma_Q/\omega_\perp \sim 0.6$ agrees well with the experiment. Still, the peak position in our calculation occurs at a larger interaction parameter than in the experiment.

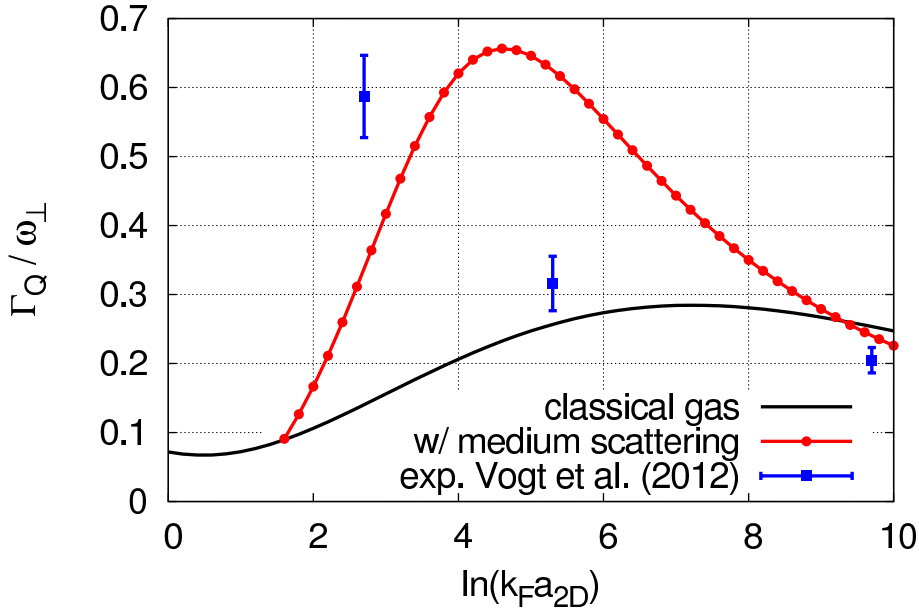


FIGURE 19: Quadrupole damping rate Γ_Q/ω_\perp vs. the interaction strength of the trapped gas at $T/T_F = 0.3$ and $\epsilon_F/h = 6.4$ kHz, with radial trapping frequency $\omega_\perp = 2\pi \times 125$ Hz and $N = 2620$ particles.

13.6 CONCLUSION AND OUTLOOK

We used the Boltzmann approach to compute the shear viscosity and the spin diffusion coefficient of the two-dimensional Fermi gas. We performed the numerical calculations with the two-body vacuum scattering matrix and the two-body medium scattering matrix and find that the medium effects lower both transport coefficients. In the case of the shear viscosity by a factor of four, cf. Eq. (267) and Eq. (268), and in the case of the spin diffusion by a factor of six, cf. Eq. (269) and Eq. (270). We also computed the ratio shear viscosity over entropy density η/s (see Eq. (271)) and obtain a result that is about twice the conjectured lower bound [6] of $\eta/s = \frac{1}{4\pi} \frac{\hbar}{k_B}$, computed using the AdS/CFT correspondence [7].

The Boltzmann approach we used to compute the transport coefficients is valid provided quantum interference effects are negligible and deviations from well-defined quasiparticles are small. This assumption is questionable in systems with strong interactions and at temperatures well below the Fermi temperature T_F . In our calculation with the medium scattering matrix we only go down to temperatures close to the Fermi temperature above the phase transition to the superfluid phase. We performed our calculations for different interaction parameters up to $\epsilon_B/\epsilon_F = 2$. Consequently we enter the strongly coupled regime, which is marked by a sharp decrease of the quadrupole mode frequency to $\omega_Q \sim \sqrt{2}\omega_\perp$, where ω_\perp is the frequency of the trapping potential in an ultracold atom experiment [3]. Accordingly, it would be instructive to compare our result to calculations within a formalism which

does not require the quasiparticle picture to be valid, as e.g. an approach based on the Kubo formula [53, 54].

APPENDIX

B.1 THE MANY-BODY SCATTERING MATRIX

In this section we compute the angular part of the integral

$$\int \frac{d^2\mathbf{p}}{(2\pi)^2} \frac{f(\epsilon_{\mathbf{p}\uparrow} - \mu_{\uparrow}) + f(\epsilon_{\mathbf{p}+\mathbf{q}\downarrow} - \mu_{\downarrow})}{i\omega + \mu_{\uparrow} + \mu_{\downarrow} - \epsilon_{\mathbf{p}\uparrow} - \epsilon_{\mathbf{p}+\mathbf{q}\downarrow}}, \quad (290)$$

which is part of the many-body scattering matrix, Eq. (208). We split the integral into two parts,

$$\begin{aligned} I_{\uparrow} &= \int \frac{d^2\mathbf{p}}{(2\pi)^2} \frac{f(\epsilon_{\mathbf{p}\uparrow} - \mu_{\uparrow})}{i\omega + \mu_{\uparrow} + \mu_{\downarrow} - \epsilon_{\mathbf{p}\uparrow} - \epsilon_{\mathbf{p}+\mathbf{q}\downarrow}} \\ &= \int \frac{d^2\mathbf{p}}{(2\pi)^2} \frac{f(\epsilon_{\mathbf{p}\uparrow} - \mu_{\uparrow})}{i\omega + \mu_{\uparrow} + \mu_{\downarrow} - \frac{p^2}{2m_{\uparrow}} - \frac{p^2}{2m_{\downarrow}} - \frac{q^2}{2m_{\downarrow}} - \frac{2pq \cos \theta}{2m_{\downarrow}}} \end{aligned} \quad (291)$$

and

$$\begin{aligned} I_{\downarrow} &= \int \frac{d^2\mathbf{p}}{(2\pi)^2} \frac{f(\epsilon_{\mathbf{p}+\mathbf{q}\downarrow} - \mu_{\downarrow})}{i\omega + \mu_{\uparrow} + \mu_{\downarrow} - \epsilon_{\mathbf{p}\uparrow} - \epsilon_{\mathbf{p}+\mathbf{q}\downarrow}} \\ &\stackrel{\mathbf{p} \rightarrow \mathbf{p}-\mathbf{q}}{=} \int \frac{d^2\mathbf{p}}{(2\pi)^2} \frac{f(\epsilon_{\mathbf{p}\downarrow} - \mu_{\downarrow})}{i\omega + \mu_{\uparrow} + \mu_{\downarrow} - \epsilon_{\mathbf{p}-\mathbf{q}\uparrow} - \epsilon_{\mathbf{p}\downarrow}} \\ &\stackrel{\mathbf{p} \rightarrow -\mathbf{p}}{=} \int \frac{d^2\mathbf{p}}{(2\pi)^2} \frac{f(\epsilon_{\mathbf{p}+\mathbf{q}\downarrow} - \mu_{\downarrow})}{i\omega + \mu_{\uparrow} + \mu_{\downarrow} - \frac{p^2}{2m_{\uparrow}} - \frac{p^2}{2m_{\downarrow}} - \frac{q^2}{2m_{\uparrow}} - \frac{2pq \cos \theta}{2m_{\uparrow}}}. \end{aligned} \quad (292)$$

Now we can summarize Eq. (291) and Eq. (292) and write

$$\begin{aligned} I_{\uparrow\downarrow} &= \int_0^{\infty} \frac{pdp}{(2\pi)^2} f(\epsilon_{\mathbf{p}\uparrow\downarrow} - \mu_{\uparrow\downarrow}) \int_0^{2\pi} d\theta \frac{1}{A_{\uparrow\downarrow} - B_{\uparrow\downarrow} \cos \theta} \\ &= \int_0^{\infty} \frac{pdp}{(2\pi)^2} f(\epsilon_{\mathbf{p}\uparrow\downarrow} - \mu_{\uparrow\downarrow}) \frac{2\pi}{\sqrt{A_{\uparrow\downarrow}^2 - B_{\uparrow\downarrow}^2}} \end{aligned} \quad (293)$$

with

$$A_{\uparrow\downarrow} = i\omega + \mu_{\uparrow} + \mu_{\downarrow} - \frac{p^2}{2m_{\uparrow}} - \frac{p^2}{2m_{\downarrow}} - \frac{q^2}{2m_{\downarrow\uparrow}} \quad \text{and} \quad B_{\uparrow\downarrow} = \frac{pq}{m_{\downarrow\uparrow}}. \quad (294)$$

B.2 PROOF: MAXIMIZING $\mathcal{Q}[\chi^{ij}]$ LEADS TO THE BOLTZMANN EQUATION

In this section we will maximize the functional $\mathcal{Q}[\chi^{ij}] = \mathcal{S}_\alpha[\chi^{ij}] + \mathcal{C}[\chi^{ij}]$ with respect to χ^{ij} and we will see that this leads to the Boltzmann equation, Eq. (222). For this purpose we will take the derivative of the functionals, $\mathcal{S}_\alpha[\chi^{ij}]$ and $\mathcal{C}[\chi^{ij}]$.

$$\begin{aligned} \frac{\delta \mathcal{S}[\chi^{ij}]}{\delta \chi_\sigma^{ij}(\mathbf{k})} &= -\frac{1}{T} \frac{\delta}{\delta \chi_\sigma^{ij}(\mathbf{k})} \sum_{\sigma'} \int_{\mathbf{k}'} f_{\sigma'}^0(\mathbf{k}') (1 - f_{\sigma'}^0(\mathbf{k}')) I_{\sigma'}^{ij}(\mathbf{k}') \chi_{\sigma'}^{ij}(\mathbf{k}') \\ &= -\frac{1}{T} \sum_{\sigma'} \int_{\mathbf{k}'} f_{\sigma'}^0(\mathbf{k}') (1 - f_{\sigma'}^0(\mathbf{k}')) I_{\sigma'}^{ij}(\mathbf{k}') \delta(\mathbf{k} - \mathbf{k}') \delta_{\sigma'\sigma} \\ &= -\frac{1}{T} f_\sigma^0(\mathbf{k}) (1 - f_\sigma^0(\mathbf{k})) I_\sigma^{ij}(\mathbf{k}) = S_\alpha^\sigma \end{aligned} \quad (295)$$

and

$$\begin{aligned} \frac{\delta \mathcal{C}[\chi^{ij}]}{\delta \chi_\sigma^{ij}(\mathbf{k})} &= \frac{\delta}{\delta \chi_\sigma^{ij}(\mathbf{k})} \frac{1}{2} \left(\int_{\mathbf{k}'} \chi_\sigma^{ij}(\mathbf{k}') \mathcal{C}[\chi_{-\sigma}^{ij}(\mathbf{k}'), \chi_{-\sigma}^{ij}(\mathbf{k}')] \right. \\ &\quad \left. + \int_{\mathbf{k}'} \chi_{-\sigma}^{ij}(\mathbf{k}') \mathcal{C}[\chi_{-\sigma}^{ij}(\mathbf{k}'), \chi_\sigma^{ij}(\mathbf{k}')] \right) \end{aligned} \quad (296)$$

with

$$\begin{aligned} &\int_{\mathbf{k}'} \chi_\sigma^{ij}(\mathbf{k}') \mathcal{C}[\chi_\sigma^{ij}(\mathbf{k}'), \chi_{-\sigma}^{ij}(\mathbf{k}')] = \\ &\frac{1}{T} \int_{\mathbf{k}'} \int_{\mathbf{k}_1, \mathbf{q}} \delta(\varepsilon_{\mathbf{k}'\sigma} + \varepsilon_{\mathbf{k}_1-\sigma} - \varepsilon_{\mathbf{k}'+\mathbf{q}\sigma} - \varepsilon_{\mathbf{k}_1-\mathbf{q}-\sigma}) \\ &\times \left| \mathcal{T}(\mathbf{k}' + \mathbf{k}_1, \varepsilon_{\mathbf{k}'\sigma} + \varepsilon_{\mathbf{k}_1-\sigma} - \mu_\sigma - \mu_{-\sigma}) \right|^2 \\ &\times \left[f_\sigma^0(\mathbf{k}') f_{-\sigma}^0(\mathbf{k}_1) (1 - f_\sigma^0(\mathbf{k}' + \mathbf{q})) (1 - f_{-\sigma}^0(\mathbf{k}_1 - \mathbf{q})) \right] \\ &\times \chi_\sigma^{ij}(\mathbf{k}') \left[\chi_\sigma^{ij}(\mathbf{k}') + \chi_{-\sigma}^{ij}(\mathbf{k}_1) - \chi_\sigma^{ij}(\mathbf{k}' + \mathbf{q}) - \chi_{-\sigma}^{ij}(\mathbf{k}_1 - \mathbf{q}) \right] \end{aligned} \quad (297)$$

and

$$\begin{aligned} &\int_{\mathbf{k}'} \chi_{-\sigma}^{ij}(\mathbf{k}') \mathcal{C}[\chi_{-\sigma}^{ij}(\mathbf{k}'), \chi_\sigma^{ij}(\mathbf{k}')] = \\ &\frac{1}{T} \int_{\mathbf{k}'} \int_{\mathbf{k}_1, \mathbf{q}} \delta(\varepsilon_{\mathbf{k}'-\sigma} + \varepsilon_{\mathbf{k}_1\sigma} - \varepsilon_{\mathbf{k}'+\mathbf{q}-\sigma} - \varepsilon_{\mathbf{k}_1-\mathbf{q}\sigma}) \\ &\times \left| \mathcal{T}(\mathbf{k}' + \mathbf{k}_1, \varepsilon_{\mathbf{k}'-\sigma} + \varepsilon_{\mathbf{k}_1\sigma} - \mu_\sigma - \mu_{-\sigma}) \right|^2 \\ &\times \left[f_{-\sigma}^0(\mathbf{k}') f_\sigma^0(\mathbf{k}_1) (1 - f_{-\sigma}^0(\mathbf{k}' + \mathbf{q})) (1 - f_\sigma^0(\mathbf{k}_1 - \mathbf{q})) \right] \\ &\times \chi_{-\sigma}^{ij}(\mathbf{k}') \left[\chi_{-\sigma}^{ij}(\mathbf{k}') + \chi_\sigma^{ij}(\mathbf{k}_1) - \chi_{-\sigma}^{ij}(\mathbf{k}' + \mathbf{q}) - \chi_\sigma^{ij}(\mathbf{k}_1 - \mathbf{q}) \right] \end{aligned} \quad (298)$$

Taking the derivative we get for the first part (297):

$$\begin{aligned}
 & \frac{\delta}{\delta \chi_{\sigma}^{ij}(\mathbf{k})} \int_{\mathbf{k}'} \chi_{\sigma}^{ij}(\mathbf{k}') C[\chi_{\sigma}^{ij}(\mathbf{k}'), \chi_{-\sigma}^{ij}(\mathbf{k}')] = \\
 & \frac{1}{T} \int_{\mathbf{k}'} \int_{\mathbf{k}_1, \mathbf{q}} \delta(\varepsilon_{\mathbf{k}'\sigma} + \varepsilon_{\mathbf{k}_1-\sigma} - \varepsilon_{\mathbf{k}'+\mathbf{q}\sigma} - \varepsilon_{\mathbf{k}_1-\mathbf{q}-\sigma}) \\
 & \times \left| \mathcal{T}(\mathbf{k}' + \mathbf{k}_1, \varepsilon_{\mathbf{k}'\sigma} + \varepsilon_{\mathbf{k}_1-\sigma} - \mu_{\sigma} - \mu_{-\sigma}) \right|^2 \\
 & \times \left[f_{\sigma}^0(\mathbf{k}') f_{-\sigma}^0(\mathbf{k}_1) \left(1 - f_{\sigma}^0(\mathbf{k}' + \mathbf{q})\right) \left(1 - f_{-\sigma}^0(\mathbf{k}_1 - \mathbf{q})\right) \right] \\
 & \times \delta(\mathbf{k} - \mathbf{k}') \left[\chi_{\sigma}^{ij}(\mathbf{k}') + \chi_{-\sigma}^{ij}(\mathbf{k}_1) - \chi_{\sigma}^{ij}(\mathbf{k}' + \mathbf{q}) - \chi_{-\sigma}^{ij}(\mathbf{k}_1 - \mathbf{q}) \right] + \\
 & \frac{1}{T} \int_{\mathbf{k}'} \int_{\mathbf{k}_1, \mathbf{q}} \delta(\varepsilon_{\mathbf{k}'\sigma} + \varepsilon_{\mathbf{k}_1-\sigma} - \varepsilon_{\mathbf{k}'+\mathbf{q}\sigma} - \varepsilon_{\mathbf{k}_1-\mathbf{q}-\sigma}) \\
 & \times \left| \mathcal{T}(\mathbf{k}' + \mathbf{k}_1, \varepsilon_{\mathbf{k}'\sigma} + \varepsilon_{\mathbf{k}_1-\sigma} - \mu_{\sigma} - \mu_{-\sigma}) \right|^2 \\
 & \times \left[f_{\sigma}^0(\mathbf{k}') f_{-\sigma}^0(\mathbf{k}_1) \left(1 - f_{\sigma}^0(\mathbf{k}' + \mathbf{q})\right) \left(1 - f_{-\sigma}^0(\mathbf{k}_1 - \mathbf{q})\right) \right] \\
 & \times \chi_{\sigma}^{ij}(\mathbf{k}') [\delta(\mathbf{k} - \mathbf{k}') - \delta(\mathbf{k} - \mathbf{k}' - \mathbf{q})]. \tag{299}
 \end{aligned}$$

Here the first summand just yields $C[\chi_{\sigma}^{ij}, \chi_{-\sigma}^{ij}]$. The second summand we split once more and discuss the two addends therein separately. For the first one, which contains the factor $\delta(\mathbf{k} - \mathbf{k}')$ we get

$$\begin{aligned}
 c_1 &= \frac{1}{T} \int_{\mathbf{k}_1, \mathbf{q}} \delta(\varepsilon_{\mathbf{k}\sigma} + \varepsilon_{\mathbf{k}_1-\sigma} - \varepsilon_{\mathbf{k}+\mathbf{q}\sigma} - \varepsilon_{\mathbf{k}_1-\mathbf{q}-\sigma}) \\
 & \times \left| \mathcal{T}(\mathbf{k} + \mathbf{k}_1, \varepsilon_{\mathbf{k}\sigma} + \varepsilon_{\mathbf{k}_1-\sigma} - \mu_{\sigma} - \mu_{-\sigma}) \right|^2 \\
 & \times \left[f_{\sigma}^0(\mathbf{k}) f_{-\sigma}^0(\mathbf{k}_1) \left(1 - f_{\sigma}^0(\mathbf{k} + \mathbf{q})\right) \left(1 - f_{-\sigma}^0(\mathbf{k}_1 - \mathbf{q})\right) \right] \chi_{\sigma}^{ij}(\mathbf{k}), \tag{300}
 \end{aligned}$$

and the second one with the factor $\delta(\mathbf{k} - \mathbf{k}' - \mathbf{q})$ yields

$$\begin{aligned}
c_2 &= -\frac{1}{T} \int_{\mathbf{k}_1, \mathbf{q}} \delta(\varepsilon_{\mathbf{k}-\mathbf{q}\sigma} + \varepsilon_{\mathbf{k}_1-\sigma} - \varepsilon_{\mathbf{k}\sigma} - \varepsilon_{\mathbf{k}_1-\mathbf{q}-\sigma}) \\
&\times \left| \mathcal{T}(\mathbf{k} - \mathbf{q} + \mathbf{k}_1, \varepsilon_{\mathbf{k}-\mathbf{q}\sigma} + \varepsilon_{\mathbf{k}_1-\sigma} - \mu_\sigma - \mu_{-\sigma}) \right|^2 \\
&\times \left[f_\sigma^0(\mathbf{k} - \mathbf{q}) f_{-\sigma}^0(\mathbf{k}_1) \left(1 - f_\sigma^0(\mathbf{k})\right) \left(1 - f_{-\sigma}^0(\mathbf{k}_1 - \mathbf{q})\right) \right] \chi_\sigma^{ij}(\mathbf{k} - \mathbf{q}) \\
&\stackrel{\mathbf{q} \rightarrow -\mathbf{q}}{=} -\frac{1}{T} \int_{\mathbf{k}_1, \mathbf{q}} \delta(\varepsilon_{\mathbf{k}+\mathbf{q}\sigma} + \varepsilon_{\mathbf{k}_1-\sigma} - \varepsilon_{\mathbf{k}\sigma} - \varepsilon_{\mathbf{k}_1+\mathbf{q}-\sigma}) \\
&\times \left| \mathcal{T}(\mathbf{k} + \mathbf{q} + \mathbf{k}_1, \varepsilon_{\mathbf{k}+\mathbf{q}\sigma} + \varepsilon_{\mathbf{k}_1-\sigma} - \mu_\sigma - \mu_{-\sigma}) \right|^2 \\
&\times \left[f_\sigma^0(\mathbf{k} + \mathbf{q}) f_{-\sigma}^0(\mathbf{k}_1) \left(1 - f_\sigma^0(\mathbf{k})\right) \left(1 - f_{-\sigma}^0(\mathbf{k}_1 + \mathbf{q})\right) \right] \chi_\sigma^{ij}(\mathbf{k} + \mathbf{q}) \\
&\stackrel{\mathbf{k}_1 \rightarrow \mathbf{k}_1 - \mathbf{q}}{=} -\frac{1}{T} \int_{\mathbf{k}_1, \mathbf{q}} \delta(\varepsilon_{\mathbf{k}+\mathbf{q}\sigma} + \varepsilon_{\mathbf{k}_1-\mathbf{q}-\sigma} - \varepsilon_{\mathbf{k}\sigma} - \varepsilon_{\mathbf{k}_1-\sigma}) \\
&\times \left| \mathcal{T}(\mathbf{k} + \mathbf{k}_1, \varepsilon_{\mathbf{k}+\mathbf{q}\sigma} + \varepsilon_{\mathbf{k}_1-\mathbf{q}-\sigma} - \mu_\sigma - \mu_{-\sigma}) \right|^2 \\
&\times \left[f_\sigma^0(\mathbf{k} + \mathbf{q}) f_{-\sigma}^0(\mathbf{k}_1 - \mathbf{q}) \left(1 - f_\sigma^0(\mathbf{k})\right) \left(1 - f_{-\sigma}^0(\mathbf{k}_1)\right) \right] \chi_\sigma^{ij}(\mathbf{k} + \mathbf{q}) \\
&= -\frac{1}{T} \int_{\mathbf{k}_1, \mathbf{q}} \delta(\varepsilon_{\mathbf{k}\sigma} + \varepsilon_{\mathbf{k}_1-\sigma} - \varepsilon_{\mathbf{k}+\mathbf{q}\sigma} - \varepsilon_{\mathbf{k}_1-\mathbf{q}-\sigma}) \\
&\times \left| \mathcal{T}(\mathbf{k} + \mathbf{k}_1, \varepsilon_{\mathbf{k}\sigma} + \varepsilon_{\mathbf{k}_1-\sigma} - \mu_\sigma - \mu_{-\sigma}) \right|^2 \\
&\times \left[f_\sigma^0(\mathbf{k}) f_{-\sigma}^0(\mathbf{k}_1) \left(1 - f_\sigma^0(\mathbf{k} + \mathbf{q})\right) \left(1 - f_{-\sigma}^0(\mathbf{k}_1 - \mathbf{q})\right) \right] \chi_\sigma^{ij}(\mathbf{k} + \mathbf{q})
\end{aligned} \tag{301}$$

where in the last step we used energy conservation during the scattering process and the identity $f_\sigma^0(\mathbf{k}) f_{-\sigma}^0(\mathbf{k}_1) (1 - f_\sigma^0(\mathbf{k} + \mathbf{q})) (1 - f_{-\sigma}^0(\mathbf{k}_1 - \mathbf{q})) = f_\sigma^0(\mathbf{k} + \mathbf{q}) f_{-\sigma}^0(\mathbf{k}_1 - \mathbf{q}) (1 - f_\sigma^0(\mathbf{k})) (1 - f_{-\sigma}^0(\mathbf{k}_1))$ which holds for the equilibrium distribution function f^0 .

Now we look at the derivative of Eq. (298)

$$\begin{aligned}
&\frac{\delta}{\delta \chi_\sigma^{ij}(\mathbf{k})} \int_{\mathbf{k}'} \chi_{-\sigma}^{ij}(\mathbf{k}') C[\chi_{-\sigma}^{ij}(\mathbf{k}'), \chi_\sigma^{ij}(\mathbf{k}')] = \\
&\frac{1}{T} \int_{\mathbf{k}'} \int_{\mathbf{k}_1, \mathbf{q}} \delta(\varepsilon_{\mathbf{k}'-\sigma} + \varepsilon_{\mathbf{k}_1\sigma} - \varepsilon_{\mathbf{k}'+\mathbf{q}-\sigma} - \varepsilon_{\mathbf{k}_1-\mathbf{q}\sigma}) \\
&\times \left| \mathcal{T}(\mathbf{k}' + \mathbf{k}_1, \varepsilon_{\mathbf{k}'-\sigma} + \varepsilon_{\mathbf{k}_1\sigma} - \mu_\sigma - \mu_{-\sigma}) \right|^2 \\
&\times \left[f_{-\sigma}^0(\mathbf{k}') f_\sigma^0(\mathbf{k}_1) \left(1 - f_{-\sigma}^0(\mathbf{k}' + \mathbf{q})\right) \left(1 - f_\sigma^0(\mathbf{k}_1 - \mathbf{q})\right) \right] \\
&\times \chi_{-\sigma}^{ij}(\mathbf{k}') [\delta(\mathbf{k} - \mathbf{k}_1) - \delta(\mathbf{k} - \mathbf{k}_1 + \mathbf{q})].
\end{aligned} \tag{302}$$

Here again we discuss the two summands separately. For the first one with the factor $\delta(\mathbf{k} - \mathbf{k}_1)$ we find

$$\begin{aligned}
 c_3 &= \frac{1}{T} \int_{\mathbf{k}', \mathbf{q}} \delta(\varepsilon_{\mathbf{k}'-\sigma} + \varepsilon_{\mathbf{k}\sigma} - \varepsilon_{\mathbf{k}'+\mathbf{q}-\sigma} - \varepsilon_{\mathbf{k}-\mathbf{q}\sigma}) \\
 &\quad \times \left| \mathcal{T}(\mathbf{k}' + \mathbf{k}, \varepsilon_{\mathbf{k}'-\sigma} + \varepsilon_{\mathbf{k}\sigma} - \mu_\sigma - \mu_{-\sigma}) \right|^2 \\
 &\quad \times \left[f_{-\sigma}^0(\mathbf{k}') f_\sigma^0(\mathbf{k}) \left(1 - f_{-\sigma}^0(\mathbf{k}' + \mathbf{q})\right) \left(1 - f_\sigma^0(\mathbf{k} - \mathbf{q})\right) \right] \chi_{-\sigma}^{ij}(\mathbf{k}') \\
 &\stackrel{\mathbf{q} \rightarrow -\mathbf{q}}{=} \frac{1}{T} \int_{\mathbf{k}', \mathbf{q}} \delta(\varepsilon_{\mathbf{k}'-\sigma} + \varepsilon_{\mathbf{k}\sigma} - \varepsilon_{\mathbf{k}'-\mathbf{q}-\sigma} - \varepsilon_{\mathbf{k}+\mathbf{q}\sigma}) \\
 &\quad \times \left| \mathcal{T}(\mathbf{k}' + \mathbf{k}, \varepsilon_{\mathbf{k}'-\sigma} + \varepsilon_{\mathbf{k}\sigma} - \mu_\sigma - \mu_{-\sigma}) \right|^2 \\
 &\quad \times \left[f_{-\sigma}^0(\mathbf{k}') f_\sigma^0(\mathbf{k}) \left(1 - f_{-\sigma}^0(\mathbf{k}' - \mathbf{q})\right) \left(1 - f_\sigma^0(\mathbf{k} + \mathbf{q})\right) \right] \chi_{-\sigma}^{ij}(\mathbf{k}').
 \end{aligned} \tag{303}$$

And the result after transformations for the second summand with the factor $\delta(\mathbf{k} - \mathbf{k}_1 + \mathbf{q})$ is

$$\begin{aligned}
 c_4 &= -\frac{1}{T} \int_{\mathbf{k}', \mathbf{q}} \delta(\varepsilon_{\mathbf{k}'-\sigma} + \varepsilon_{\mathbf{k}+\mathbf{q}\sigma} - \varepsilon_{\mathbf{k}'+\mathbf{q}-\sigma} - \varepsilon_{\mathbf{k}\sigma}) \\
 &\quad \times \left| \mathcal{T}(\mathbf{k}' + \mathbf{k} + \mathbf{q}, \varepsilon_{\mathbf{k}'-\sigma} + \varepsilon_{\mathbf{k}+\mathbf{q}\sigma} - \mu_\sigma - \mu_{-\sigma}) \right|^2 \\
 &\quad \times \left[f_{-\sigma}^0(\mathbf{k}') f_\sigma^0(\mathbf{k} + \mathbf{q}) \left(1 - f_{-\sigma}^0(\mathbf{k}' + \mathbf{q})\right) \left(1 - f_\sigma^0(\mathbf{k})\right) \right] \chi_{-\sigma}^{ij}(\mathbf{k}') \\
 &\stackrel{\mathbf{k}' \rightarrow \mathbf{k}' - \mathbf{q}}{=} -\frac{1}{T} \int_{\mathbf{k}', \mathbf{q}} \delta(\varepsilon_{\mathbf{k}'-\mathbf{q}-\sigma} + \varepsilon_{\mathbf{k}+\mathbf{q}\sigma} - \varepsilon_{\mathbf{k}'-\sigma} - \varepsilon_{\mathbf{k}\sigma}) \\
 &\quad \times \left| \mathcal{T}(\mathbf{k}' + \mathbf{k}, \varepsilon_{\mathbf{k}'-\mathbf{q}-\sigma} + \varepsilon_{\mathbf{k}+\mathbf{q}\sigma} - \mu_\sigma - \mu_{-\sigma}) \right|^2 \\
 &\quad \times \left[f_{-\sigma}^0(\mathbf{k}' - \mathbf{q}) f_\sigma^0(\mathbf{k} + \mathbf{q}) \left(1 - f_{-\sigma}^0(\mathbf{k}')\right) \left(1 - f_\sigma^0(\mathbf{k})\right) \right] \chi_{-\sigma}^{ij}(\mathbf{k}' - \mathbf{q}) \\
 &= -\frac{1}{T} \int_{\mathbf{k}', \mathbf{q}} \delta(\varepsilon_{\mathbf{k}'-\sigma} + \varepsilon_{\mathbf{k}\sigma} - \varepsilon_{\mathbf{k}'-\mathbf{q}-\sigma} - \varepsilon_{\mathbf{k}+\mathbf{q}\sigma}) \\
 &\quad \times \left| \mathcal{T}(\mathbf{k}' + \mathbf{k}, \varepsilon_{\mathbf{k}'-\sigma} + \varepsilon_{\mathbf{k}\sigma} - \mu_\sigma - \mu_{-\sigma}) \right|^2 \\
 &\quad \times \left[f_{-\sigma}^0(\mathbf{k}') f_\sigma^0(\mathbf{k}) \left(1 - f_{-\sigma}^0(\mathbf{k}' - \mathbf{q})\right) \left(1 - f_\sigma^0(\mathbf{k} + \mathbf{q})\right) \right] \chi_{-\sigma}^{ij}(\mathbf{k}' - \mathbf{q}).
 \end{aligned} \tag{304}$$

Here, again, we used energy conservation and the identity we used in the last step of Eq. (301).

Adding all components we find

$$\begin{aligned}
\frac{\delta \mathcal{C}[\chi^{ij}]}{\delta \chi_{\sigma}^{ij}(\mathbf{k})} &= \frac{1}{2} \left(C[\chi_{\sigma}^{ij}, \chi_{-\sigma}^{ij}] + \right. \\
&\frac{1}{T} \int_{\mathbf{k}_1, \mathbf{q}} \delta(\varepsilon_{\mathbf{k}\sigma} + \varepsilon_{\mathbf{k}_1-\sigma} - \varepsilon_{\mathbf{k}+\mathbf{q}\sigma} - \varepsilon_{\mathbf{k}_1-\mathbf{q}-\sigma}) \\
&\times \left| \mathcal{T}(\mathbf{k} + \mathbf{k}_1, \varepsilon_{\mathbf{k}\sigma} + \varepsilon_{\mathbf{k}_1-\sigma} - \mu_{\sigma} - \mu_{-\sigma}) \right|^2 \\
&\times \left[f_{\sigma}^0(\mathbf{k}) f_{-\sigma}^0(\mathbf{k}_1) \left(1 - f_{\sigma}^0(\mathbf{k} + \mathbf{q}) \right) \left(1 - f_{-\sigma}^0(\mathbf{k}_1 - \mathbf{q}) \right) \right] \\
&\times \left[\chi_{\sigma}^{ij}(\mathbf{k}) - \chi_{\sigma}^{ij}(\mathbf{k} + \mathbf{q}) + \chi_{-\sigma}^{ij}(\mathbf{k}') - \chi_{-\sigma}^{ij}(\mathbf{k}' - \mathbf{q}) \right] \\
&= C[\chi_{\sigma}^{ij}, \chi_{-\sigma}^{ij}]
\end{aligned} \tag{305}$$

Thus we find

$$\frac{\delta \mathcal{Q}[\chi^{ij}]}{\delta \chi_{\sigma}^{ij}(\mathbf{k})} = 0 \Leftrightarrow S_{\alpha}^{\sigma} - C[\chi_{\sigma}^{ij}, \chi_{-\sigma}^{ij}] = 0, \tag{306}$$

which is the Boltzmann equation (cf. Eq. (222) and Eq. (224)).

BIBLIOGRAPHY

- [1] J. M. Luttinger and J. C. Ward, *Phys. Rev.* **118**, 1417 (1960).
- [2] Y. Adamov, I. V. Gornyi, and A. D. Mirlin, *Phys. Rev. B* **73**, 045426 (2006).
- [3] E. Vogt, M. Feld, B. Fröhlich, D. Pertot, M. Koschorreck, and M. Köhl, *Phys. Rev. Lett.* **108**, 070404 (2012).
- [4] T. Schäfer, *Phys. Rev. A* **85**, 033623 (2012).
- [5] G. M. Bruun, *Phys. Rev. A* **85**, 013636 (2012).
- [6] P. K. Kovtun, D. T. Son, and A. O. Starinets, *Phys. Rev. Lett.* **94**, 111601 (2005).
- [7] G. Policastro, D. T. Son, and A. O. Starinets, *Phys. Rev. Lett.* **87**, 081601 (2001).
- [8] L. D. Landau, *Sov. Phys. JETP* **3**, 920 (1957).
- [9] V. N. Kotov, B. Uchoa, V. M. Pereira, F. Guinea, and A. H. Castro Neto, *Rev. Mod. Phys.* **84**, 1067 (2012).
- [10] J. González, F. Guinea, and M. A. H. Vozmediano, *Phys. Rev. B* **59**, R2474 (1999).
- [11] J. González, F. Guinea, and M. Vozmediano, *Nuclear Physics B* **424**, 595 (1994).
- [12] D. C. Elias, R. V. Gorbachev, A. S. Mayorov, S. V. Morozov, A. A. Zhukov, P. Blake, L. A. Ponomarenko, I. V. Grigorieva, K. S. Novoselov, F. Guinea, and A. K. Geim, *Nat Phys* **7**, 701 (2011).
- [13] G. L. Yu, R. Jalil, B. Belle, A. S. Mayorov, P. Blake, F. Schedin, S. V. Morozov, L. A. Ponomarenko, F. Chiappini, S. Wiedmann, U. Zeitler, M. I. Katsnelson, A. K. Geim, K. S. Novoselov, and D. C. Elias, *Proc. Natl Acad. Sci. USA* **110**, 3282 (2013).
- [14] J. E. Drut and T. A. Lähde, *Phys. Rev. Lett.* **102**, 026802 (2009).
- [15] J. E. Drut and T. A. Lähde, (2013), [arxiv:1304.1711v2](https://arxiv.org/abs/1304.1711v2) .
- [16] D. Shoenberg, *Magnetic Oscillations in Metals* (Cambridge University Press, 1984).
- [17] G. W. Martin, D. L. Maslov, and M. Y. Reizer, *Phys. Rev. B* **68**, 241309 (2003).
- [18] K. S. Novoselov, A. K. Geim, S. V. Morozov, D. Jiang, Y. Zhang, S. V. Dubonos, I. V. Grigorieva, and A. A. Firsov, *Science* **306**, 666 (2004).
- [19] A. K. Geim, *Rev. Mod. Phys.* **83**, 851 (2011).
- [20] R. Peierls, *Ann. I.H. Poioncare* **5** (1935).
- [21] L. D. Landau, *Phys. Z. Sowjetunion* **11** (1937).

- [22] N. D. Mermin and H. Wagner, *Phys. Rev. Lett.* **17**, 1133 (1966).
- [23] N. D. Mermin, *Phys. Rev.* **176**, 250 (1968).
- [24] N. Garcia, (2007), [arxiv:cond-mat/0703515](https://arxiv.org/abs/0703515) .
- [25] A. Fasolino, J. H. Los, and M. I. Katsnelson, *Nat Mater* **6**, 858 (2007).
- [26] V. Crespi, *Physics* **1**, 15 (2008).
- [27] A. H. Castro Neto, F. Guinea, N. M. R. Peres, K. S. Novoselov, and A. K. Geim, *Rev. Mod. Phys.* **81**, 109 (2009).
- [28] A. Kretinin, G. L. Yu, R. Jalil, Y. Cao, F. Withers, A. Mishchenko, M. I. Katsnelson, K. S. Novoselov, A. K. Geim, and F. Guinea, *Phys. Rev. B* **88**, 165427 (2013).
- [29] L. Landau and E. Lifshitz, *Quantum Mechanics: Non-Relativistic Theory*, Course of Theoretical Physics (Elsevier Science, 1981).
- [30] L. Onsager, *Phil. Mag.* **43**, 1006 (1952).
- [31] C. Kittel, *Introduction to solid state physics* (Wiley India Pvt. Limited, 2007).
- [32] C. D. Castro and R. Raimondi, (2004), [arxiv:cond-mat/0402203](https://arxiv.org/abs/cond-mat/0402203) .
- [33] A. Altland and B. Simons, *Condensed Matter Field Theory* (Cambridge University Press, 2006).
- [34] M. Fowler and R. E. Prange, *Physics* **1** (1965).
- [35] H. Bruus and K. Flensberg, *Many-Body Quantum Theory in Condensed Matter Physics: An Introduction*, Oxford Graduate Texts (OUP Oxford, 2004).
- [36] D. T. Son, *Phys. Rev. Lett.* **98**, 020604 (2007), [arXiv:cond-mat/0511721](https://arxiv.org/abs/cond-mat/0511721) .
- [37] U. Briskot, I. A. Dmitriev, and A. D. Mirlin, *Phys. Rev. B* **87**, 195432 (2013).
- [38] T. Ando, Y. Matsumoto, Y. Uemura, M. Kobayashi, and K. F. Komatsubara, *Journal of the Physical Society of Japan* **32**, 859 (1972).
- [39] T. Ando, *Journal of the Physical Society of Japan* **37**, 1233 (1974).
- [40] T. Schäfer and D. Teaney, *Reports on Progress in Physics* **72**, 126001 (2009).
- [41] M. Müller, J. Schmalian, and L. Fritz, *Phys. Rev. Lett.* **103**, 025301 (2009), [arXiv:0903.4178](https://arxiv.org/abs/0903.4178) .
- [42] A. Turlapov, J. Kinast, B. Clancy, L. Luo, J. Joseph, and J. Thomas, *Journal of Low Temperature Physics* **150**, 567 (2008).
- [43] C. Cao, E. Elliott, J. Joseph, H. Wu, J. Petricka, T. Schäfer, and J. E. Thomas, *Science* **331**, 58 (2011), [arXiv:1007.2625](https://arxiv.org/abs/1007.2625) .
- [44] C. Cao, E. Elliott, H. Wu, and J. E. Thomas, *New Journal of Physics* **13**, 075007 (2011).
- [45] L. D. Landau and I. M. Khalatnikov, **19**, 637,709 (1949), english translation in *Collected Papers of L. D. Landau* (Pergamon Press, Ltd., Oxford,

- England, 1965), p. 494.
- [46] C. J. Pethick, H. Smith, and P. Bhattacharyya, *Phys. Rev. Lett.* **34**, 643 (1975).
- [47] G. Rupak and T. Schäfer, *Phys. Rev. A* **76**, 053607 (2007), arXiv:0707.1520 .
- [48] P. Massignan, G. M. Bruun, and H. Smith, *Phys. Rev. A* **71**, 033607 (2005), arXiv:cond-mat/0409660 .
- [49] G. M. Bruun and H. Smith, *Phys. Rev. A* **72**, 043605 (2005), arXiv:cond-mat/0504734 .
- [50] S. Riedl, E. R. Sánchez Guajardo, C. Kohstall, A. Altmeyer, M. J. Wright, J. H. Denschlag, R. Grimm, G. M. Bruun, and H. Smith, *Phys. Rev. A* **78**, 053609 (2008).
- [51] T. Enss, *Phys. Rev. A* **86**, 013616 (2012).
- [52] G. M. Bruun and H. Smith, *Phys. Rev. A* **75**, 043612 (2007), arXiv:cond-mat/0612460 .
- [53] T. Enss, R. Haussmann, and W. Zwerger, *Annals of Physics* **326**, 770 (2011).
- [54] G. Wlazłowski, P. Magierski, and J. E. Drut, *Phys. Rev. Lett.* **109**, 020406 (2012).
- [55] G. M. Bruun, *New Journal of Physics* **13**, 035005 (2011).
- [56] A. Sommer, M. Ku, G. Roati, and M. W. Zwierlein, *Nature* **472**, 201 (2011).
- [57] A. Sommer, M. Ku, and M. W. Zwierlein, *New Journal of Physics* **13**, 055009 (2011).
- [58] I. Bloch, J. Dalibard, and W. Zwerger, *Rev. Mod. Phys.* **80**, 885 (2008).
- [59] H. Stoof, K. Gubbels, and D. Dickerscheid, *Ultracold Quantum Fields*, Theoretical and Mathematical Physics (Springer, 2008).
- [60] A. Messiah, *Quantum Mechanics*, Dover books on physics (Dover Publications, 1961).
- [61] Duk, H. Padleckas, and Stannerd, *Image: Laminarshear.png* (English Wikipedia, Share Alike 3.0 Unported license) <https://en.wikipedia.org/wiki/Viscosity> .
- [62] M. Koschorreck, D. Pertot, E. Vogt, and M. Kohl, *Nat Phys* **9**, 405 (2013).
- [63] S. K. Adhikari, *American J. Phys.* **54**, 362 (1986).
- [64] M. Randeria, J.-M. Duan, and L.-Y. Shieh, *Phys. Rev. Lett.* **62**, 981 (1989).
- [65] L. Landau and E. Lifshitz, *Quantum Mechanics: Non-relativistic Theory*, Butterworth Heinemann (Butterworth-Heinemann, 1977).
- [66] J. R. Engelbrecht and M. Randeria, *Phys. Rev. B* **45**, 12419 (1992).

- [67] R. Schmidt, T. Enss, V. Pietilä, and E. Demler, *Phys. Rev. A* **85**, 021602(R) (2012).
- [68] L. Boltzmann, *Wiener Berichte* **66**, 275 (1872).
- [69] J. Ziman, *Electrons and Phonons: The Theory of Transport Phenomena in Solids*, International series of monographs on physics (OUP Oxford, 1960).
- [70] P. Arnold, G. D. Moore, and L. G. Yaffe, *Journal of High Energy Physics* **2000**, 001 (2000).
- [71] E. Fermi, *Nuclear Physics* (University of Chicago Press, 1950).
- [72] H. Smith and H. Jensen, *Transport Phenomena*, Oxford science publications (Clarendon Press, 1989).
- [73] M. Müller and H. C. Nguyen, *New Journal of Physics* **13**, 035009 (2011).
- [74] X.-J. Liu, *Phys. Rev. A* **88**, 043607 (2013).
- [75] X.-J. Liu and H. Hu, *EPL (Europhysics Letters)* **75**, 364 (2006).
- [76] C. A. R. Sá de Melo, M. Randeria, and J. R. Engelbrecht, *Phys. Rev. Lett.* **71**, 3202 (1993).
- [77] R. J. Donnelly, *Print edition* **62**, 34 (2009).
- [78] M. Braby, J. Chao, and T. Schäfer, *New Journal of Physics* **13**, 035014 (2011).
- [79] E. Taylor and M. Randeria, *Phys. Rev. A* **81**, 053610 (2010), [arXiv:1002.0869](https://arxiv.org/abs/1002.0869) .

STATEMENT OF AUTHORSHIP / SELBSTSTÄNDIGKEITSERKLÄRUNG

Ich versichere, dass ich die von mir vorgelegte Dissertation selbständig angefertigt, die benutzten Quellen und Hilfsmittel vollständig angegeben und die Stellen der Arbeit - einschließlich Tabellen, Karten und Abbildungen -, die anderen Werken im Wortlauf oder dem Sinn nach entnommen sind, in jedem Einzelfall als Entlehnung kenntlich gemacht habe; dass diese Dissertation, abgesehen von der Universität Utrecht, noch keiner anderen Fakultät oder Universität zur Prüfung vorgelegen hat; dass sie - abgesehen von unten angegebenen Teilpublikationen - noch nicht veröffentlicht worden ist, sowie, dass ich eine solche Veröffentlichung vor Abschluss des Promotionsverfahrens nicht vornehmen werde. Die Bestimmungen der Promotionsordnung sind mir bekannt. Die von mir vorgelegte Dissertation ist von Prof. Dr. Achim Rosch (Köln), Prof. Dr. Cristiane de Morais Smith (Utrecht) und Dr. Lars Fritz (Utrecht) betreut worden.

Carolin Sarah Küppersbusch

Teilpublikationen

- Tilman Enss, Carolin Küppersbusch and Lars Fritz, "*Shear viscosity and spin diffusion in a two-dimensional Fermi gas*", *Phys. Rev. A* **86**, 013617 (2012)